IN-20
1658
P192

NASA Technical Memorandum 103731

Multi-Dimensional Modeling of a Thermal Energy Storage Canister

Thomas W. Kerslake
Lewis Research Center
Cleveland, Ohio

(NASA-TM-103731) MULTI-DIMENSIONAL MODELING N91-19177
OF A THERMAL ENERGY STORAGE CANISTER M.S.
Thesis - Cleveland State Univ., Dec. 1990
(NASA) 192 p CSCL 10C Unclas
G3/20 0001658

January 1991

MULTI-DIMENSIONAL MODELING
OF A
THERMAL ENERGY STORAGE CANISTER

Thomas W. Kerslake
National Aeronautics and Space Administration
Lewis Research Center
Cleveland, Ohio 44135

ABSTRACT

The Solar Dynamic Power Module being developed for Space Station Freedom uses a eutectic mixture of LiF-CaF_2 phase change material (PCM) contained in toroidal canisters for thermal energy storage. Presented herein are the results from heat transfer analyses of a PCM containment canister. One- and two-dimensional finite-difference computer models are developed to analyze heat transfer in the canister walls, PCM, void, and heat engine working fluid coolant. The modes of heat transfer considered include conduction in canister walls and solid PCM, conduction and pseudo - free convection in liquid PCM, conduction and radiation across PCM vapor filled void regions and forced convection in the heat engine working fluid. Void shape, location, growth or shrinkage (due to density difference between the solid and liquid PCM phases) are prescribed based on engineering judgement. The PCM phase change process is analyzed using the enthalpy method. The discussion of results focuses on how canister thermal performance is affected by free convection in the liquid PCM and void heat transfer. Characterizing these effects is important for interpreting the relationship between ground-based canister performance (in 1-g) and expected on-orbit performance (in micro-g). Void regions accentuate canister hot spots and temperature gradients due to their large thermal resistance. Free convection reduces the extent of PCM superheating and lowers canister temperatures during a portion of the PCM thermal charge period. Surprisingly small differences in canister thermal performance result from operation on the ground and operation on-orbit. This lack of a strong gravity dependency is attributed to the large contribution of container walls in overall canister energy redistribution by conduction.

TABLE OF CONTENTS

NOMENCLATURE

c = Specific Heat, J/g-K

A = Void Surface Element Area, cm^2 or constant

B = Constant

C5 = Constant

D = Cooling Fluid Tube Inner Diameter, cm

div = Divergence Operator

e = Specific Enthalpy, J/g

F = View Factor

g = Gravitational Acceleration, cm/sec^2

h = Film coefficient, W/cm^2-K

H = PCM Heat of Fusion, J/g

He-Xe= Helium-Xenon Gas Mixture

i = Grid Element Index

iv = Grid Element Which Contains X_v

iv′ = Combined Grid Element

k = Thermal Conductivity, W/cm-K

L = Annular Canister Length, cm

L′ = Slab Canister Thickness, cm

LH = Liquid PCM Vertical Layer Height, cm

LiF-CaF_2 = Lithium Fluoride-Calcium Fluoride

$\dot{m}$ = He/Xe Mass Flow Rate, g/sec

MF = Mass Fraction PCM in Element iv

MFL = PCM Mass Fraction Liquid

NRS = Number of Void Radiating Surface Elements

n3 = Constant
Nu = Nusselt Number
PCM = Phase Change Material
Pr = Prandtl Number
q = Heat flux, W/cm^2
Q = Thermal Power, W
r = Radial Coordinate, cm
R = Thermal Resistance, cm^2-K/W
Ra = Rayleigh Number
Re = Reynolds number
s = Conduction path length, cm
St = Stefan Number
t = Time, sec
T = Temperature, K
TES = Thermal Energy Storage
u = Velocity of Void-PCM Interface, cm/sec
U = Overall Heat Transfer Coefficient, W/cm^2-K
VVF = Void Volume Fraction
w = Liquid PCM Width, cm
x = One-Dimensional Coordinate, cm
X = Melt or Void Front Position, cm
XF = Mushy Zone Liquid PCM Mass Fraction
YF = Mushy Zone Liquid PCM Volume Fraction
z = Axial Coordinate, cm
● = Dot Product
∇ = Gradient Operator

Greek Symbols

α = Thermal Diffusivity, cm^2/sec

β = Volumetric Thermal Expansion Coefficient, 1/K

δ = Canister Wall Thickness, cm

Δ = Kronecker Delta Function

Δr = Radial Grid Spacing, cm

Δt = Time Step, sec

ΔT = Temperature Difference, K

Δx = One-Dimensional Grid Spacing, cm

Δz = Axial Grid Spacing, cm

ϵ = Emittance

π = Pi Constant, $2*\sin^{-1}(1)$

ρ = Density, g/cm^3

σ = Stefan-Boltzmann Constant, $5.67051\text{x}10^{-12}$ W/cm^2-K^4

ν = Kinematic Viscosity, cm^2/sec

ψ = Dimensionless Function of Δr and r

Subscripts and Superscripts

E = Enhanced

EFF = Effective

f = He-Xe Fluid

i = Inner Radius or Grid Element Index

j = Void Surface Element

k = Void Surface Element

L = Liquid PCM

m = PCM Melt

n = Current Time Step

n+1 = Future Time Step

O = Outer Radius

PCM = Phase Change Material

rad = Radiation

S = Solid PCM

v = Void

VAP = Vapor

w = Canister Wall

WS = Side Wall

\+ = Slightly Above

\- = Slightly Below

ACKNOWLEDGEMENTS

I would like to express my thanks to several people whose valuable contributions made possible, this work:

- Dr. Mounir B. Ibrahim, who served as thesis committee chairman, for his thoughtful technical insights and guidance in conducting this work.

- Mr. Chris A. Gallo, NASA Lewis Research Center, for writing the required PATRAN-interfacing programs and for producing many of the PATRAN temperature contour and phase plots contained in this thesis.

- The staff of the NASA Lewis Research Center GVIS Lab (advanced Graphics Visualization Laboratory) for producing video animations of the numerical results.

CHAPTER I

SUMMARY

Phase change thermal energy storage is a particularly attractive approach to meet energy storage requirements for the space station Freedom electrical power system. In this application, the ability to produce continuous electrical power with the intermittent solar source of low earth orbit is crucial. The solar dynamic power module proposed for use on Freedom incorporates a solid-to-liquid phase change material (PCM) encapsulated in multiple, annular containment canisters to meet thermal energy storage requirements. Detailed heat transfer analyses of the canister are necessary to determine temperature histories for subsequent use in thermal-stress and material durability calculations.

The nature of canister heat transfer is very complex. Solid-liquid phase change along with many modes of heat transfer are encompassed in this time-dependent, three-dimensional problem. Although there are several methods available for solving classical moving boundary or Stefan

problems, a weak numerical solution technique is the only feasible approach for the canister problem. This is due to the combination of canister geometry and periodic boundary conditions which can create multiple, complex-shape phase boundaries whose locations are not known a priori. Moreover, the enthalpy formulation appears to be the best suited weak solution technique to employ on the basis accuracy and reliability.

The TES canister problem has been analyzed by several researchers using a variety of different approaches. Many of these approaches either 1) over simplify the problem by ignoring modes of heat transfer, void effects, and/or free convection effects or 2) over complicate the problem by rigorously analyzing nearly all facets of canister heat transfer in the three-dimensional domain. The need exists for canister analyses that provide a balanced approach which captures the salient facets of canister heat transfer in a step-by-step fashion and analyzes them with a minimum amount of required rigor. With the aim of providing timely and accurate solutions useful for engineering purposes, this approach, described in Chapter II, is adopted for conducting canister analyses in the work presented herein.

In Chapter III, the governing equations for one-dimensional semi-infinite PCM, one-dimensional PCM slab canister, and two-dimensional (r,z) canister problem geometries are developed. Conservation of energy is formulated with enthalpy as the dependent variable which can in turn be related to temperature through a set of constitutive equations. Void heat transfer is formulated as uncoupled conduction and radiation processes. Void shape and location are prescribed while void size is determined based on conservation of mass. Liquid PCM free convection heat transfer effects are modeled through use of a thermal conductivity enhancement factor (i.e., the Nusselt number) based on existing empirical correlations.

Chapter IV contains a discussion of the finite-difference, simple explicit numerical solution approach selected to solve the conservation of energy equation. This approach was selected on the basis of simplicity and accuracy. Stability requirements and grid size selection analyses are also discussed along with a method employed to modify the computational domain to account for PCM expansion and contraction.

In Chapter V, numerical solution accuracy is compared with available exact solutions and good agreement exists. Furthermore, numerical consistency checks confirm that a high degree of computational integrity is present in the calculations. Initial analyses on one-dimensional canister models show that thermal performance is sensitive to the type of boundary conditions employed. In addition, the effects of void heat transfer and free convection on canister performance are shown to be substantial. Two-dimensional canister analyses show that the effects of a void and free convection are much less pronounced since a large portion heat transfer takes place via conduction in canister walls. Thus, the difference in canister performance during ground-based tests, in 1-g, and flight operation, in micro-g, are predicted to be only moderate.

In Chapter VI, major conclusions drawn from the one-dimensional analyses and two-dimensional analyses are listed. In addition, suggested areas for future work are discussed.

CHAPTER II

INTRODUCTION

Solidification heat transfer plays an important role in many engineering problems. Casting processes, ice accretion on vehicles, cryosurgical procedures, structural design in permafrost regions, and advanced residential and commercial cooling systems are but a few examples. Solid-to-liquid phase change materials (PCM's) have also been incorporated into the designs of many thermal control and thermal energy storage (TES) systems due to their inherent advantages of small operating temperature range and efficient, high specific energy storage capability. A review of the literature yields many references to theoretical and experimental work on such systems (see Blumenberg and Weingartner (1988), Tanaka et al. (1989), Torab (1989), and Sheffield (1981)). PCM TES systems are particularly well suited to solar thermal-electric power conversion systems. In this application, the ability to adapt the energy supply to the energy demand is essential since terrestrial systems must contend with transient cloud cover conditions and spacecraft-based systems must adapt to the intermittent solar energy supply provided in low earth orbits with substantial eclipse periods.

Perhaps the most notable spacecraft solar power system is the one currently under development for the NASA/International Space Station Freedom (SSF). SSF electrical power will be generated by photovoltaic solar arrays initially and later augmented with Solar Dynamic Power Modules (SDPM's). The SDPM, shown conceptually in Figure 2.1, employs a concentrator to collect and focus solar energy into a cylindrical cavity heat receiver where it is converted to thermal energy. A fraction of the thermal energy is transferred to a circulating working fluid to operate the power conversion unit (PCU) (a Brayton cycle heat engine) which generates electrical power. The remaining thermal energy melts a eutectic composition LiF-CaF_2 Phase Change Material (PCM) contained in multiple canisters brazed concentrically around working fluid tubes. The working fluid tubes run the length of the heat receiver cavity which is shown conceptually in Figure 2.2. A single PCM containment canister is shown in Figure 2.3. The PCM stores and releases thermal energy by undergoing phase change at its critical temperature of 1040 K. This permits continuous operation of the heat engine during the substantial eclipse periods (up to 36 minutes) of Freedom's low earth orbit. The design life requirement for the heat

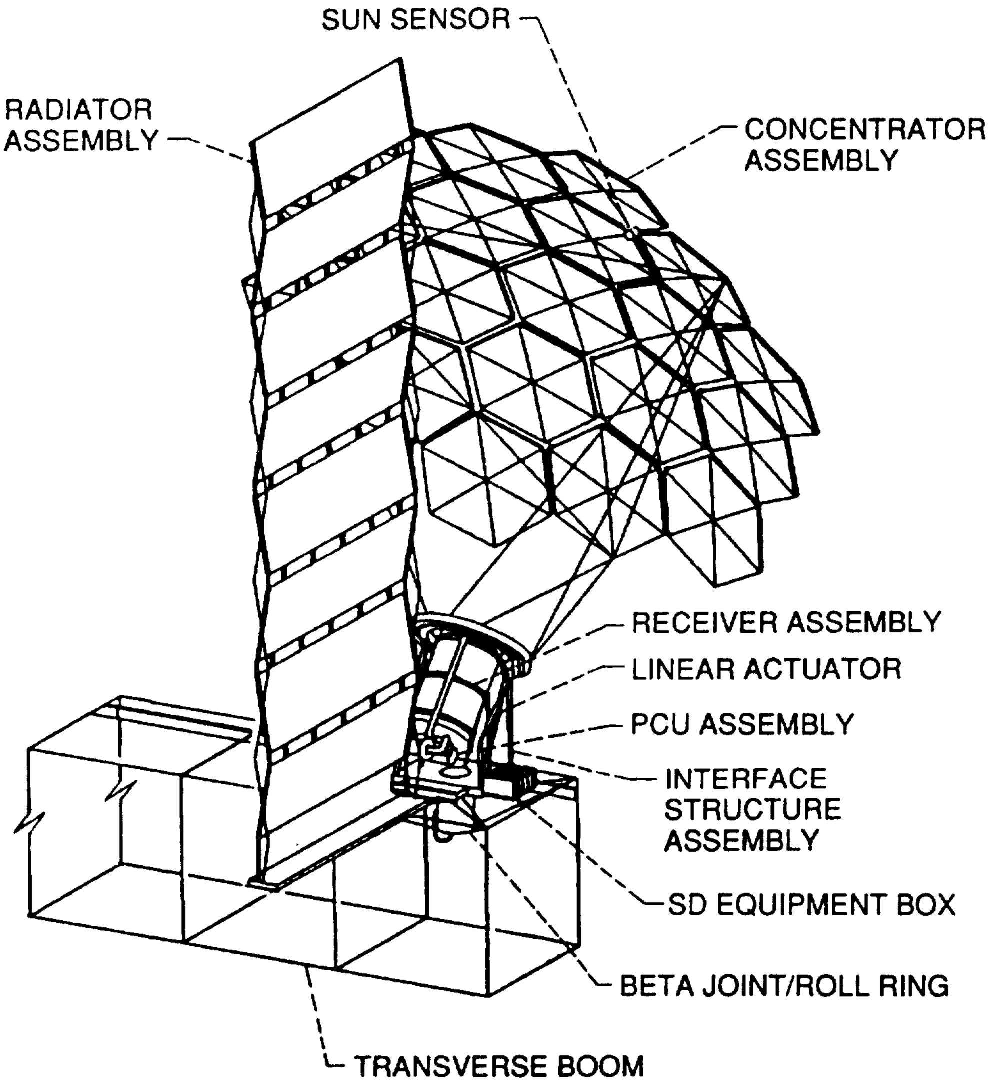

Figure 2.1. Solar Dynamic Power Module.

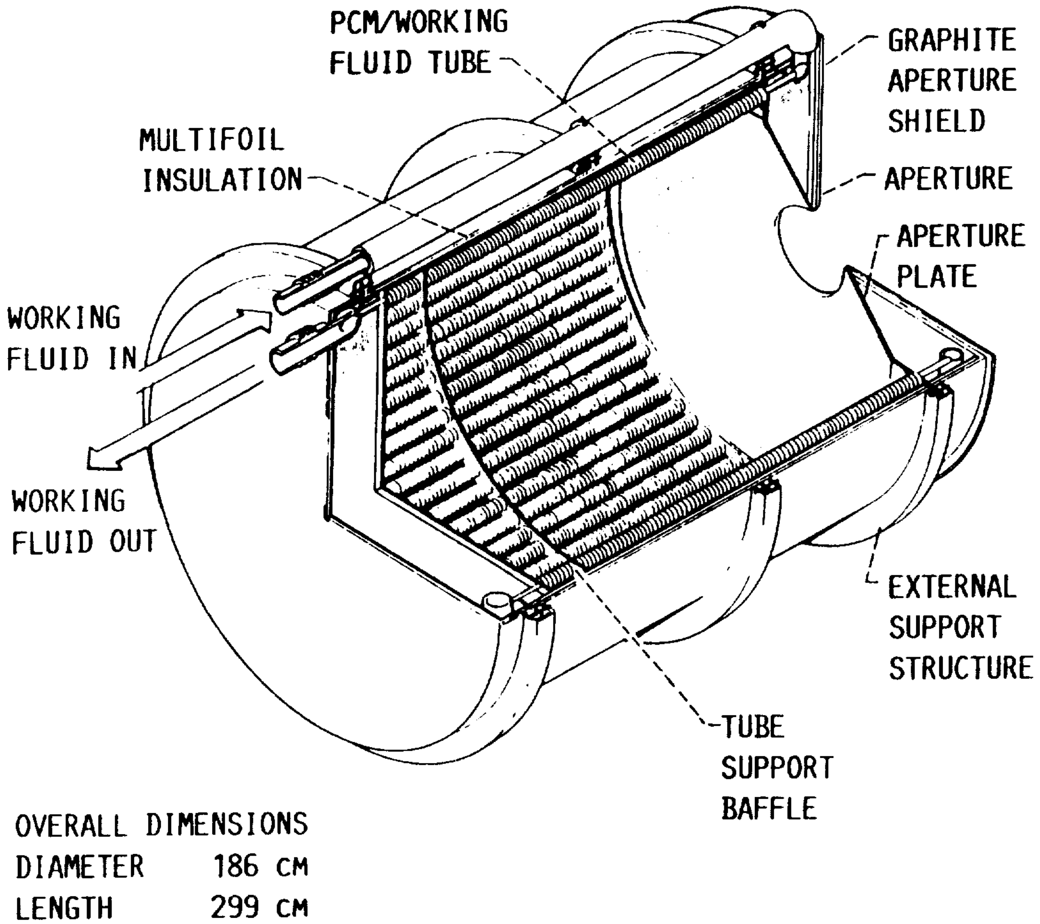

Figure 2.2. Heat Receiver.

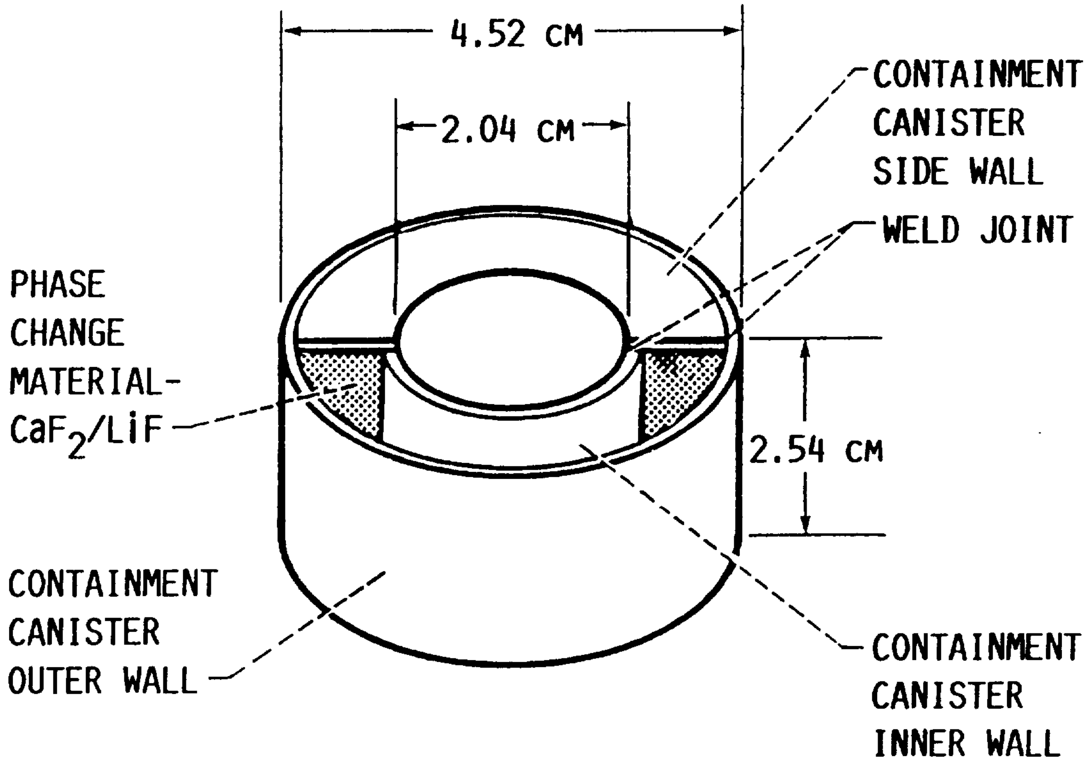

Figure 2.3. PCM Containment Canister.

receiver is 30 years.

A detailed understanding of containment canister heat transfer is important to ensure that an efficient heat receiver design (that meets all requirements) is developed. Three primary technical requirements driving the receiver design are: 1) supplying the required thermal power to the heat engine working fluid, 2) storing adequate thermal energy for use during the eclipse portion of Freedom's orbit, and 3) meeting a 30 year design life. The first two requirements can be addressed by relatively coarse receiver heat transfer analyses. However, the last requirement, a 30 year receiver design life, is probably driven by canister life. Therefore, detailed canister heat transfer analyses are required to accurately determine temperature histories for subsequent use in thermal-stress and material durability calculations. In addition, it is likely that analytical models, verified with ground-based experiments, will be required to predict on-orbit, flight performance due to the limited availability of funds to perform flight experiments.

To address the need for detailed TES canister analyses, a numerical heat transfer model was developed. This thesis documents the step-by-step development of this TES canister heat transfer model and discusses the numerical results from analyses conducted with this model.

2.1 Attributes of Canister Heat Transfer

2.1.1 Thermal Loading

During nominal TES charge-discharge operation, energy is added or removed from the canister outer peripheral surface via radiation exchange within the heat receiver cavity. The magnitude and sign of this energy exchange varies with time and circumferential canister position. Energy is removed from the canister inner peripheral surface via forced convection cooling by the heat engine working fluid, a 39.94 molecular weight helium-xenon gas mixture. The temperature of the gas varies with time. Canister sidewalls are thermally insulated and can be considered adiabatic.

2.1.2 Role of Conduction Within Canister Walls

For this TES concept, canister walls are required to contain the PCM and to act as effective heat transfer fins due to poor PCM thermal conductivity, 0.0382 and 0.0170 W/cm-K for the solid and liquid phases, respectively. Energy is distributed radially, axially, and circumferentially by conduction within the canister walls. This distribution of heat is required to efficiently heat the working fluid and melt the PCM in addition to controlling canister wall temperature gradients that give rise to thermal stresses.

2.1.3 Void Behavior

During the melting process, the PCM expands approximately 20% by volume. As a result, during the canister PCM fill process, ullage volume must be left in the canister to accommodate melting phase change expansion. This ullage volume, or void space, is filled with PCM vapor and as a function of time, grows and shrinks during PCM freezing and melting, respectively. The void shape and location within the canister is determined by a combination of surface-tension and buoyancy forces. During ground operation in 1-g, it is expected that buoyancy forces would dominate and the void would be located in the uppermost canister volume. However, it has been shown by post-test radiographs that voids associated with PCM solidification shrinkage can form on the canister bottom for certain cooling conditions, Tong et al. (1987). This situation resulted from the combination of high PCM wettability, canister geometry, and cooling conditions which permitted PCM on the bottom to freeze last.

The exact shape and location of the void in microgravity has not been quantified as of this writing. However, it is believed that the void shape will be essentially spherical (to minimize surface free energy) and will be located in the region containing the warmest liquid

PCM (liquid LiF-CaF_2 data indicate that surface tension decreases with increasing temperature which would result in a propulsive force to move a freely suspended void from cool liquid to hot liquid).

2.1.4 Void Heat Transfer

Across the void, energy is transferred by means of conduction, convection, radiation, and evaporation-condensation. Scoping calculations have shown that PCM vapor convection heat transfer is negligible, Whichner et al. (1987). Yet at typical canister operating temperatures (950 to 1150 K), conduction, radiation and evaporation-condensation heat transfer modes can be comparable in magnitude. Kerslake and Ibrahim (1990) showed in one-dimensional analyses that void vapor conduction and radiation heat transfer are of the same order-of-magnitude and are highly dependent on void size.

2.1.5 PCM Radiant Transmission Characteristics

There is evidence that suggests significant radiant heat transfer through the liquid PCM will likely take place. Data show that both solid LiF and CaF_2 PCM components have optical "windows" in the 0 to 6 micrometer wavelength range where highly polished and monocrystalline specimens exhibit ~95% transmittance at room temperature. For a black body at 1100 K, ~80% of the emissive power occurs at wavelengths in this 0 to 6 micrometer window. Thus, a good potential exists for substantial radiant interchange between interior canister walls. However, the "as-cast" PCM has polycrystalline structure and is visually opaque which suggests that the shorter wavelength portion of the window has been "closed". Hence, radiant transfer through liquid PCM regions is likely to be more important than in solid PCM regions.

2.1.6 Convection in the PCM Melt

Convection in the liquid PCM is driven by buoyancy forces, thermal-capillary forces, and by PCM phase change expansion/contraction at the solid-liquid interface. Under 1-g conditions, Whichner, et al. (1987) showed that free convective flow in a TES canister is dominant over surface tension and advective flows. Also predicted was the occurrence of peak wall temperatures located 45 to 90 degrees around the canister circumference from the location of peak heat input at the canister bottom. This occurrence was attributed to a vortex shedding mechanism within the liquid PCM region which created hot liquid vortices rising along the canister outer wall. This prediction was later qualitatively confirmed in experiments by Tong et al. (1988) where measured peak temperatures occurred at a location 45 degrees from the canister bottom for a portion of the melt-freeze cycle. In another study, Nusselt numbers (Nu) in the 4 to 5 range were predicted for a fully molten PCM containment canister during ground tests, Kerslake and Ibrahim (1990).

In micro-gravity, thermal-capillary flow is the dominant mode of convection. This type of flow arises due to surface tension variation along the PCM liquid-void interface as a result of temperature gradients. Whichner et al. (1987) showed that these flows have an order-of-magnitude lower velocity than buoyancy flows in 1-g and that the flow field is fairly localized around the void. Thus their contribution to overall canister heat in micro-gravity is expected to be small. In addition, phase change driven flows were predicted to be 7 orders-of-magnitude smaller than buoyancy flows in 1-g and thus, need not be considered in overall canister heat transfer.

2.2 Methods For Solving Phase Change Problems

There are several methods available for solving phase change problems which fall into the general classification of "moving boundary" or "Stefan" type problems. These methods of solution fall into basically four different categories: exact, approximate, strong numerical, and weak numerical. In short, exact solutions are available for only a limited number of inherently one-dimensional problems, as in Carslaw and Jaeger (1959), and for problems involving determination of multi-dimensional steady state solid-liquid interface geometry, as in Siegel (1982) and Siegel (1985). Approximate solutions, i.e. embedding methods, are limited to at most two-phase region, one-dimensional problems.

Strong numerical solutions, i.e. Douglas-Gallie method, explicitly solve for the solid-liquid interface position and are generally limited to two phase one-dimensional problems or with difficulty, single phase, two-dimensional problems. This is due to the problem formulation which requires simultaneous solution of the heat diffusion equation in the PCM solid and liquid regions and the PCM solid-liquid interface energy balance equation. The interfacial energy balance is formulated using temperature gradient and velocity terms which are normal to the PCM solid-liquid interface. Hence for multi-dimensional geometries, these terms must be evaluated via partial derivatives in the coordinate directions. This becomes a difficult task to accomplish when the PCM solid-liquid interface position and geometry are not known a priori. A second complication arises when the second derivatives of temperature in the heat diffusion equation must be evaluated near interfaces and boundaries where temperature gradients are discontinuous. The three-point finite-difference approximation to the second derivative relies on all three points being in the same medium. However, this is not the case in the vicinity of the PCM solid-liquid interface or near canister walls. Thus, the three-point scheme must be modified in these areas continuously throughout the computer simulation to accurately determine temperatures, Springer and Olson (1962).

Weak numerical solutions, such as augmented specific heat or the enthalpy methods, eliminate complications of strong numerical techniques since knowledge of the PCM solid-liquid interface is not required. In the augmented specific heat method, an artificially high PCM specific heat value is substituted for PCM regions within an arbitrary temperature range, ΔT, near the melting point. The augmented specific heat value is defined by the PCM heat of fusion, H_m, divided by ΔT. The artificially high sensible energy storage (or release) that occurs over the specified ΔT approximates heat of fusion energy storage (or release) during PCM phase transformation. However, it is not clear how to appropriately choose the value of ΔT. Selection of a small value risks jumping over part or all of the ΔT temperature range and hence, not properly accounting for all of the heat of fusion energy. Selection of a large ΔT value is not consistent with the physics of solid-liquid phase transformation of a eutectic composition mixture which occurs at one discrete temperature.

In contrast, the enthalpy method uses enthalpy or energy content as the dependent variable in the conservation of energy equation. Unlike temperature, enthalpy is a continuous function across the solid, mushy, and liquid PCM regions and thus, can be calculated throughout the entire

PCM domain without regard to the location and shape of solid-liquid interfaces. Once enthalpy distributions are determined, phase front location is contained implicitly in the solution. The solid phase exists where the specific enthalpy (energy per unit mass), e, is less than 0, liquid phase exists where $H_m<e$, and the approximate phase front position is located in the mushy zone that exists where $0\le e\le H_m$. Thus, the enthalpy formulation lends itself nicely to TES canister type phase-change problems where multi-dimensional geometries with periodic boundary conditions can produce multiple, complex geometry phase fronts whose locations are not known a priori.

The primary disadvantages of the enthalpy formulation are that the PCM solid-liquid interface(s) are not clearly defined and that the mushy zone model does not strictly apply to the phase change process of a eutectic composition mixture. The former introduces some uncertainty in temperature gradients in the PCM mushy zone where thermal conductivity can only be estimated. The latter introduces physics into the problem analysis which do not occur in the physical phase change process, i.e. an extended two-phase zone is assumed to exist instead of a sharp solid-liquid interface. However, both of these disadvantages can be minimized to acceptable levels for engineering calculations by refining the computational grid on which the calculations are performed.

The strong inherent advantages and benign disadvantages discussed above make the enthalpy method the simplest, most logical engineering approach for accurately simulating multi-phase, multi-dimensional phase change problems without prior knowledge of the geometry of the phase front(s). A more complete discussion of the various methods and solution techniques can be found in Solomon (1986).

2.3 Literature Review

The complex nature of canister heat transfer is apparent. It is a formidable task to accurately model all facets of the canister phase change heat transfer problem. Thus, usually a compromise is made between modeling complexity and accuracy of results. Generally, researchers have concluded that PCM convection, void effects, and three-dimensionality are key features to incorporate into TES canister phase change material models. Yet as of this writing, analytical results from a three-dimensional model that describes TES canister phase change heat transfer with PCM convection and void effects have not been published. Several computer models of varying sophistication have been developed (or are currently under development) to analyze this type of PCM Thermal Energy Storage (TES) canister. These analyses reported in the literature have modeled many aspects of the TES canister heat transfer problem.

The model described by Solomon (1986) is relatively straight forward in that it predicts temperature and phase distributions in the PCM based solely on conduction heat transfer. PCM container walls and PCM void formation (due to density difference in the PCM solid and liquid phases) are not modeled. This model is used to determine the feasibility and overall performance of a TES device comprised of PCM canisters.

Tong et al. (1988) modeled transient, three-dimensional conduction heat transfer using a finite-element technique and solved the problem using the commercially available general purpose thermal-structural analyzer program MARC. The phase change process was modeled using a modified specific heat capacity value over a small temperature range above the PCM melting point. However, liquid PCM convection and radiation across the PCM vapor void were not modeled. Consequently, analytical results generated could only be roughly correlated with ground-based test data. Using a similar approach, Strumpf and Coombs (1988) used the ANSYS general purpose thermal-structural analysis program to predict TES canister thermal-stress performance in micro-g. The short-fall of using general purpose computer programs is the inability to change or add software necessary to explore various PCM and void heat transfer modeling techniques.

Sedgwick et al. (1989) modeled the three-dimensional, transient heat transfer of a high length-to-diameter ratio annular TES canister containing PCM in a matrix of felt metal. The model used an implicit, finite difference approach with an iterative solution technique to solve the energy equation. The phase change process was modeled by employing an artificially high PCM specific heat value over a small temperature range above the PCM melting point to simulate the latent heat effects. Use of the felt metal more or less uniformly distributes PCM void volume and eliminates natural convection effects. Thus, the PCM can be analytically treated as a homogenous solid thermal conductor with effective material properties dependent on the amounts of solid PCM, liquid PCM, and felt metal.

Viterna (1989) modeled transient, two-dimensional PCM heat transfer including conduction and convection in the PCM. The continuity, momentum, and energy equations were simultaneously solved using a finite element technique with a Galerkin formulation (method of weighted residuals). The phase change process was analyzed using an enthalpy formulation of the PCM conservation of energy equation combined with a thermodynamic equation of state. Analytical predictions were verified using a variety of published results from the literature.

Wichner et al. (1988) modeled two-dimensional (r,θ), transient canister heat transfer including conduction, convection, radiation, and PCM evaporation-condensation. The continuity, momentum, and energy equations were simultaneously solved using a simple explicit, finite difference technique. The phase change process was modeled using the enthalpy method and a prescribed PCM vapor void behavior was included for both 1-g and micro-g environments.

Work has been continuing to extend the canister model to three dimensions and improve the void model. Wilson and Flanery (1988) describe the analytical formulation of the transient, three-dimensional PCM problem. However, no results have been published to date. Although such a model offers the potential for a very refined solution, its practical utility is diminished by large computer memory and execution time requirements as well as extensive computer code development/check-out requirements.

Several conclusions can be drawn from these references. First, convection and radiation modes of heat transfer are important and must be considered. Secondly, TES canister heat transfer is strongly three-dimensional due to asymmetric boundary conditions and orientation with respect to gravity (ground operation only). Thirdly, as more fidelity is built into the canister heat transfer model (fluid flow and three-dimensionality), the practical utility of the computer code rapidly decreases since computer storage requirements and execution times start to challenge computer system capabilities. In some cases, insufficient computer memory space has been the limiting factor in conducting three-dimensional analyses.

The need exists for a "design-oriented" computer model with moderate sophistication to analyze a PCM canister. Such a model would have moderate computer memory and run time requirements yet would be capable of multi-dimensional PCM canister analysis including simplified models of void behavior and liquid PCM convection. This type of model could serve as a canister design tool generating detailed temperature distributions for use in structural models and for validating less detailed heat receiver models. In addition, this model could address key questions about canister analyses such as: How should void heat transfer be modeled? What effect does the void have on canister heat transfer? What are the differences in canister heat transfer during ground tests (in the presence of free convection) and during flight operation under micro-gravity conditions? It seems logical that these questions should first be addressed by relatively simplified analyses which are likely to yield error-free answers in a timely manner. Then, if required, important phenomena identified can be modeled in greater detail to refine predictions.

2.4 Thesis Approach

In keeping with the "design-oriented" philosophy discussed above, the primary thrust of the work herein is to develop a PCM canister heat transfer computer code with low-to-moderate run time and sufficient accuracy to conduct design trade-off or optimization studies and the ability to answer the questions posed above. The approach to PCM canister code development incorporates an incremental build-up of code complexity. This allows the resulting analytical predictions to be interpreted without ambiguity by comparison with previously verified solutions.

Initially, one-dimensional models are analyzed. A semi-infinite PCM geometry is first analyzed primarily to check the accuracy of numerical methods against a limited group a exact solutions. Secondary objectives include exploring the effects of applied boundary conditions, void heat transfer models, and liquid PCM free convection on the solutions to classical Stefan problems.

A PCM slab canister is next analyzed to evaluate the heat transfer performance of an idealized TES canister with boundary conditions typical of heat receiver operation. Initially, void and free convection models are not incorporated into the analyses. Results from these analyses are compared with the previously verified results for the semi-infinite PCM geometry. Then the numerical model is modified to determine the impacts of a vapor void and liquid free convection on canister heat transfer performance.

Finally, a two-dimensional (2D(r,z)) PCM canister model is analyzed, first without considering void and free convection effects, and then later modified to include these effects. Results from these analyses are discussed in a comparative manner, highlighting significant differences in PCM containment canister temperature and phase distributions that arise from the presence of a void and/or free convection.

The transient, multi-dimensional PCM canister heat transfer is analyzed using the simple explicit, finite difference numerical method. Conduction, convection, and radiation modes of heat transfer are included. The PCM vapor void model includes a prescribed void shape and location. Void heat transfer occurs via uncoupled vapor thermal conduction and internal void surface radiation. To limit complexity and computational requirements, liquid PCM flow analysis is not performed. Instead, an effective liquid PCM thermal conductivity is calculated based on an existing Nusselt number correlation. The phase change process is numerically analyzed using a solution technique based on an "enthalpy" formulation of the conservation of energy equation.

Canister thermal performance for ground-based (in 1-g) and orbital flight (in micro-g) operating modes is predicted. Two primary differences in canister PCM behavior are anticipated as a consequence of these different operating modes: 1) the magnitude and direction of PCM liquid velocities and 2) the location and shape of the vapor void. During flight operation, it is assumed that only conduction heat transfer takes place in the solid and liquid PCM. During ground-based operation, it is assumed that conduction heat transfer takes place in the solid PCM and that conduction and free convection heat transfer take place in the liquid PCM. The void shape and location are assumed to be the same for ground-based and flight canister operating modes. In both operating modes, the void is conservatively located adjacent to the canister surface where heat input is applied.

CHAPTER III

PROBLEM FORMULATION

3.1 Problem Statement

The problem considered in this work is to analytically predict the transient temperatures, heat transfer rates, and PCM phase distributions in a TES canister comprised of a metallic shell containing a eutectic composition LiF-CaF_2 PCM. The temperatures of the TES canister gaseous cooling fluid are also predicted. Conduction heat transfer is analyzed in the container walls, solid PCM, and liquid PCM. Conduction and radiation (subject to diffuse, gray assumptions) heat transfer is analyzed in the void region. Void shape and position are specified while void growth or shrinkage obeys conservation of mass. Liquid PCM free convection is modeled using a modified liquid PCM conductivity in a conduction heat transfer analysis. The selected problem geometries are a one-dimensional, semi-infinite PCM, a one-dimensional PCM slab canister of infinite cross section, and a two-dimensional (r,z) annular canister. Constant material thermophysical properties are used.

Phenomena that are not analyzed include PCM vapor evaporation-condensation, liquid PCM circulation patterns arising from buoyancy or surface tension forces, dynamic void shape and position, PCM solid-liquid interface kinetics, liquid PCM supercooling, and radiant transmission through the PCM.

3.2 Governing Equations

3.2.1 PCM Canister Energy Balance

PCM and canister wall energy redistribution are formulated using "the enthalpy method" described by Whichner et al. (1988) and Solomon (1986). Based on conservation of energy, the governing equation is

$$\frac{\partial(\rho e)}{\partial t} = \mathrm{div}\,(k\nabla T) \quad . \tag{3.1}$$

In this equation, e is the specific enthalpy (i.e., given in Joules per gram), T is the temperature, ρ is the PCM or canister wall density, k is the PCM or canister wall thermal conductivity, and t is time. For a special case examined with the one-dimensional, semi-infinite geometry, the solid

PCM region is translated at a velocity, u, equal to the rate of void growth. Therefore, a transport term, $u \bullet \nabla(\rho e)$, must be added to the left hand side of equation (3.1) when evaluating the energy balance in the solid PCM.

When evaluating the discrete form of equation (3.1) in the vicinity of the PCM solid-liquid interface or near canister wall boundaries, special consideration must be given to the conduction heat transfer between adjacent finite-difference elements possessing different conductivities. This is accomplished by evaluating k in equation (3.1) as a "net conductivity", k_{net}, which is defined below for the example case of two different material slabs placed together in perfect thermal contact:

$$k_{net} = k_1 * k_2 * (s_1 + s_2) / (k_1 * s_2 + k_2 * s_1) \quad . \qquad (3.2)$$

The net conductivity is based on the individual material conductivities, k_1 and k_2, and conduction path lengths, s_1 and s_2. In equation (3.2), materials 1 and 2 could be any combination of solid, liquid, or mushy PCM or canister wall material.

As a simplifying assumption, internal PCM radiation terms were not included in the solid or liquid PCM energy balances. Data indicate that highly-polished and monocrystalline specimens of solid LiF and CaF_2 (and presumably liquid LiF-CaF_2) are semi-transparent to radiant energy with wavelengths less than 6 micrometers. Thus, a finite portion of energy is transmitted, absorbed, and re-emitted within the PCM.

3.2.2 Constitutive Relationships

Specific enthalpy is coupled to temperature through the following set of constitutive equations:

$$T = \begin{cases} T_m + e/c_S & : \quad e<0 \quad \text{Solid PCM} \\ T_m & : \quad 0 \le e \le H_m \quad \text{Mushy PCM} \\ T_m + (e-H_m)/c_L & : \quad H_m<e \quad \text{Liquid PCM} \\ T_m + e/c_W & : \quad -\infty<e<\infty \quad \text{Canister Walls} \; . \end{cases} \tag{3.3}$$

Here, T_m is the PCM melting temperature, H_m is the PCM heat of fusion, and c_S, c_L, and c_W are the specific heat values for the solid PCM, liquid PCM, and canister wall material, respectively.

3.2.3 Mushy Zone Properties

A so-called "mushy" zone exists when $0<e<H_m$. This zone usually consists of dendritic solid phase surrounded by liquid although the exact mushy zone characteristics are functions of material properties, temperature gradients, and interface kinetics, Flemings (1974) and Grodzka et al. (1968). Since extended mushy zones do not exist for eutectic mixtures undergoing phase change

(i.e., solidification interfaces remain planar or stable to within the distance of interlamellar spacing for low freezing rates typical of TES PCM's), the mushy zone model is only an approximation to the actual phase change process. However, this approach greatly simplifies the numerical solution technique and the option to shrink the finite-difference control volumes to an arbitrarily small size (within the limits imposed by computational requirements) is available. This, in turn, reduces the mushy zone size and hence, reduces the extent of approximation introduced.

For the purpose of this analysis, the density and thermal conductivity of control volumes in the mushy zone are treated as linear functions of the liquid PCM volume fraction, YF, and mass fraction, XF, such that

$$\rho = (1-YF)*\rho_S + YF*\rho_L \quad , \tag{3.4}$$

$$k = (1-XF)*k_S + XF*k_L \quad , \tag{3.5}$$

where XF and YF are defined as

$$XF = e/H_m \quad , \tag{3.6}$$

$$YF = [\ 1 + (\rho_L/\rho_S)*(1/XF - 1)\ ]^{-1} \quad . \tag{3.7}$$

In these equations, the subscripts S and L denote the PCM solid and liquid phases, respectively.

3.2.4 Void Models

3.2.4.1 One-Dimensional Analyses

For the one-dimensional PCM slab geometry (see Figure 3.1), the fraction of total canister volume occupied by the void, defined as the void volume fraction (VVF), varies between 0.0 percent, when the PCM is completely liquid, and 15.44 percent, when the PCM is totally solid. The same situation exists for the semi-infinite PCM geometry if an arbitrarily large control volume of PCM (or imaginary "container") is defined. The PCM growth and shrinkage associated with phase transformation is accommodated numerically by the combination of variable grid size and a variable PCM computational domain. This procedure, known as the "combined grid element technique," is described in section 4.4.

Void heat transfer is formulated as conduction, radiation, or conduction plus radiation processes. The void is assumed to be filled with LiF vapor with negligible thermal capacitance and at a pressure equal to the vapor pressure of LiF at 1040 K, i.e. $7\text{x}10^{-3}$ torr. These assumptions seem reasonable since the vapor pressure of CaF_2 at 1040 K, as reported by Borucka (1975), is ten orders-of-magnitude lower than that of LiF and the void vapor mass is very small (10^{-8} g). The void occupies the prescribed regions $0 \le x \le X_v(t)$ and $\delta_w \le x \le X_v(t)$ for the semi-

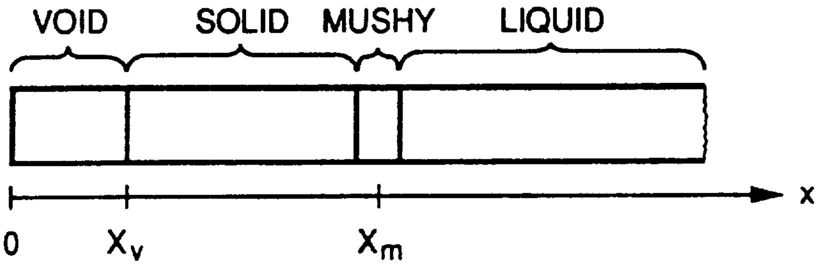

(a) Semi-infinite PCM.

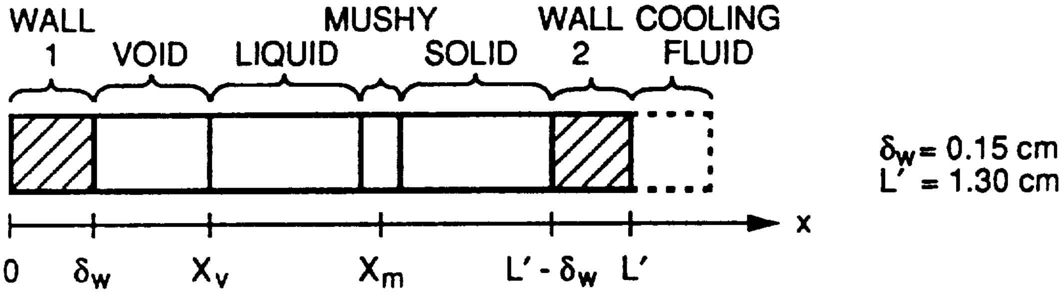

(b) PCM slab canister.

Figure 3.1. Schematic One-Dimensional Problem Geometries.

(a) Semi-infinite PCM
(b) PCM Slab Canister

infinite PCM and slab PCM geometries, respectively. Here $X_v(t)$ represents the time dependent location of the void-PCM interface and δ_w represents the thickness of the PCM containment canister wall.

The time dependent void heat flux, q_v, is given by

$$q_v(t) = R_v^{-1}*[\ T(0,t)-T(X_v(t),t)\ ] \quad , \qquad (3.8a)$$

for the semi-infinite PCM geometry and by

$$q_v(t) = R_v^{-1}*[\ T(\delta_w,t)-T(X_v(t),t)\ ] \quad , \qquad (3.8b)$$

for the PCM slab geometry where R_v is the void thermal resistance. The void thermal resistance is comprised of two components: one associated with heat conduction and one associated with radiation. The conduction component of thermal resistance is given by $X_v(t)/k_v$ and $[X_v(t)-\delta_w]/k_v$ for the semi-infinite and slab geometries, respectively, where the void thermal conductivity, k_v, is equal to the thermal conductivity of LiF vapor, k_{LiFVap}. Using the kinetic theory of gases as done by Wichner et al. (1988), the value of k_{LiFVap} is 4.7×10^{-4} W/cm-K at 1040 K.

The radiation component of void thermal resistance, assuming gray optical properties and that LiF vapor is a non-participating medium, is given in terms of a "radiation" conductivity, k_{rad}, by

$$X_v(t)/k_{rad} = \frac{[1/\epsilon_0 + 1/\epsilon_{PCM} - 1]*[T(0,t)-T(X_v(t),t)]}{\sigma*[T^4(0,t)-T^4(X_v(t),t)]} , \qquad (3.9a)$$

for the semi-infinite PCM geometry and by

$$[X_v(t)-\delta_w]/k_{rad} = \frac{[1/\epsilon_w+1/\epsilon_{PCM}-1]*[T(\delta_w,t)-T(X_v(t),t)]}{\sigma*[T^4(\delta_w,t)-T^4(X_v(t),t)]} , \qquad (3.9b)$$

for the slab PCM geometry where σ is the Stefan-Boltzmann constant, ϵ_{PCM} is the PCM emittance, and ϵ_0 and ϵ_w are the emittance values of the surface at x=0 and the containment wall at $x=\delta_w$, respectively.

Void heat transfer can be evaluated based on the individual conduction and radiation thermal resistance components alone or on the basis of an uncoupled, effective thermal resistance term incorporating both conduction and radiation. Since the void heat transfer components are uncoupled, superposition is possible. Using the rule of parallel resistances, the effective void thermal resistance from conduction and radiation, $R_{V\ EFF}$, is given by

$$R_{V\ EFF} = \left[\frac{k_{LiFVap}}{X_v(t)} + \frac{\sigma*[T^4(0,t)-T^4(X_v(t),t)]}{[1/\epsilon_0+1/\epsilon_{PCM}-1]*[T(0,t)-T(X_v(t),t)]}\right]^{-1} , \qquad (3.10a)$$

for the semi-infinite PCM geometry and by

$$R_{V\ EFF} = \left[k_{LiFVap}/[X_V(t)-\delta_W] \quad + \quad \frac{\sigma*[T^4(\delta_W,t)-T^4(X_V(t),t)]}{[1/\epsilon_W+1/\epsilon_{PCM}-1]*[T(\delta_W,t)-T(X_V(t),t)]} \right]^{-1}, \qquad (3.10b)$$

for the slab PCM geometry. Note that the conduction component of void thermal resistance is dependent on void size and independent of temperature while the converse is true for the radiation component. It is also worth noting that if the void boundaries of interest consist of PCM only, void heat transfer by evaporation/condensation can be significant. Scoping calculations by Wichner et al. (1988) show that under certain conditions, void heat transfer by radiation and vaporization in a LiF PCM are comparable in magnitude while heat transfer by conduction is an order-of-magnitude smaller.

3.2.4.2 Two-Dimensional Analyses

For two-dimensional canister analyses, the VVF varies between 8 percent, when all PCM is liquid at the melting point (T_m), to 22 percent, when all PCM is solid at T_m. This VVF range is the result of receiver fabrication requirements and PCM contraction during solidification. Unlike the idealized one-dimensional models with no additional VVF margin, a fraction of the two-dimensional canister model volume must consist of PCM vapor void at all times during the orbital cycle. The small volume changes associated with cyclic thermal expansion of the PCM and containment canister walls are ignored.

The void geometry selected is a cylindrical annulus which easily conforms to a cylindrical finite-difference element grid network. The void is placed adjacent to the canister outer wall, a location that generates conservatively high canister wall temperature distributions (see Figure 3.2). Void growth or shrinkage occur uniformly across the PCM-void interface defined as r_v. As PCM liquifies or freezes, r_v increases or decreases, respectively, about 0.1 cm which changes void volume. An attempt was made to accommodate PCM growth-shrinkage in the two-dimensional canister analyses by applying a modified version of the one-dimensional combined grid element technique. However, problems with PCM mass and energy balances were encountered. Non-uniform PCM-void interface growth-shrinkage approaches were considered, but numerical implementation of such approaches are considered beyond the scope of the current work. Therefore, as an engineering approximation, a constant 15 percent VVF is assumed.

Uncoupled void vapor conduction and radiation are considered in two-dimensional canister analyses. Since void vapor mass is negligible, the void vapor temperature distribution is determined by the steady state heat diffusion equation:

$$\frac{1}{r}\frac{\partial}{\partial r}\left(r\,\frac{\partial T}{\partial r}\right)+\frac{\partial}{\partial z}\left(\frac{\partial T}{\partial z}\right) = 0 \quad . \tag{3.11}$$

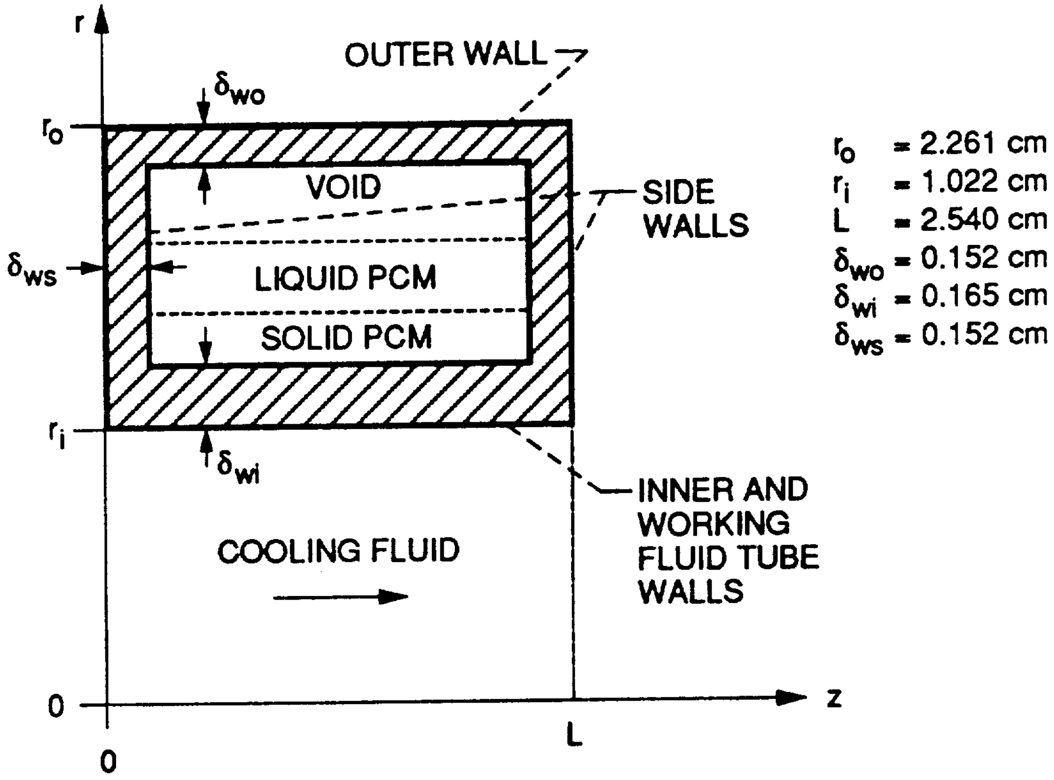

Figure 3.2. Schematic Two-Dimensional Problem Geometry.

Preliminary void conduction calculations show that axial temperature gradients are small and can be ignored for engineering calculations. This eliminates the second term in equation (3.11) and the resulting solution has the familiar logarithmic form

$$T(r) = A*\ln(r) + B \quad , \tag{3.12}$$

with the term $A=[T(r_o)-T(r_v)]/\ln(r_o/r_v)$ and the term $B=T(r_o)-\ln(r_o)[T(r_o)-T(r_v)]/\ln(r_o/r_v)$. Equation (3.12) is evaluated as a function of time at each axial void grid element to determine the void vapor temperature distributions.

Void radiation heat transfer is calculated based on the assumptions that, 1) all void surfaces are diffuse and gray, 2) PCM surfaces are opaque to all wavelengths of radiation, and 3) void vapor is a non-participating medium. With these assumptions, the governing equation set for void radiation heat transfer, found in Siegel and Howell (1981), is:

$$\sum_{j=1}^{NRS}\left[\frac{\Delta_{kj}}{\epsilon_j} - \left(\frac{1-\epsilon_j}{\epsilon_j}\right)F_{kj}\right]\frac{Q_j}{A_j} = \sum_{j=1}^{NRS} F_{kj}\sigma(T_k^4-T_j^4) \quad , \tag{3.13}$$

where k indexes from 1 to NRS. In equation (3.13), the subscripts k and j are void surface element numbers that take on all integer values between 1 and NRS. NRS is the total number of radiating surfaces in the void enclosure.

The term Δ_{kj} is the Kronecker delta equal to 1 for k=j and equal to 0 for k≠j. Given that each surface element temperature, T_j, emittance, ϵ_j, and element-to-element view factor, F_{kj}, are known, the surface element net radiative heat loss matrix, Q_j/A_j, can be determined. These heat loss terms are then added to the energy balance equation (equation 3.1) for the appropriate finite-difference grid elements in the canister outer wall, canister side walls, and outermost PCM.

An emittance value of 0.52 is selected for canister walls which are fabricated of Haynes alloy 188 (HA 188). This value is based on experimental measurements from diffuse (grit blasted) HA 188 test coupons for the temperature range 1000 K to 1100 K. An emittance value of 0.6 is selected for PCM surfaces. This value is an estimate based on emittance data for similar dielectric materials in the temperature range of interest.

Element-to-element view factors, F_{kj}, were determined using existing closed-form view factor solutions and considerable view factor algebra (see Rea (1975), Minning (1970), Leuenberger and Person (1956), and Sparrow et al. (1962)). View factors are recalculated for the various void sizes encountered during a simulated melt-freeze cycle. In the current work, however, view factors are calculated only once for the single void size assumed, i.e. the 15 percent VVF case.

3.2.3 Liquid PCM Free Convection Models

A rigorous treatment of liquid PCM free convection requires simultaneous solution of the three conservation equations: namely, conservation of mass, momentum, and energy. In light of the presence of solid-liquid phase change, void vapor regions, and multi-dimensional problem geometry, the numerical solution of the TES canister problem with PCM liquid circulation becomes extremely complex. Since wall temperature distributions (which determine heat transfer rates and thermal stresses) are of primary concern in TES canister analyses, it seems reasonable to approximate the gross behavior of liquid PCM circulation in terms of its overall contribution to heat transfer. To this end, a substantial simplification in the problem formulation and numerical solution is achieved when the conservation of mass and momentum equations are eliminated and a modified conservation of energy equation is used.

In the conservation of energy equation, the thermal conductivity term, k, is modified based on a simplified model of liquid PCM free convection. Free convection models are based on existing empirical heat transfer correlations in the literature. Enhanced heat transfer due to liquid PCM circulation is accounted for by modifying or enhancing the value of liquid PCM thermal conductivity, k_L, such that

$$k_{LE} = Nu*k_L \quad , \tag{3.14}$$

where k_{LE} is the enhanced PCM liquid conductivity and Nu is the Nusselt number. This approach was successfully used by Humphries (1974) to predict PCM melt zone height during ground testing of a finned thermal capacitor and by other researchers (see Szekeley and Chhabra (1970) and Chiesa and Guthrie (1974)) to study phase change processes in metals and alloy systems.

There are three concerns to consider with this approach: 1) exact temperature distributions in the liquid PCM are not predicted, 2) empirical Nu correlations for the exact, time-varying liquid region geometries and boundary conditions do not exist, and 3) existing empirical Nu correlations were generated without the presence of phase change. The first concern is not critical for these analyses since canister wall temperatures are primarily controlled by overall heat transfer rates and the solid-liquid interface position and not local liquid temperature gradients. The second concern also does not appear to introduce major difficulties into the analysis. This is based on numerical evaluation of several existing correlations shown in Table I which indicate that calculated Nu numbers are not extremely sensitive to geometry or type of boundary condition. For values representative of a canister with fully liquified PCM, i.e. $Ra=2.7*10^5$ and Prandtl number, $Pr=2.4$, the variation in calculated Nu number is only ±13 percent for a variety of geometries and boundary conditions.

Table I. Various Nu Correlations with Ra=2.7×10^5 and Pr=2.4

Geometry	Boundary Condition	Correlation	Nu	Restrictions	Reference
Horizontal Cylindrical Annulus	Isothermal	$0.386\left[\frac{Pr*Ra}{0.861+Pr}\right]^{0.25}\frac{d^{-3/4}*\ln(D_o/D_i)}{(D_i^{-3/5}+D_o^{-3/5})^{5/4}}$	4.92	$2\times10^2<Ra<2\times10^7$	Raithby and Hollands (1975)
Spherical Annulus	Isothermal	$0.74\left[\frac{Pr*Ra}{0.861+Pr}\right]^{0.25}\frac{d^{1/4}/(D_i*D_o)}{(D_i^{-7/5}+D_o^{-7/5})^{5/4}}$	4.38	$4\times10^2<Ra<4\times10^4$	Raithby and Hollands (1975)
Horizontal Layer	Isothermal	$1+1.44\left[1-\frac{1708}{Ra}\right]^{+}+\left[\left(\frac{Ra}{5830}\right)^{1/3}-1\right]^{+}$	5.02	High H/d, $Pr\simeq0.7$ $[\ ]^{+}<0 \Rightarrow =0$	Hollands et al.(1976)
	Isothermal	$0.13*Ra^{0.3}$	5.53	$3.7\times10^4<Ra<10^8$	Özisik (1985)
Vertical Layer	Isothermal	$0.242\left(\frac{Ra*d}{LH}\right)^{0.272}$	4.85	$5<LH/d<110$ $10^2<Ra<2\times10^7$ $Pr\simeq0.7$	El-Sherbiny et al.(1982)
	Isothermal or Isoflux	$0.42*Pr^{0.012}*Ra^{1/4}*(LH/d)^{-0.3}$	4.84	$10^4<Ra<10^7$ $10<LH/d<40$	Özisik (1985)

The third concern has been addressed in experimental studies and again, does not appear to present a problem for this approach. Kemink and Sparrow (1981) found that standard free convection correlations could be accurately applied to the problem of PCM melting in open or closed containers. In addition, Sparrow et al. (1978) found that calculated film coefficients during melting experiments were within 12 percent of those calculated for free convection experiments with the liquid phase alone. These experiments were conducted with the same materials and test apparatus so that a direct, quantitative comparison could be made.

Therefore, the simplest Nu number correlations, for horizontal and vertical layers from Özisik (1985), are selected for one- and two-dimensional canister analysis. Since the assumption of axisymmetry in two-dimensional analyses requires the gravity vector to be parallel with the canister axis of symmetry, only the vertical layer correlation is used. This restricts the simulated canister ground-test orientation to one with the axis of symmetry vertical.

For the semi-infinite PCM geometry, the Nu number correlation from Table I for a horizontal layer heated isothermally from the bottom is used, Özisik (1985) . The correlation has the form

$$Nu = C5*Ra^{n3} \quad , \tag{3.15}$$

which is valid for the Prandtl number range $1 < Pr < 20$. Values for C5 and n3 are given in Table II. Here the Rayleigh number, Ra, is defined by

$$Ra = \frac{g*\beta*[T(0,t)-T_m]*X_m^3(t)}{\alpha*\nu} \quad , \tag{3.16}$$

where g is gravitational acceleration, $X_m(t)$ is the PCM liquid zone height equal to the characteristic length, and α, β, ν, and T_m are the PCM thermal diffusivity, volumetric thermal expansion coefficient, kinematic viscosity, and melting temperature, respectively.

The Nu number correlation used for the one-dimensional PCM slab and two-dimensional annulus canister geometries, also from Özisik (1985) in Table I, is valid for a vertical layer with isothermal or isoflux heating from one side. It is given as

$$Nu = C5*Ra^{n3}*(LH/w)^{-0.3} \quad , \tag{3.17}$$

with the restrictions of $1 < Pr < 20,000$ and vertical layer height to width ratio, LH/w, $10 < LH/w < 40$. Values of the constants are given in Table II. The Ra number in equation (3.17) is given as

$$Ra = \frac{g*\beta*[T(X_v(t),t)-T_m]*(X_m(t)-X_v(t))^3}{\alpha*\nu} \quad , \tag{3.18}$$

Table II. Selected Nusselt Number Correlations For Liquid PCM Free Convection

Geometry	Correlation	c5	n3	LH/w	Ra range
Horizontal layer (semi-infinite PCM)	Nu = $c5*Ra^{n3}$	1	0	--	<1700
		0.012	0.6	--	1.7×10^3 - 6×10^3
		0.375	0.2	--	6×10^3 - 3.7×10^4
		0.13	0.3	--	3.7×10^4 - 10^8
		0.057	1/3	--	$>10^8$
Vertical layer (PCM slab)	Nu = $c5*Ra^{n3}*(LH/w)^{-0.3}$	0.42 $Pr^{0.012}$	1/4	40	10^4 - 10^7

for PCM slab canister analyses. Here, the characteristic length is the liquid PCM layer thickness which can be obtained from the difference between the PCM solid-liquid interface and the PCM-void interface, $X_m(t)-X_v(t)$. For the two-dimensional canister analyses, the Ra number is given as

$$Ra = \frac{g*\beta*[T(r_v,z,t)-T_m]*[r_v-r_m(z,t)]^3}{\alpha*\nu} \quad , \tag{3.19}$$

where the characteristic length, $r_v-r_m(z,t)$, is the radial liquid PCM layer thickness which is a function of axial position, z. The axial dependence of the Ra number is removed by substituting integrated average values for the PCM-void interface temperature, $T(r_v,z,t)$, and the PCM solid-liquid interface position, $r_m(z,t)$.

3.2.6 Canister Cooling Fluid Heat Transfer

A constant film coefficient, h, is determined based on a Nu number correlation discussed by Taylor et al. (1988) which is valid for fully developed turbulent flow in circular tubes with a low Pr number fluid. The canister cooling fluid (or heat engine working fluid), a 39.94 molecular weight helium-xenon (He/Xe) mixture, has a Pr of 0.24. The correlation has the form

$$Nu = 0.022*Re^{0.8}*Pr^{0.6} \quad , \tag{3.20}$$

where Re is the Reynolds number. The film coefficient can then be evaluated by

$$h = Nu*k_f/D \quad , \tag{3.21}$$

where k_f is the cooling fluid conductivity and D is the cooling fluid tube inner diameter.

The cooling fluid mean temperature profile, $T_f(z,t)$, is determined by a quasi-steady state analysis. This approach eliminates extremely small time steps required for transient numerical temperature solutions of the cooling fluid which has negligible thermal inertia. $T_f(z,t)$ is evaluated as a function of time such that

$$\int_0^L \{U*\pi*D*[T_w(z,t)-T_f(z,t)]\}dz = \dot{m}*c_f*[T_f(L,t)-T_f(0,t)], \tag{3.22}$$

where $T_w(z,t)$ is the canister inner wall-cooling fluid tube central temperature, $\dot{m}$ and c_f are the cooling fluid mass flow rate and specific heat, respectively, and U is the overall heat transfer coefficient given by

$$U = [\ 1/h + D*\ln(1+\delta_i/D)/(2*k_w)\ ]^{-1} . \tag{3.23}$$

In this equation, δ_i is the cooling fluid tube plus canister inner wall combined thickness and k_w is the tube/canister thermal conductivity.

3.3 Boundary and Initial Conditions

The boundary and initial conditions for the semi-infinite PCM, slab PCM canister, and the two-dimensional (r,z) PCM canister problems are contained in Table III. Exact solutions for the Stefan problem are available in Solomon (1979) and Solomon (1981) for semi-infinite PCM geometries initially at uniform temperature with an imposed constant temperature at one face, i.e. problem numbers 1 and 2 in Table III. A specialized exact solution to the Stefan problem with void formation is given in Solomon et al. (1986).

For the semi-infinite PCM problems 1 and 2 in Table III, the Stefan number (St), defined by $c*\Delta T/H_m$, is selected to be 0.10. Here ΔT is the absolute value of the difference between initial PCM temperature and the imposed temperature at x=0. This small Stefan number value is representative of phase change processes in TES canisters. For problem 3, the value of q is chosen such that the same amount of PCM energy change occurs as with the constant temperature boundary condition phase change process.

For the PCM slab geometry, problem 4, values typical of a LiF-CaF_2 filled TES canister are selected for the length, L', initial temperature, T_S, heat flux input, q(t), film coefficient, h, and cooling fluid temperature, T_f. Values selected also permitted full PCM melting and freezing during

Table III. Boundary And Initial Conditions

Problem number	Geometry	Initial condition	Initial PCM phase	Boundary conditions	Exact solution available?
1	Semi-infinite PCM	$T(x,0) = T_m$	Liquid	$T(0,t) = T_W < T_m$ $T(\infty,t) = T_m$	Yes
2	Semi-infinite PCM	$T(x,0) = T_S < T_m$	Solid	$T(0,t) = T_L > T_m$ $T(\infty,t) = T_S$	Yes
3	Semi-infinite PCM	$T(x,0) = T_m$	Liquid	$-k\partial/\partial x[T(0,t)] = q < 0$ $T(\infty,t) = T_m$	No
4	PCM slab	$T(x,0) = T_S < T_m$	Solid	$-k\partial/\partial x[T(0,t)] = q(t)$ $-k\partial/\partial x[T(L',t)] = h[T(L',t) - T_f]$ $h,\ T_f$ = constants	No
5	2D(r,z)	$T(r,z,0) = T_S < T_m$	Solid	$k\partial/\partial r[T(r_o,z,t)] = q(t)$ $k\partial/\partial r[T(r_i,z,t)] = h[T(r_i,z,t) - T_f(z,t)]$ $\partial/\partial z[T(r,0,t)] = \partial/\partial z[T(r,L,t)] = 0$	No

the canister simulated charge-discharge cycle.

Boundary condition values for the two-dimensional canister geometry, problem 5, are based on results obtained from the heat receiver analysis computer code described by Strumpf and Coombs (1988). Figure 3.3 shows the absorbed heat input function, q(t), applied to the canister outer surface at $r=r_0$ and the cooling fluid inlet temperature function, $T_f(0,t)$, for a canister located about 115 cm behind the conceptual heat receiver aperture plane (see Figure 2.2). During a simulated 91 minute Space Station Freedom orbit, canisters in this region of the receiver experience maximum heat input and undergo complete PCM melting and freezing. Note that q(t) is negative for about the first half of the eclipse period when the hottest canisters lose heat to the remaining canisters in the receiver cavity which are at a cooler average temperature. For the second half of the eclipse period, however, relatively cold heat engine working fluid from the receiver inlet manifold preferentially cools what were the hottest canisters at the beginning of eclipse to a temperature below that of the remaining canisters in the receiver cavity. Therefore, q(t) is positive during this period. It will be shown later that the period of canister outer wall heat loss for the first half of eclipse significantly affects PCM freezing patterns and canister temperature distributions.

Variations in the inlet cooling fluid temperature, $T_f(0,t)$, are the result of variations in the average

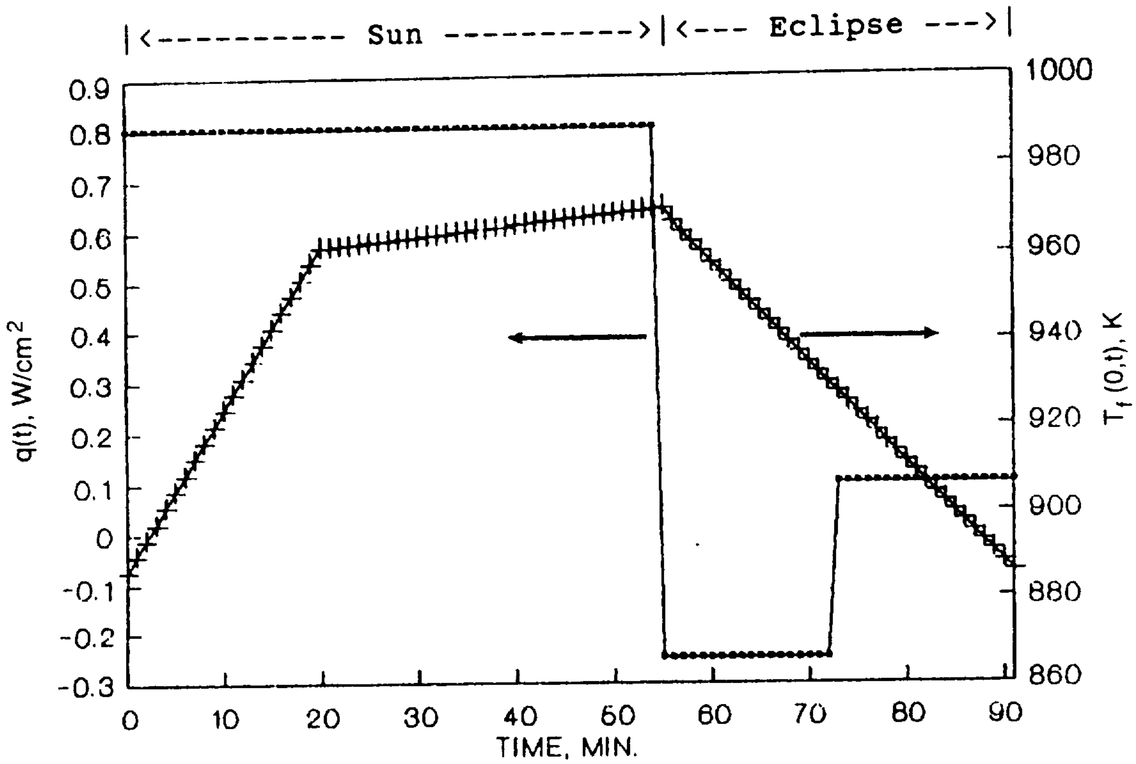

Figure 3.3. Boundary Conditions For Two-Dimensional Analyses.

receiver cavity temperature. It will be shown later that interesting local fluid heat transfer rates occur as the result of different temperature transients between the canister, driven by local absorbed heat fluxes and local PCM quality, and the cooling fluid, driven by the average receiver temperature and PCM quality.

Canister side wall boundaries at z=0 and at z=L are treated as adiabatic. This assumption is justified by the fact that adjacent canisters on a given working fluid tube experience nearly the same heating and cooling boundary conditions and thus, operate at nearly identical temperatures. Furthermore, the canisters are physically separated by ceramic paper spacers during tube assembly which minimizes any axial heat transfer that could occur due to small side wall temperature differences in adjacent canisters.

3.4 Thermophysical Properties

For the purpose of this analysis, constant material properties are assumed. These properties are given in Table IV. Note that the LiF-CaF$_2$ PCM and Haynes alloy 188 (HA 188) containment canister material properties are evaluated at 1040 K while the He/Xe working fluid properties are evaluated at 900 K. During cyclic canister operation, temperatures generally remain within a range ±100 K from the PCM melting point. Over this limited temperature range, HA

Table IV. Material Properties

Property	80.5 LiF-19.5 CaF_2 at 1040 K		Haynes alloy 188 at 1040 K	39.94 mol wt He/Xe at 900 K
	Solid	Liquid		
ρ, g/cm3	2.59	2.19	8.813	1.862×10^{-3}
c, J/g-K	1.77	1.77	0.548	0.5202
k, w/cm-K	0.038	0.017	0.246	1.333×10^{-3}
T_m, K	1040		1575 - 1630	----------
H_m, J/g	816		-----------	----------
ν, cm^2/sec	-----	0.0105	-----------	----------
β, 1/K	-----	2.87×10^{-4}	-----------	----------
μ, g/cm-sec	-----	0.023	-----------	5.982×10^{-4}
Pr	-----	2.4	-----------	0.24
ε	0.6	0.6	0.52	----------

188 thermophysical properties vary by less than 5 percent while PCM properties generally vary by less than 15 percent. The only deviation from "flat" property temperature dependence occurs for the liquid PCM density which decreases by 31 percent over the temperature range from 1040 K to 1140 K. However, temperature-dependent properties can readily be incorporated into future analyses if deemed necessary.

CHAPTER IV

NUMERICAL APPROACH

4.1 Solution Algorithm

The simple explicit numerical method is implemented to solve equation 3.1. This method is selected primarily because of the ease in numerical equation development and programming. In addition, Thibault (1985) ranked the simple explicit method third best numerical scheme to solve the three-dimensional heat diffusion equation in a parallelepiped. In this study, nine different numerical methods, including explicit, fully implicit, alternating-direction-implicit (ADI), and Crank-Nicolson methods, are compared on the basis of accuracy, ease of programming, computation time and computer storage requirements. Ranking first and second best are two similar ADI methods which make use of the efficient Thomas algorithm to solve the tridiagonal system of equations successively in each coordinate direction.

4.2 Stability Requirements

Based on the local maximum principle discussed by Solomon et al. (1986), the simple explicit scheme is stable as long as the time step, Δt, is chosen such that

$$\Delta t < \Delta x^2/(2*\alpha) \quad , \tag{4.1}$$

for central PCM grid elements in the one-dimensional PCM canister analyses. For two-dimensional canister analyses, stability is ensured as long as

$$\Delta t < \frac{\Delta r^2/(2*\alpha_w)}{\psi+\Delta r^2*k_s/(k_s*\delta_{ws}{}^2+k_w*\delta_{ws}*\Delta z)} \tag{4.2}$$

for canister sidewall grid elements. In equation (4.1), Δx is the grid size and α is the PCM thermal diffusivity of the solid or liquid phase. This dictates that Δt values less than 0.0375 seconds and 0.0199 seconds must be selected to ensure stability for one-dimensional cases with and without the presence of free convection, respectively. In equation (4.2), Δr and Δz are the radial and axial grid spacings and k_w, δ_{ws}, and α_w are the canister side wall element thermal conductivity, thickness, and thermal diffusivity. The term ψ is given by

$$\psi = \frac{\Delta r}{2*r_i}\left[\frac{1}{\ln(r_{i+1}/r_i)} + \frac{1}{\ln(r_i/r_{i-1})}\right] \tag{4.3}$$

where r_i is the radial coordinate of canister sidewall grid element i. This dictates that a Δt value less than 0.0254 seconds must be selected to ensure stability.

The exact Δt value used as input to the two-dimensional canister computer program is 0.0234375 or 3/128 seconds. This value is essentially the largest number that is less than 0.0254 seconds and belongs to the family of fractions defined by

$$\Delta t = (i1)/2^{(i2)} \quad , \qquad (4.4)$$

where i1 and i2 are natural numbers. Fractions in this family have the unique ability to be converted from decimal to hexadecimal format and vice versa without computer round-off error. This measure helps to reduce cumulative numerical errors in equations containing Δt, such as energy balances, which can become significant after a large number of repeated calculations (over 230,000 time steps are used for one TES charge-discharge cycle).

4.3 Grid Selection

Grid independence tests were performed using the PCM slab canister model to determine the appropriate grid size for good solution accuracy and resolution. The numerical tests were conducted by selecting a fixed time step and evaluating several temperature solutions for increasingly smaller grid spacings. Based on these tests, ~40 grids per cm of PCM were used in one-dimensional analyses where computation times are small. For two-dimensional analyses, ~20 grids per cm of PCM in the radial direction (the primary heat transfer direction) and ~5 grids per cm of PCM in the axial direction (the secondary heat transfer direction) were selected. The larger, two-dimensional grid size essentially maintains the solution accuracy of the smaller one-dimensional grid but decreases solution resolution in order to limit computational time.

The two-dimensional finite-difference element model is shown in Figure 4.1. For this model, the nominal PCM radial and axial grid spacings are 0.05115 cm and 0.27940 cm, respectively. Note, however, that the radial grid spacing is non-uniform. For analyses with the void model, the size of two radial grid spacings is adjusted so that adjacent void and PCM element boundaries are coincident with the PCM-void interface. The location of the PCM-void interface is a function of the total PCM mass and the relative percentages of solid and liquid PCM that exist at any given time.

4.4 Combined Grid Element Technique

Because of the time-varying void size in the one-dimensional PCM slab analyses, the PCM computational domain, $X_v(t) \le x \le L' - \delta_w$, must be continually up-dated throughout the

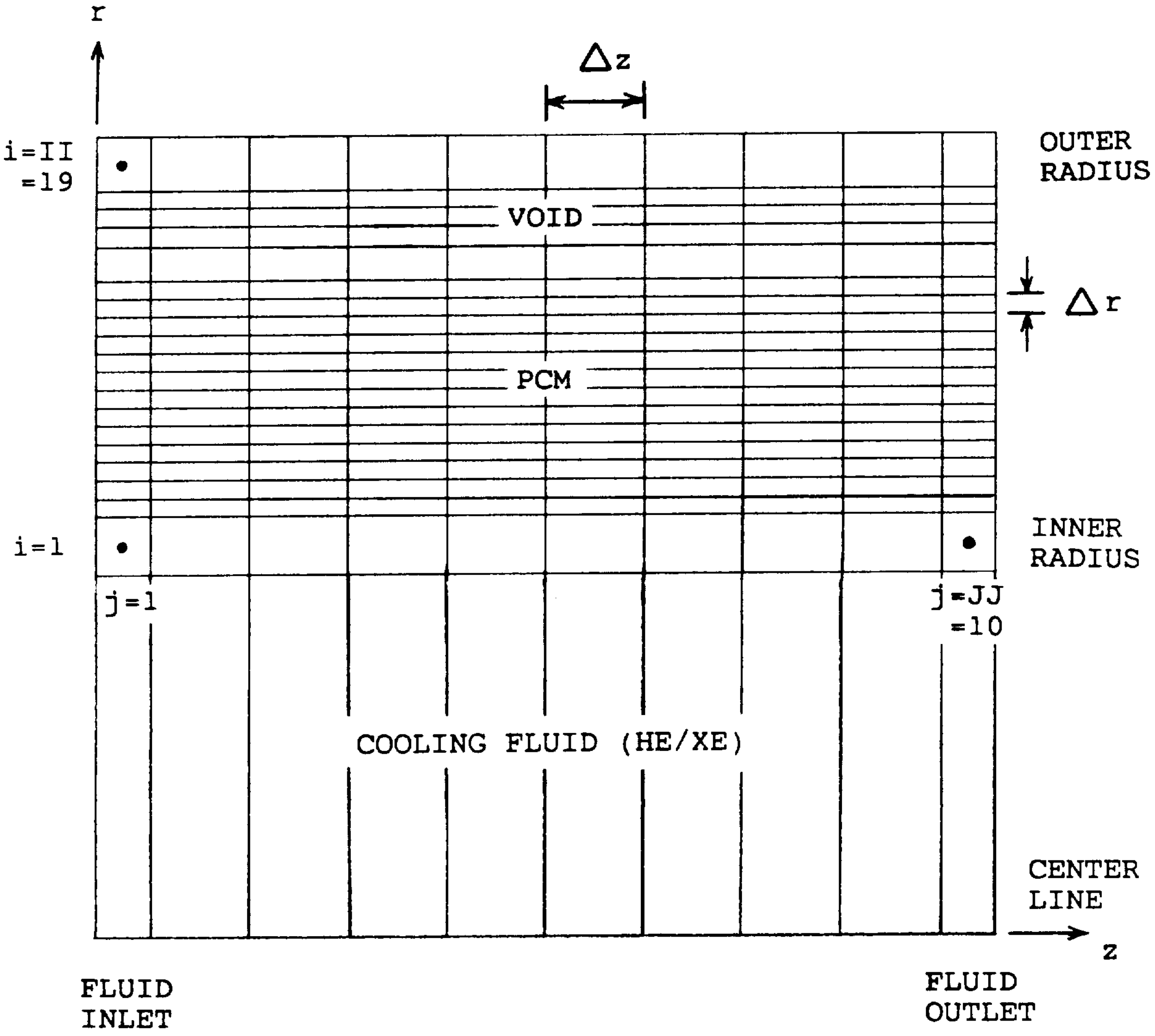

Figure 4.1. Two-Dimensional Finite-Difference Element Model.

simulation to prevent computations from being made in the void region. This preventative measure is taken because void elements are considered to be massless which forces numerical computations to quickly go unstable and terminate computer program execution. Up-dating the PCM computational domain is accomplished by calculating the position of $X_v(t)$ based on conservation of PCM mass and by implementing a "combined grid element" technique. This technique simply combines the element that contains the void-PCM interface, iv, with the adjacent PCM element, iv+1, to form one larger element, iv', of width Δx_v given by

$$\Delta x_v = \Delta x*(1+MF_v) \quad , \tag{4.5}$$

where MF_v is the mass fraction PCM contained in element iv at any given time. Since $\Delta x_v > \Delta x$, this grid space adjustment does not affect numerical stability. As the void front translates during the simulation, the value iv will "jump" at discrete instances of time. Once a jump condition has been detected, properties of element iv' are updated for the future time step based on the average properties of the new elements iv and iv+1 from the current time step.

4.5 Computer Resource Requirements

Computer programs are coded in FORTRAN 77 and executed on an AMDAHL 5860 computer using double precision variables. Single precision runs were also made to compare run time requirements and accuracy. Table V shows the normalized computer execution time requirements for running each canister analysis program. Single precision runs reduce central processor unit (CPU) time requirements by factors of 1.1 and 1.6 for the one and two-dimensional models, respectively. Generally, single and double precision calculations are in agreement to within 1 percent for temperature predictions and to within 2 to 3 percent for melt front predictions. Addition of the void model to the two-dimensional canister computer program increases CPU time by 25 percent while addition of the free convection model has essentially no impact on required CPU time. See Appendix A2 for a discussion of the two-dimensional canister analysis computer program NUCAM2DV (Numerical Canister Model: Two-Dimensional With Void).

Table V. Normalized Computer Program Execution Times In CPU Seconds/Simulation Seconds

	One-Dimensional Programs		Two-Dimensional Programs	
	Free Convection Off	Free Convection On	Without Void	With Void
	$\Delta x=0.025$ cm $\Delta t=0.025$ sec	$\Delta x=0.025$ cm $\Delta t=0.010$ sec	$\Delta r=0.05115$ cm $\Delta z=0.27940$ cm $\Delta t=0.025$ sec	$\Delta r=0.05115$ cm $\Delta z=0.27940$ cm $\Delta t=0.025$ sec
Single Precision	0.02433	0.06166	0.37729	*****
Double Precision	0.02666	0.07000	0.63736	0.79308

CHAPTER V

RESULTS AND DISCUSSION

5.1 Numerical Solution Accuracy

Numerical solutions were obtained to the one-dimensional, temperature controlled freezing and melting problems, problems 1 and 2 in Table III, respectively, in which exact solutions also existed. Exact and numerical temperature and phase front solutions were then compared to assess the accuracy of the numerical computations. That comparison is shown in Table VI. Numerical melt front solutions are within 0.6 percent of the exact solutions without voids and within 1.8 percent of the exact solution with void. Numerical temperature solutions are within 0.5 K of the exact solutions for all problems. These results indicate that the numerical scheme is accurate and properly implemented.

To assure proper implementation of the numerical equations, the two-dimensional canister computer program

Table VI. Numerical Versus Exact Solutions For Problems 1 And 2

(a) Melt and void front solutions

Time, min	$X_m(t)$, cm						$X_v(t)$, cm	
	Problem 1		Problem 1 with void		Problem 2		Problem 1 with void	
	Numerical	Exact	Numerical	Exact	Numerical	Exact	Numerical	Exact
0.0	0.00000	0.00000	0.00000	0.00000	0.00000	0.00000	0.00000	0.00000
10.0	1.06220	1.07000	0.29491	0.29660	0.44390	0.44430	0.04555	0.04581
20.0	1.50470	1.51320	0.41681	0.41950	0.62587	0.62830	0.06437	0.06479
30.0	1.84420	1.85330	0.50933	0.51380	0.76559	0.76950	0.07866	0.07935
40.0	2.12950	2.14000	0.58637	0.59330	0.88337	0.88860	0.09056	0.09163
50.0	2.37940	2.39260	0.65123	0.66330	0.98732	0.99340	0.10058	0.10244

(b) Temperature solutions

T(x, t = 45 min)/phase											
Problem 1				Problem 1 with void				Problem 2			
x, cm	Numerical	Phase	Exact	x, cm	Numerical	Phase	Exact	x, cm	Numerical	Phase	Exact
0.0000	994.0	SOL	994.0	0.0000	994.0	VOID	994.0	0.0000	1063.0	LIQ	1063.0
0.1125	996.3	SOL	996.2	0.0525	******	VOID	******	0.1125	1060.2	LIQ	1060.2
0.3125	1000.5	SOL	1000.3	0.1104	1037.2	SOL	******	0.2125	1057.7	LIQ	1057.8
0.5125	1004.6	SOL	1004.5	0.1125	******	SOL	1036.6	0.3125	1055.3	LIQ	1055.3
0.7125	1008.7	SOL	1008.6	0.1625	1037.5	SOL	1037.5	0.4125	1052.8	LIQ	1052.9
0.9125	1012.8	SOL	1012.7	0.2125	1037.8	SOL	1037.7	0.5125	1050.3	LIQ	1050.4
1.1125	1016.9	SOL	1016.8	0.2625	1038.0	SOL	1038.0	0.6125	1047.9	LIQ	1048.0
1.3125	1020.9	SOL	1020.8	0.3125	1038.3	SOL	1038.3	0.7125	1045.4	LIQ	1045.5
1.5125	1025.0	SOL	1024.9	0.3625	1038.6	SOL	1038.5	0.8125	1043.0	LIQ	1043.1
1.7125	1029.0	SOL	1028.9	0.4125	1038.9	SOL	1038.8	0.9125	1040.5	LIQ	1040.7
1.9125	1032.9	SOL	1032.9	0.4625	1039.2	SOL	1039.1	0.9625	1039.9	SOL	1039.9
2.1125	1036.9	SOL	1036.9	0.5125	1039.4	SOL	1039.4	1.0125	1039.8	SOL	1039.8
2.2125	1038.9	SOL	1038.9	0.5625	1039.7	SOL	1039.6	1.0625	1039.6	SOL	1039.7
2.3125	1040.0	MUSH	1040.0	0.6125	1040.0	MUSH	1039.9	1.1625	1039.4	SOL	1039.4
2.4125	1040.0	LIQ	1040.0	0.6625	1040.0	LIQ	1040.0	1.2625	1039.1	SOL	1039.2

(without a void model) was exercised independently in the r and z coordinate directions and the results were compared to the exact solution of problem 2 in Table III. As with the one-dimensional analyses, numerical and exact solutions agreed to within 0.6 percent. In addition, the computer model global energy balance was checked to assure that boundary conditions were properly implemented. An energy balance was maintained to within 0.003 percent.

In the absence of applicable exact or analytical solutions, previous numerical solutions, and experimental data, numerical consistency checks were performed to assess the validity of numerical solutions from two-dimensional analyses with the void model. A numerical check of canister model energy balance and void surface element view factor summation was carried out for each computer run. For all cases, an energy balance was maintained within 0.0015 percent and all surface element view factors summed to 1.0 within machine accuracy.

5.2 One-Dimensional Analyses

5.2.1 Semi-infinite PCM

5.2.1.1 Effects of the Void

The temperature controlled freezing problem (problem 1 in Table III) was solved for three cases: 1) without a void, 2) with a void considering only vapor conduction heat transfer, and 3) with a void considering only radiation heat transfer. The effect of a void on the PCM freezing process is evident in Figure 5.1 which illustrates freeze front position, X_m, versus time for the three cases outlined above. Here, the presence of the void reduces the amount of PCM frozen by factors of ~4 or ~5 assuming void heat transfer via conduction only or radiation only, respectively. For small St number freezing processes, the amount of energy removal is essentially proportional to the amount of PCM frozen. Therefore, in this problem where void size is small (i.e., 15 percent of X_m), the magnitude of void heat transfer via conduction and radiation are comparable.

5.2.1.2 Effects of Boundary Conditions

The effect of boundary conditions on the freezing processes in problems 1 and 3 of Table III is examined next. For these problems, comparison of results between constant temperature and constant heat flux boundary conditions is made on the basis of equal energy removal. This is accomplished by first integrating the boundary heat flux at x=0 over the 50 minute period for the constant temperature case to determine the total energy removed from the PCM. This total energy is then divided by 50 minutes to determine the required boundary condition at x=0 for the constant

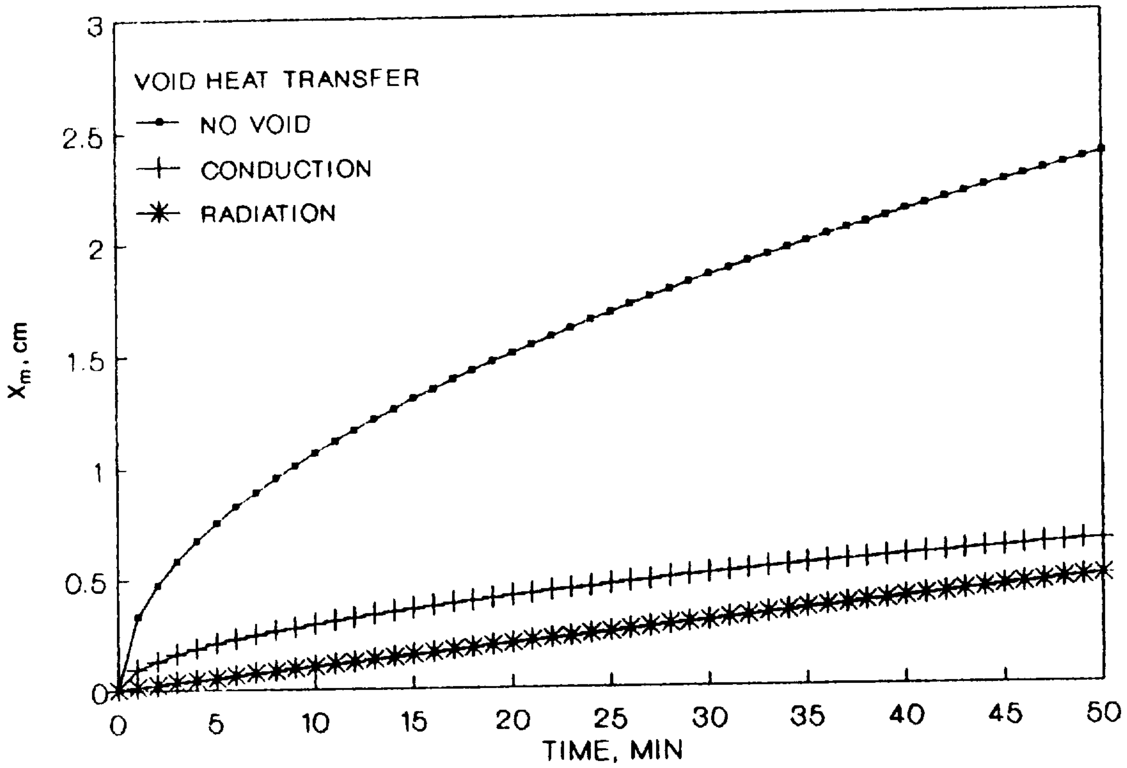

Figure 5.1. Melt Front Location For Freezing Process With St=0.10.

cooling heat flux case. This basis of comparison is consistent with a thermal energy storage application in which a finite amount of energy must be stored and released.

Plots of boundary temperature, T(0,t), and freeze front location, X_m, versus time are contained in Figures 5.2 and 5.3, respectively. Boundary temperature decreases linearly versus time with constant wall heat flux (see Figure 5.2). However, with radiation void heat transfer, variation in T(0,t) is small. This confirms the anticipated insensitivity of radiation heat transfer to void size. Freeze front advancement differs substantially with boundary condition assuming conduction void heat transfer (see Figure 5.3). A constant temperature boundary condition generates PCM freezing ~ time$^{1/2}$ and a constant flux boundary condition generates PCM freezing ~ time. This freezing behavior is characteristic of one-phase Stefan problems (see Yao and Prusa (1989)).

5.2.1.3 Effects of Free Convection

The effect of free convection on a melting process with St=0.10 (see problem 2 in Table III) is illustrated in Figure 5.4. Figure 5.4 contains plots of melt front position, X_m, versus time, PCM temperature at time 25 minutes, T(x, 25 min), versus position, and boundary heat flux, q(0,t), versus time for cases with and without free convection present. Although constant temperature is

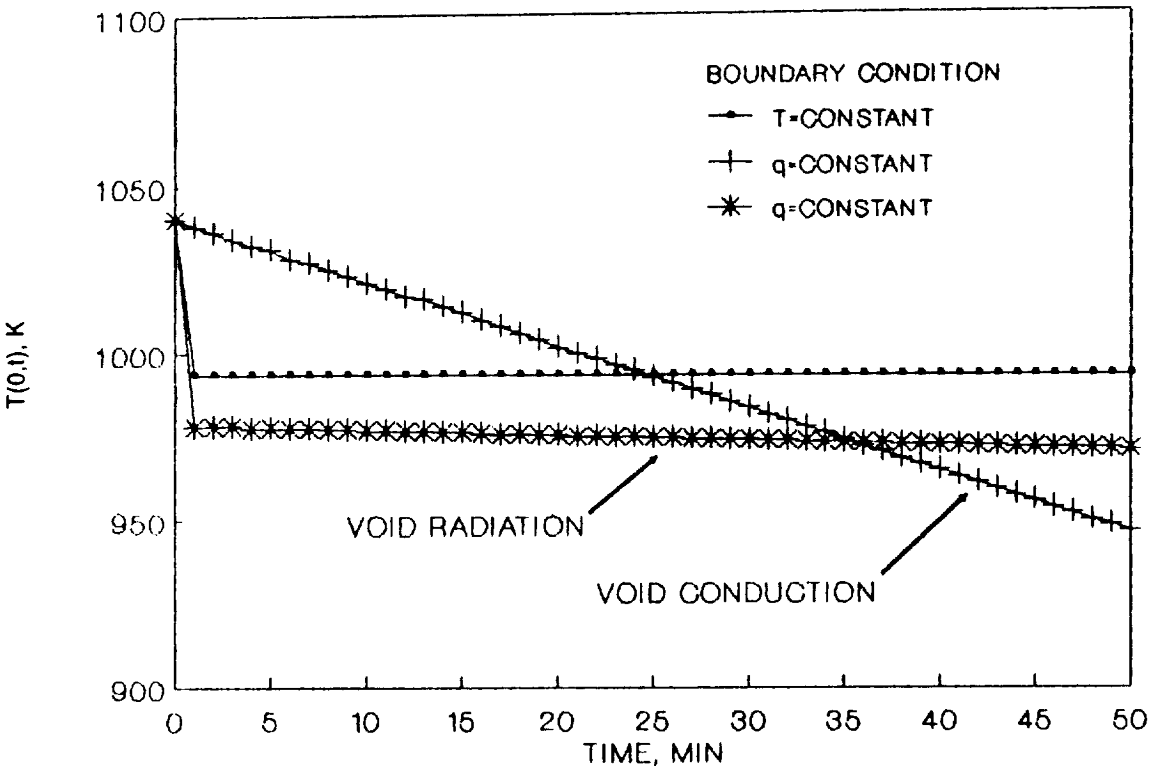

Figure 5.2. Boundary Temperatures For Equal Energy Removal Processes.

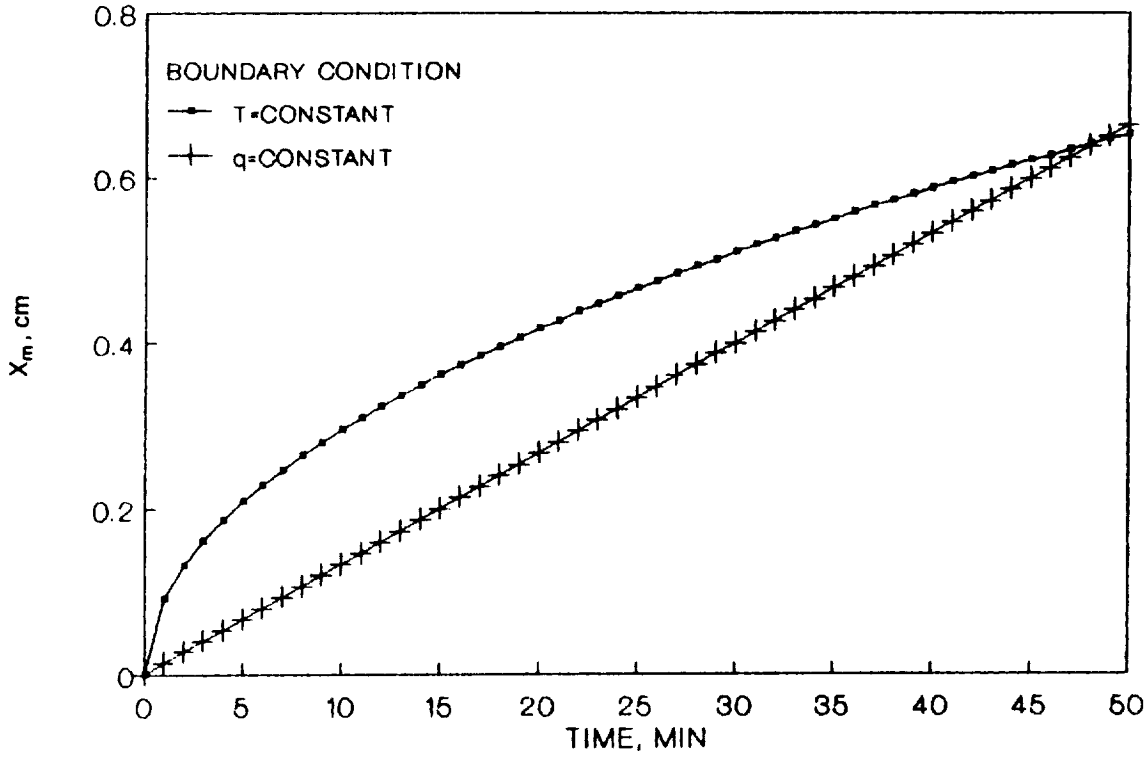

Figure 5.3. Melt Front Locations For Equal Energy Removal Processes.

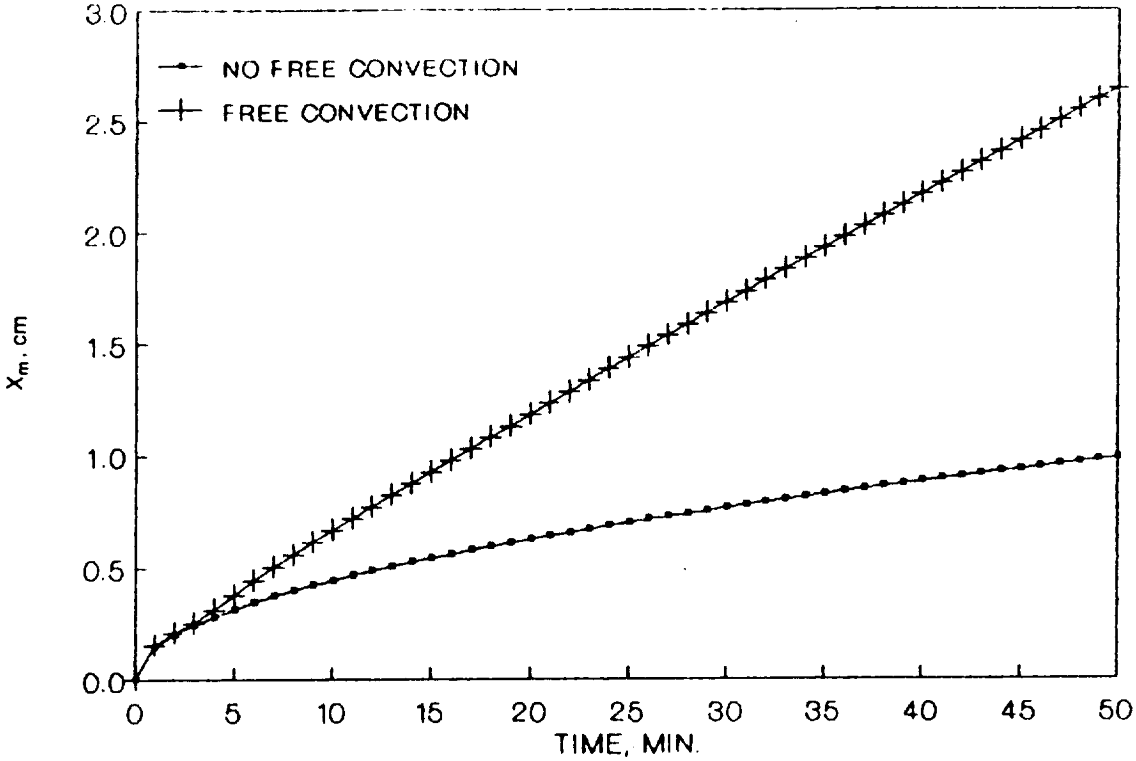

(a) Melt front location.

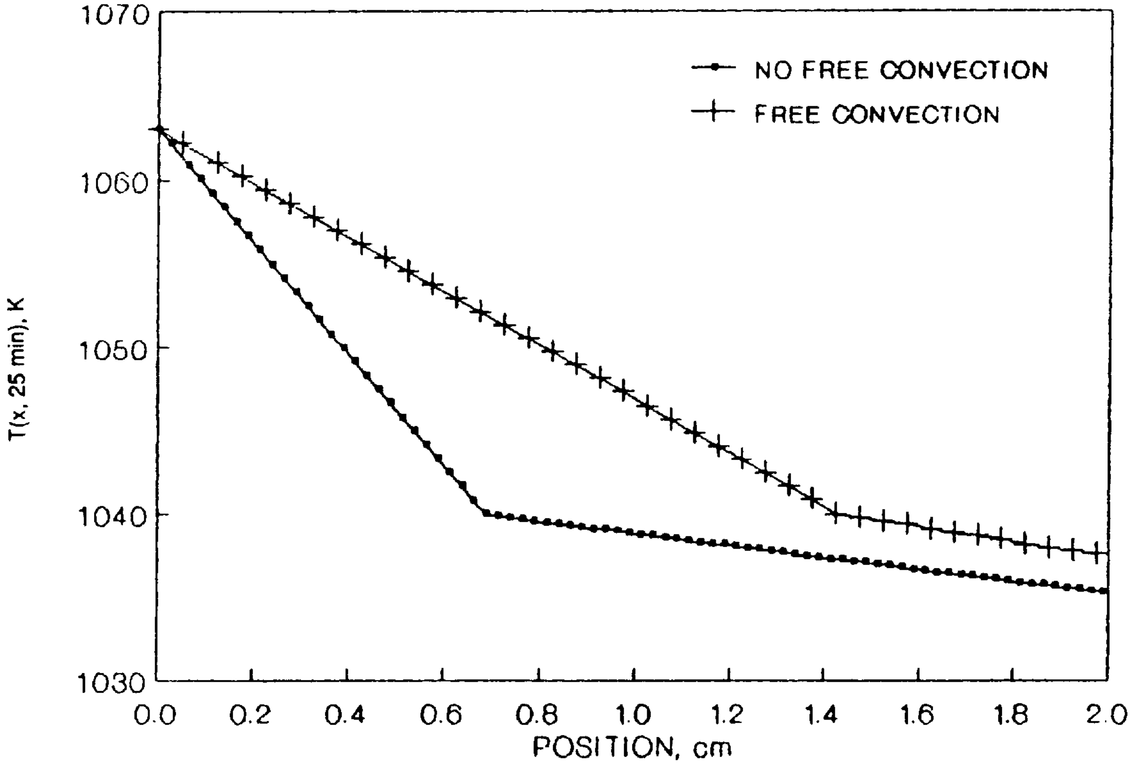

(b) PCM temperature distributions.

Figure 5.4. Problem 2 With St=0.10.

(a) Melt Front Position
(b) PCM Temperature Distributions

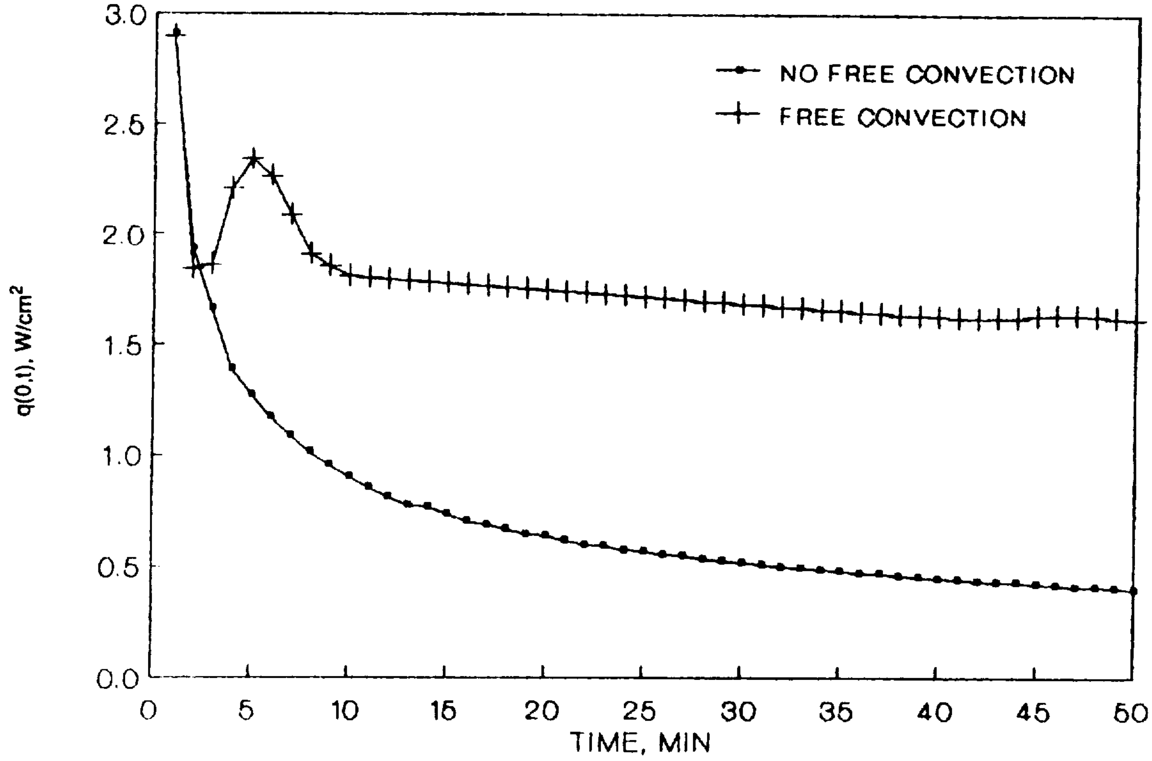

(c) Boundary heat flux.

Figure 5.4. Problem 2 With St=0.10.

(c) Boundary Heat Flux

maintained at x=0, the progression of X_m is nearly linear with the presence of free convection. This is characteristic of a conduction controlled, constant heat addition melting process (see Figure 5.4a). This same behavior was observed in experiments by Hale and Viskanta (1980). At 25 minutes, temperature gradients in the liquid PCM are reduced by a factor of ~2 while at the same time q(0,25 min) is increased by a factor of ~3 (see Figures 5.4b and 5.4c).

In Figure 5.4c, a local peak in q(0,t) exists at 5 minutes with free convection present (see the top curve). This is in sharp contrast to the monotonically decreasing behavior of q(0,t) predicted when accounting for only liquid PCM conduction heat transfer (see bottom curve). This heat transfer over-shoot phenomenon was also observed experimentally by Sparrow et al. (1978) and predicted numerically by Sparrow et al. (1977).

The over-shoot occurs when the magnitudes of convection and conduction in the liquid PCM are equal. The phenomenon can be explained physically in the following way. During the early stages of melting, liquid PCM heat transfer is controlled by conduction and decreases rapidly as the fluid layer thickness, or conduction path, increases. Fluid velocities are small and liquid temperature profiles are nearly linear. As melting proceeds, fluid velocities increase and boundary layers start to form. Moderate temperature gradients exist in both the bulk fluid and in the developing boundary layers near the heated and cooled surfaces. During this stage of melting, the rapid fall-off in conduction heat transfer is compensated for by the increasing convective heat transport. Thus, overall heat transfer rates start to increase. Fluid conduction and convection heat transfer components eventually become equal in magnitude at which time the liquid PCM heat transfer rate is locally maximized.

As melting proceeds still further, heat transfer rates fall-off again, but at a much slower rate consistent which the gradually increasing flow resistance associated with the growing liquid region size. Boundary layers become fully developed and fluid motion and temperature gradients are confined to narrow layers adjacent to the heated and cooled surfaces. Temperature gradients through the bulk liquid are essentially zero as the heat transport through the liquid layer is due solely to liquid recirculation.

A similar situation arises in constant flux melting experiments. In these tests, the measured heat source temperature exhibits a maxima (i.e., the film coefficient exhibits a local minima) near the transition from conduction dominated to convection dominated liquid heat transfer, Goldstein and Ramsey (1979).

It is interesting to note for the case with free convection, that although the liquid PCM region continues to grow in size, q(0,t) reaches a near steady state value by 50 minutes (see Figure 5.4c). This suggests that the free convection film coefficient and liquid PCM region thermal resistance are independent of X_m. A check of the free convection correlation in Table II reveals that for $Ra>10^5$, the Nu number essentially increases linearly with X_m. This is to be expected since in this Ra number range, $Nu \sim Ra^{0.3} \sim X_m^{0.9}$. Thus, the film coefficient exhibits a very weak dependence on the melt zone size during the later stages of melting when large Ra numbers exist. Experiments by Bathelt et al. (1979) also confirm this behavior.

5.2.1.4 Observations

Although semi-infinite PCM analyses were performed primarily to check the accuracy of numerical predictions, a few observations regarding the general performance of TES canisters can be made. First, dramatically different problem solutions are obtained depending on whether a void is present or not. Consequently, any reasonable analysis of a PCM with appreciable volume change (i.e., >5 percent) must include a model of void behavior. Furthermore, the void model must properly take into account the primary modes of heat transfer for the given void size and void vapor thermophysical properties.

This point is illustrated by considering two separate LiF vapor void problems that lead to two separate conclusions: 1) the freezing process shown in Figure 5.1 where void size is small (i.e., < 0.1 cm) and the temperature difference across the void is moderate (i.e., ~40 K) and 2) scoping calculations by Whichner et al. (1988) where a large void size is considered (i.e., 1 cm) and a large void temperature difference exists (i.e., ~100 K). In the first problem, it is concluded that void heat transfer by radiation and conduction are nearly equal since nearly equal quantities of PCM are frozen in each case. However, in the second problem, radiation heat transfer is predicted to be ~35 times larger than conduction heat transfer. Therefore, void heat transfer modeling must be consistent with the void geometry analyzed and the anticipated temperature conditions. A further discussion of void heat transfer is given in the next section.

A second observation can be made concerning the wide range of solidification rates, boundary temperatures, and boundary heat fluxes predicted for equal energy removal processes depending on the type of boundary condition assumed (see Figures 5.2 and 5.3). This suggests that the type of boundary conditions that a TES canister experiences will influence, to some extent, items such as solid PCM crystalline structure and void distribution (which are both functions of the solidification rate).

PCM containment canister material durability will also be influenced by the type of boundary condition since results indicate that a constant temperature heat sink (or heat source), such as a nearly isothermal heat pipe, maintains the boundary temperature closer to T_m than does a constant flux boundary condition. The practical implication of this result is that lower PCM containment wall temperatures will occur with heat pipe receiver concepts versus direct absorption receiver concepts. Keeping canister wall temperatures close to T_m is important for achieving long component design lives since increasing temperature enhances the PCM corrosion rate and reduces canister material strength. However, the benefit of lower canister wall temperatures must be weighed against the added complexity and mass of a heat pipe receiver concept.

A third observation can be made regarding the influence of free convection. As shown in Figure 5.4, the heat transfer differences from liquid PCM circulation (in terms of melting rates, temperature gradients, and boundary heat fluxes) are substantial. Therefore, PCM analyses must include a free convection model to enable correlation with ground-based experiments. This same conclusion has been reached by researchers referenced in the preceding section and by others (see Bathelt et al. (1979), Deal and Solomon (1981), and Humphries (1974)) after completing phase change experiments which focus on the effects of free convection in the PCM melt. Furthermore, it is essential to be able to accurately predict ground-based performance of flight-design TES units since full scale flight tests may not be practical on the basis of cost. If this is the case, extrapolation of TES unit flight performance (in micro-g) can be calculated with a satisfactory confidence level. A further discussion of this point is given in the following sections.

5.2.2 PCM Slab Canister

5.2.2.1 Void Thermal Resistance

Void thermal resistance is plotted as a function of time in Figure 5.5 for a representative size slab PCM containment canister undergoing a 30 minute, constant heat input melting period and a 20 minute, zero heat input freezing period. Conduction and radiation thermal resistances are of the same order-of-magnitude and both vary significantly with time due to variations in void size and canister wall temperature, respectively. Therefore, for TES canisters of the type analyzed herein, void heat transfer is most accurately modeled as a simultaneous conduction-radiation process. The resultant thermal resistance from uncoupled conduction and radiation heat transfer modes is also shown in Figure 5.5.

5.2.2.2 Wall 1 Temperatures

The canister wall 1 temperatures, T(0,t), are shown versus time in Figure 5.6 for different void heat transfer assumptions. Note that canister heat input is applied at wall 1 which is adjacent to the void while wall 2 is convectively cooled by the heat engine working fluid (see Figure 3.1). T(0,t) predictions widely vary depending on

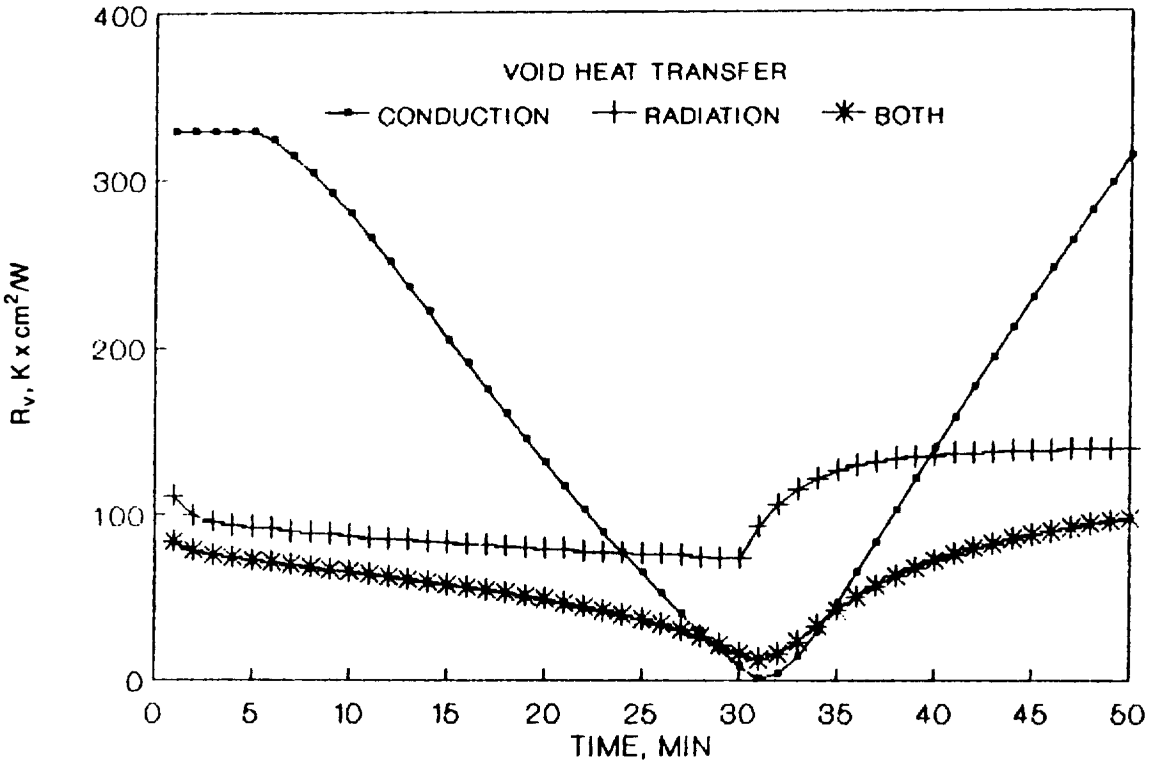

Figure 5.5. Void Thermal Resistance.

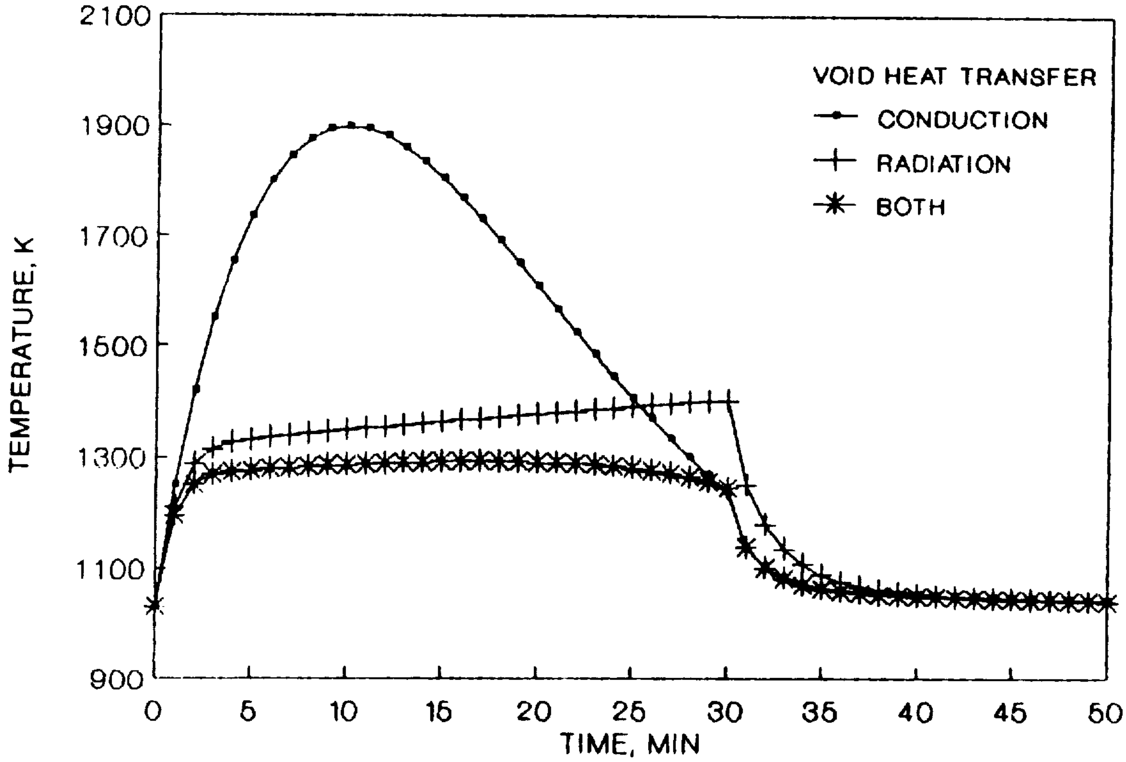

Figure 5.6. Wall 1 Temperatures With Various Modes Of Void Heat Transfer.

the assumed type of void heat transfer. With combined mode void heat transfer, T(0,t) is nearly isothermal at 1290 K during melting and at 1050 K during freezing. Ignoring the conduction component of void heat transfer increases canister wall 1 temperature predictions by 50 to 150 K over those with combined mode void heat transfer. The magnitude of this temperature difference is probably not acceptable from a canister design view point. Therefore, ignoring void vapor conduction is not a good assumption in this case since it would lead to an overly conservative canister design.

Ignoring void radiation results in wall 1 temperatures that exceed the melting range of Haynes alloy 188 (1575 to 1630 K). In all cases, wall 1 temperature predictions are too high for long term operation of containment canisters constructed with superalloys. This illustrates the need for heat transfer enhancement fins between heat addition and heat removal surfaces when dealing with low conductivity PCM's to maintain maximum wall temperatures below ~1150 K.

5.2.2.3 Effects of Void Distribution and Consequences for One-Dimensional Analyses

Since the void in actual PCM containment canisters is not evenly distributed around the circumference, Strumpf and Coombs (1988), the behavior of localized canister radial segments can roughly be approximated by the behavior of one-dimensional PCM models with or without a void. Figure 5.7

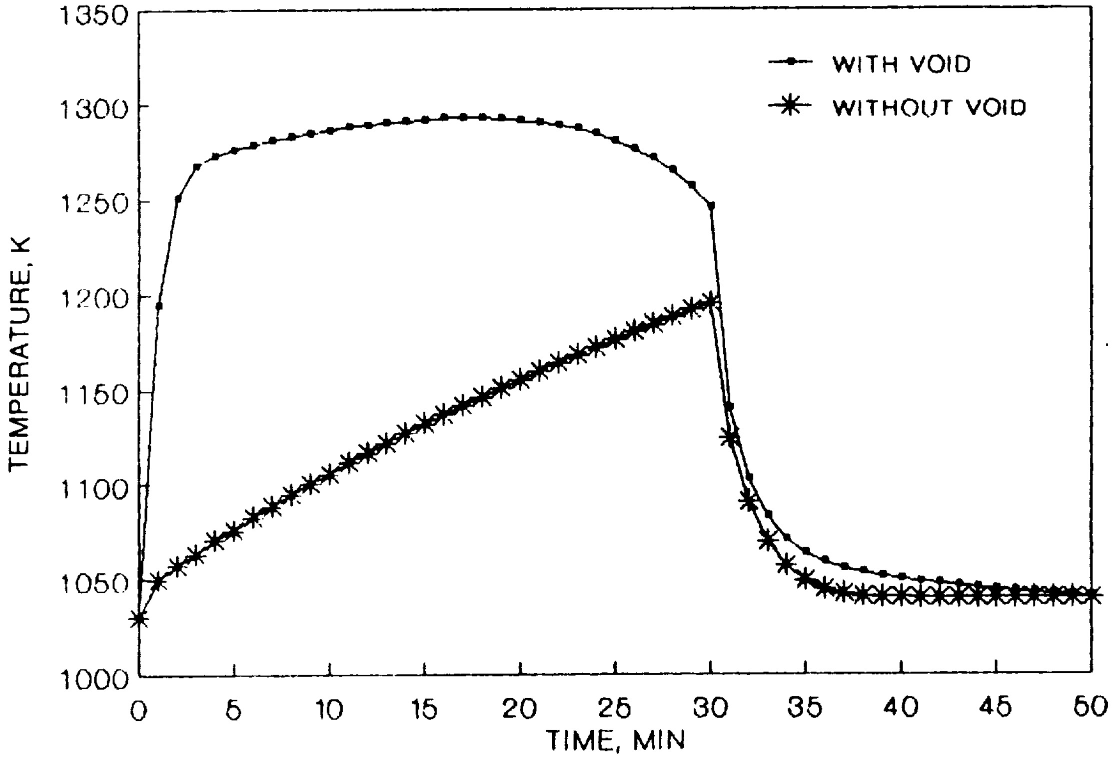

Figure 5.7. Wall 1 Temperatures With And Without A Void.

illustrates wall 1 temperature predictions versus time for cases with and without a void. The void increases wall 1 temperatures between 50 to 200 K throughout the TES charge period with constant heat input. This introduces the potential that for PCM canisters with asymmetric heat input, the maximum wall temperatures will not occur at the point of maximum heat input but instead will occur in the region of the void (i.e., the location of largest thermal resistance). Hence, the position of the void must be quantified to accurately characterize wall temperatures of canisters with high length-to-diameter ratio, i.e. canisters with small side wall end effects. However, accurate prediction of the void location in micro-g requires very complex calculations which are difficult to verify.

To avoid the difficulties in predicting void behavior, a straight-forward approach could be adopted in which the void is placed adjacent to the heat input surface to yield conservative temperature predictions. It will be shown in the two-dimensional canister analysis sections that for a low length-to-diameter ratio canister, i.e. $l/d \approx 0.5$, wall temperature sensitivity to void location is greatly reduced because of the large heat transfer contribution of canister sidewalls.

It should be noted that one-dimensional canister analysis accentuates wall temperature increases introduced by a void since all canister absorbed energy must be transferred across the void. In an actual canister, absorbed energy in the outer wall has multiple heat transfer paths in which to diffuse. Thus, wall temperature increases due to the presence of a void would be much less pronounced than indicated from one-dimensional predictions.

The sensitivity of wall temperatures to void location and to the nature of void heat transfer depends on the extent to which PCM heat transfer is required for energy redistribution within the canister. In section 5.3, two-dimensional analytical results will show that during the cycle heating period, when highest canister wall temperatures exist, roughly 30 to 70 percent of canister total radial heat transfer occurs within the side walls. Thus, it will be shown that the sensitivity of canister wall temperatures to PCM-void distribution is greatly reduced over the one-dimensional case.

It is conceivable that the magnitude of this reduction may render void heat transfer secondary in importance to canister and PCM heat conduction/convection. In this case, wall temperature predictions would be essentially independent of the method used to model void heat transfer. Results from steady state PCM canister heat transfer analyses discussed by Tong et al. (1988) support this assertion. In this study, the maximum canister wall temperature increased by only 29 K with the addition of a circumferential void at the canister outer diameter. A more detailed discussion of canister wall temperature sensitivity to a void will be given in section 5.3.

5.2.2.4 Effects of Free Convection

Figure 5.8 illustrates the impact of free convection on PCM melt and void front positions, canister wall temperatures and PCM temperature distributions. The PCM occupies the region $0.15 < x < 1.15$ cm between the two canister walls. The void occupies the region $0.15 < x \lesssim 0.30$ cm as it sequentially grows and shrinks (due to density differences in the solid and liquid PCM) during PCM freezing and melting, respectively. Little difference exists between melt/void front locations with the addition of free convection (see Figure 5.8a). However, the presence of free convection significantly lowers canister wall 1 temperatures and PCM temperature gradients during the TES charge period in addition to melting slightly more PCM (see Figures 5.8b and 5.8c).

Figure 5.9 shows the liquid PCM Nu number as a function of melt front position X_m with and without a void. Without a void, the critical Ra number is exceeded at $X_m \approx 0.50$ cm and the Nu number increases linearly with X_m until complete PCM melting has occurred. At this point, $Nu \approx 3.4$ which is about 35 percent lower than the Nu number for the semi-infinite PCM geometry with the same X_m. This seems reasonable since for the semi-infinite PCM geometry, a horizontal liquid layer with heat input from the bottom (with respect to gravity) is assumed. This orientation creates greater

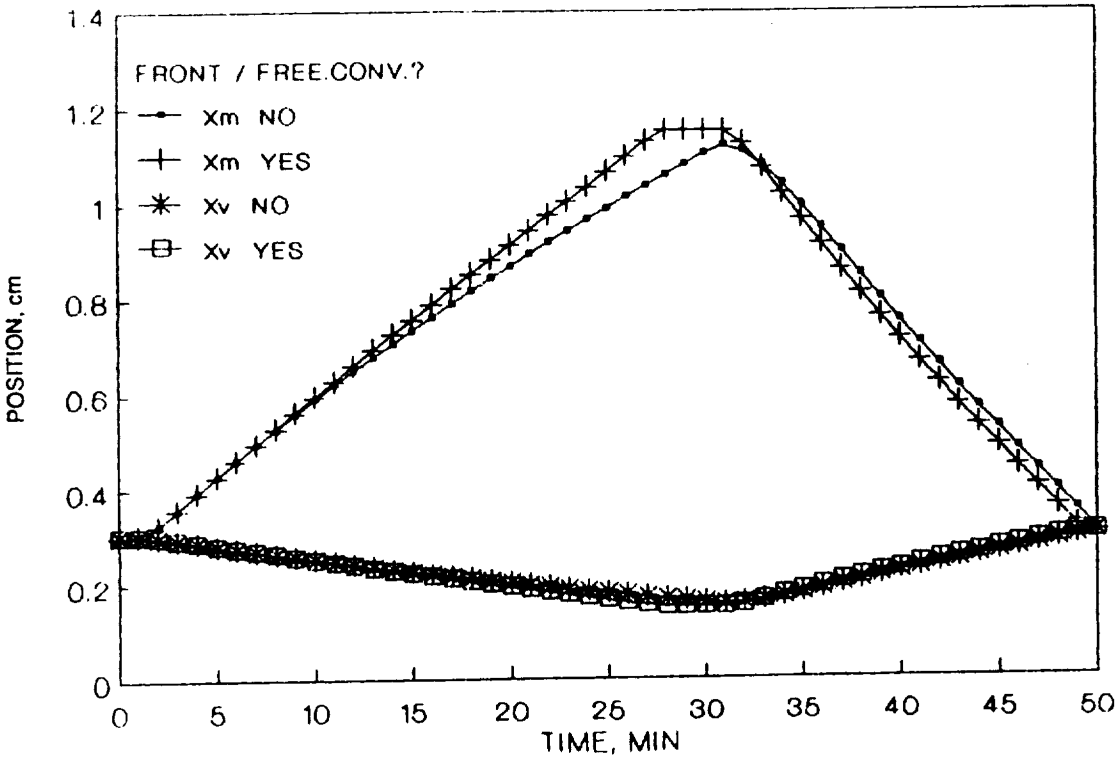

(a) Melt and void front positions.

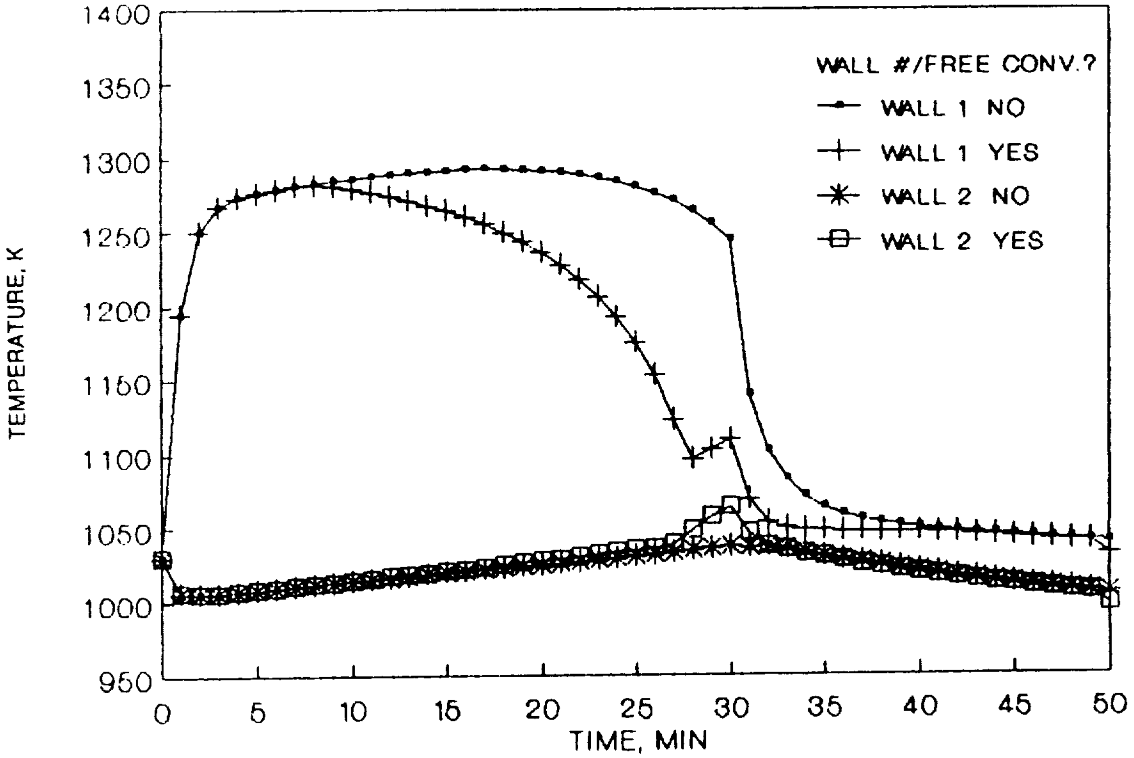

(b) Wall temperatures.

Figure 5.8. PCM Slab Canister Results.

(a) Melt And Void Front Positions
(b) Wall Temperatures

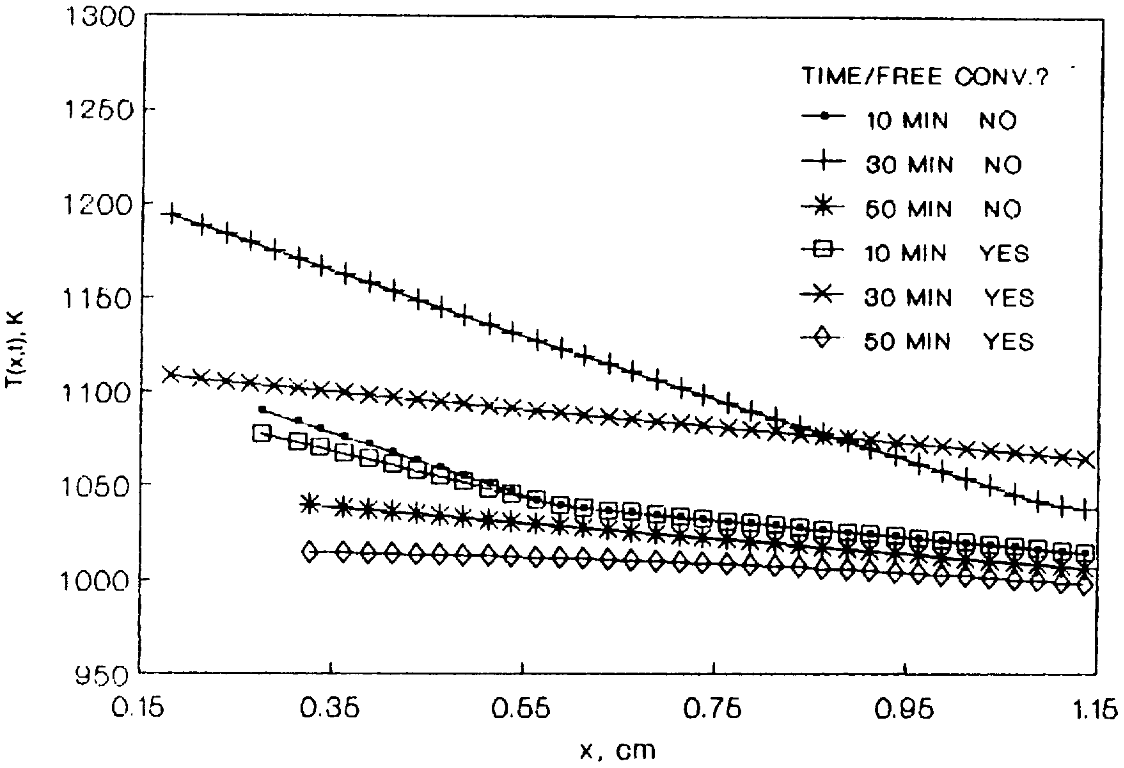

(c) PCM temperature distributions.

Figure 5.8. PCM Slab Canister Results.

(c) PCM Temperature Distributions

C-2

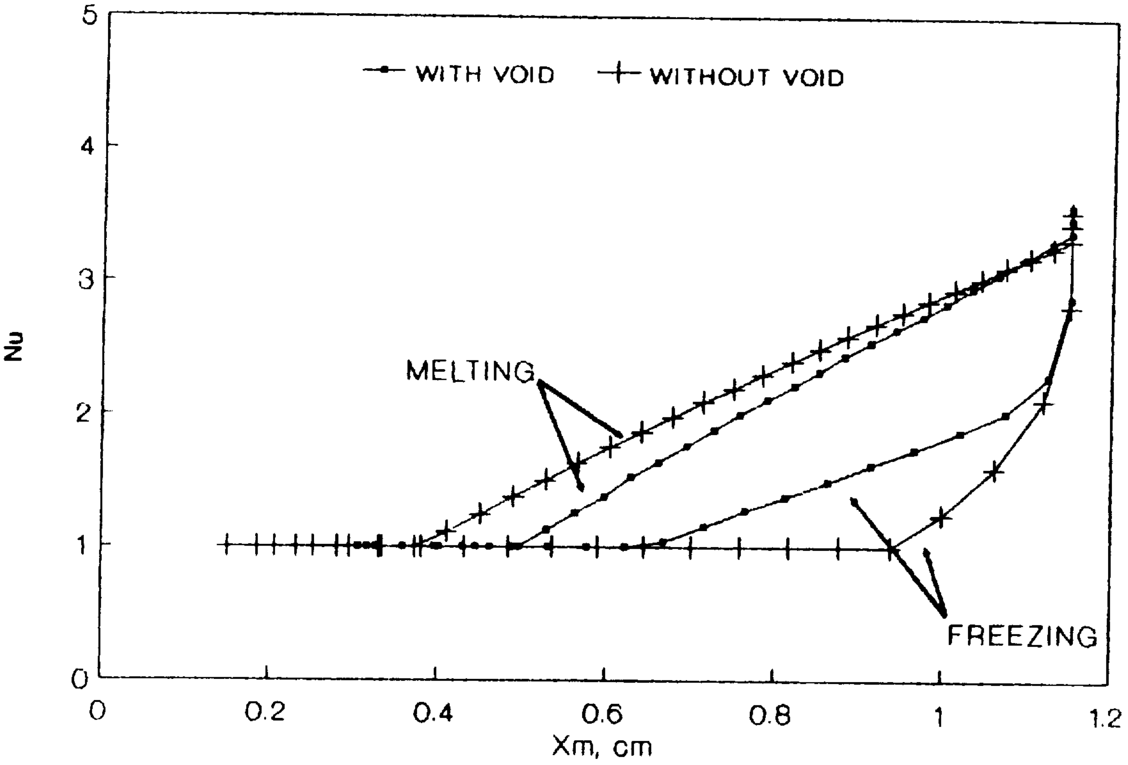

Figure 5.9. Nusselt Number Versus Melt Front Position.

convective instability than expected for the PCM slab canister which is assumed to have a vertical liquid layer heated in a direction normal to the gravity vector. During freezing, the Nu number falls off rapidly with decreasing X_m and becomes linear with a slope about 25 percent lower than during melting. This is attributed to smaller Ra numbers due to reduced temperature gradients. This suggests that h is essentially independent of X_m but does depend on whether the PCM is melting or freezing.

Note that in Figure 5.9, there is a marked difference in the curves for the cases with and without a void. During PCM melting, Nu numbers for the case with a void appear to be lower than those occurring without a void for a given melt front position, X_m. This result has no physical significance but instead is the consequence of how X_m is measured in the case with a void: namely, the value of X_m is necessarily increased by the size of the void at any given time, i.e. by 0.15 cm at the start of melting which vanishes to 0.0 cm at the conclusion of melting (see Figure 3.1b).

During PCM freezing, the larger Nu numbers in Figure 5.9 for the case with a void (compared to the case without a void) can be ascribed to physical differences between the two problems in addition to the convention adopted for measuring X_m. With a void present, slightly less PCM is liquified during the charging period. Instead, this energy manifests itself sensibly in the from of substantially increased wall 1 temperatures. When the PCM is discharging, however, wall 1 rapidly cools and effectively acts as a heat source to the liquid PCM. This sustains liquid PCM temperature gradients for a longer period of time and hence, Nu numbers greater than 1.0 persist for smaller values of X_m during freezing with a void as compared to without a void.

5.2.2.5 Ground-Based Testing of Flight Design Hardware

Several comments can be made about the effects of liquid PCM free convection and its implications for ground-based testing of the conceptual heat receiver or PCM containment canisters designed for operation in low earth orbit. Analyses have shown that liquid PCM convective flows arising from buoyancy and surface tension forces are small in a micro-gravity environment, Whichner et al. (1988). Thus, liquid PCM heat transfer during on-orbit operation will take place primarily via thermal conduction. However, for ground-based tests, the effects of free convection (based on one-dimensional analyses) are lower canister wall temperatures and increased PCM melting rate during heat input periods. These effects are enhanced for the canister orientation in which the direction of outer wall heat input is from the bottom (with respect to gravity) as opposed to normal to the gravity vector. Therefore, free convection effects should lead to improvement in overall receiver PCM utilization, greater receiver cavity isothermallity, and lower receiver heat losses. During thermal discharge periods, free convection effects are small and should not significantly affect receiver thermal performance.

These results suggest that canister ground tests should be conducted with an orientation that permits outer wall heat input from the top (with respect to gravity) or normal to the gravity vector to minimize free convection effects. Furthermore, outer wall heating in a direction normal to gravity places the canister axis of symmetry parallel to the gravity vector. In this orientation, free convective effects will tend to be more uniform around the canister circumference when compared to the canister orientation with outer wall heating directed parallel to the gravity vector.

It is interesting to note that an analogous situation arises in adiabatic, two-phase (liquid-vapor) flow in circular tubes. Researchers have found that vapor bubble shapes and distributions in 1-g, vertical tube flow tests closely match those encountered during low-g flow tests while horizontal 1-g flow tests generate substantially different vapor bubble characteristics, Siegel (1967). This observation introduces the possibility that for certain cases, vertical orientation testing in 1-g offers an adequate test simulation of anticipated micro-g operation.

The argument for canister ground test orientation can also be extended to heat receiver ground testing. The preferred heat receiver ground test orientation should be with the axis of the receiver vertical (see Figure 2.2).

This orientation permits canisters on each working fluid tube to receive outer wall heating directed normal to gravity and thereby experience uniform free convection effects. A test conducted with the receiver axis horizontal would cause canisters on top receiver tubes to be heated diametrically opposed to gravity (i.e., generating maximum convective activity) while canisters on bottom tubes would be heated in the direction with the gravity vector (i.e., generating minimum convective activity). This situation would skew tube-to-tube canister performance and introduce additional receiver cavity circumferential temperature variations not expected during on-orbit operation. A more detailed discussion of liquid PCM free convection effects based on two-dimensional canister analyses will be given in section 5.3.

5.3 Two-Dimensional Analyses

5.3.1 Canister Without Void or Free Convection Models

5.3.1.1 PCM Phase Distributions

PCM phase distributions are shown in Figure 4.10 at several times (24.28, 54.63, 66.77, and 91.05 minutes) for a 91 minute cycle in which the PCM is being charged for the first ~55 minutes and discharged for the remaining ~36 minutes. The heat transfer benefits of the canister side

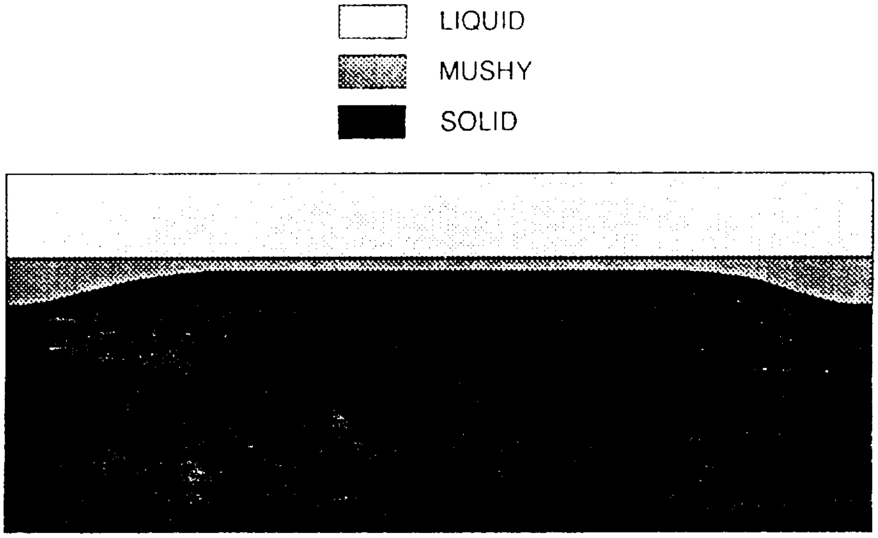

(a) Time = 24.28 min, MFL = 0.30.

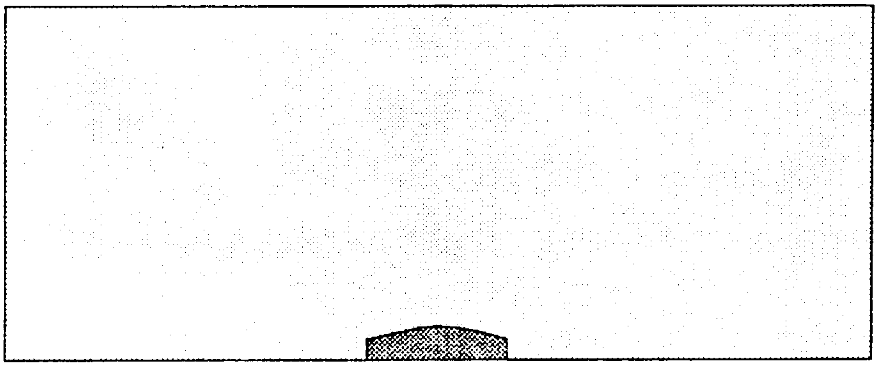

(b) Time = 54.63 min, MFL = 0.99.

Figure 5.10. PCM Phase Maps.

(a) Time=24.28 min., MFL=0.30
(b) Time=54.63 min., MFL=0.99

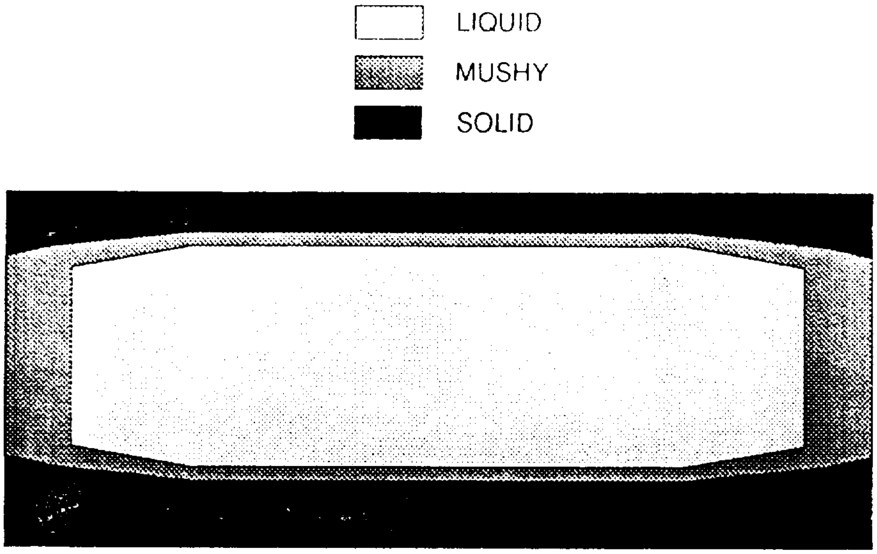

(c) Time = 66.77 min, MFL = 0.63.

(d) Time = 91.05 min, MFL = 0.00.

Figure 5.10. PCM Phase Maps.

(c) Time=66.77 min., MFL=0.63
(d) Time=91.05 min., MFL=0.00

walls are evident at 24.28 minutes into the TES charge period. The liquid and mushy PCM regions extend radially inward adjacent to canister sidewalls to a greater extent than the bulk PCM. This indicates the manner in which sidewall heat transfer enhances PCM melting in both radial and axial directions without the need for large liquid PCM temperature gradients. Nearly complete PCM melting occurs by 54.63 minutes at which time only a small mushy region exists at the canister inner radius.

At 66.77 minutes, mushy PCM and solid PCM regions completely surround a liquid PCM core region. This phase distribution is the result of heat removal at both inner and outer radial canister surfaces during the first half of the TES discharge period (see Figure 3.3). As freezing continues, the solid region growths inward from all sides until the liquid core region is consumed at about 6 minutes prior to the end of the discharge period. Thus, at 91.05 minutes, only solid PCM exists. In short, the PCM solidification process obeys 2 simple rules: 1) solid PCM forms on cooled surfaces and 2) the last liquid to solidify is situated furthest from cooling surfaces.

The simple observations of the PCM freezing pattern mentioned above have important implications for evaluating void behavior. Knowing where solid PCM formations occur narrows down the possible locations that voids can occupy. The above freezing behavior suggests that had PCM density differences been accounted for, the resultant void volume would most likely end up as a central core region surrounded by solid PCM. This prediction is based on the assumption that liquified PCM can creep into canister corners and completely cover available internal canister wall surface area. In this sense, the void in completely liquified PCM would be centrally located within the canister volume prior to the start of PCM freezing.

Langbein et al. (1990) found from micro-g experiments and Concus and Finn (1990) proved mathematically that a liquid will creep into container corners if the sum of the liquid contact angle plus the corner half angle is less than 90 degrees. This situation does in fact exist for liquid LiF-CaF_2 at temperatures below ~1100 K. Furthermore, ground-based observations of canister PCM distributions by Strumpf and Coombs (1989) show a centrally located void position after repeated freeze-thaw cycles in an air furnace where cooling takes place on all canister surfaces. In other ground-based experiments by Blumenberg and Weingartner (1988), LiF-filled coaxial cylinders were found to have voids located at or near non-cooled surfaces. In experiments by Sparrow et al. (1978), guard heaters were incorporated into the apparatus specifically to control void formation during PCM solidification in preparation for subsequent melting experiments. As intended, voids formed near the guard heaters and therefore, essentially eliminated solid PCM porosity and potential over-stress conditions in the PCM containment vessel from undesirable void distributions. In the present analyses, cooling occurs along all canister walls which confirms the above assertion that void formation will likely result in the canister central volume.

5.3.1.2 Temperature Distributions

Canister temperature contour maps that correspond to the PCM phase maps are shown in Figure 5.11. The isotherms just above and below 1040 K reveal the approximate position of the PCM solid-liquid interface. Noticeable isotherm compression occurs in the vicinity of the melt front as evidence of the relatively high heat transfer rates needed to support PCM melting (see Figure 5.11a) or PCM freezing (see Figure 5.11c). At times when only liquid PCM or only solid PCM exists, isotherms are spaced in a relatively uniform fashion (see Figures 5.11b and 5.11d, respectively). Noticeable bending in the isotherms occurs near canister walls. This illustrates the effect of canister wall heat transfer enhancement that effectively behaves as a heat sink for the outer wall and as a heat source for the inner wall.

5.3.1.3 Temperature and Heat Transfer Variations

Figure 5.12 illustrates the variation in maximum canister wall temperature and heat transfer to the cooling fluid as a function of cycle time. The maximum canister

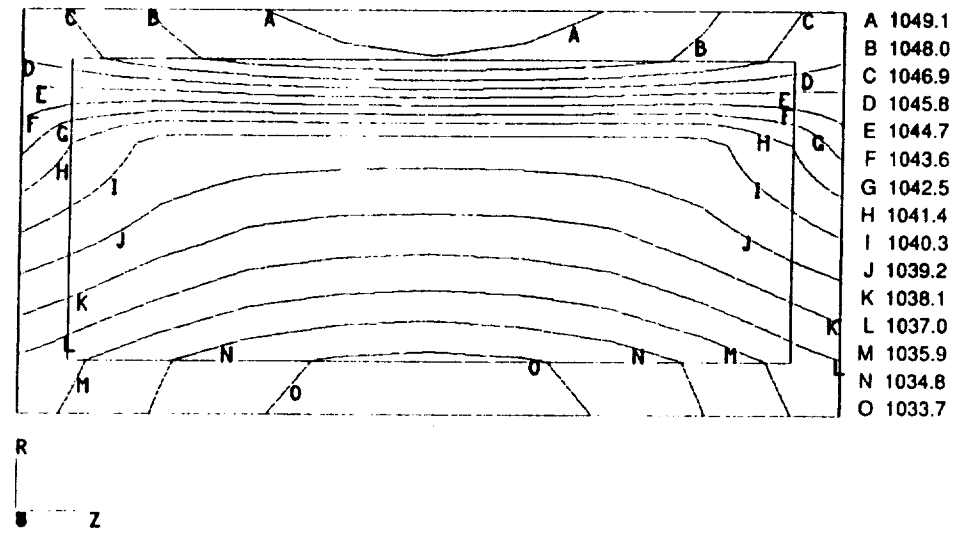

(a) Time = 24.28 min.

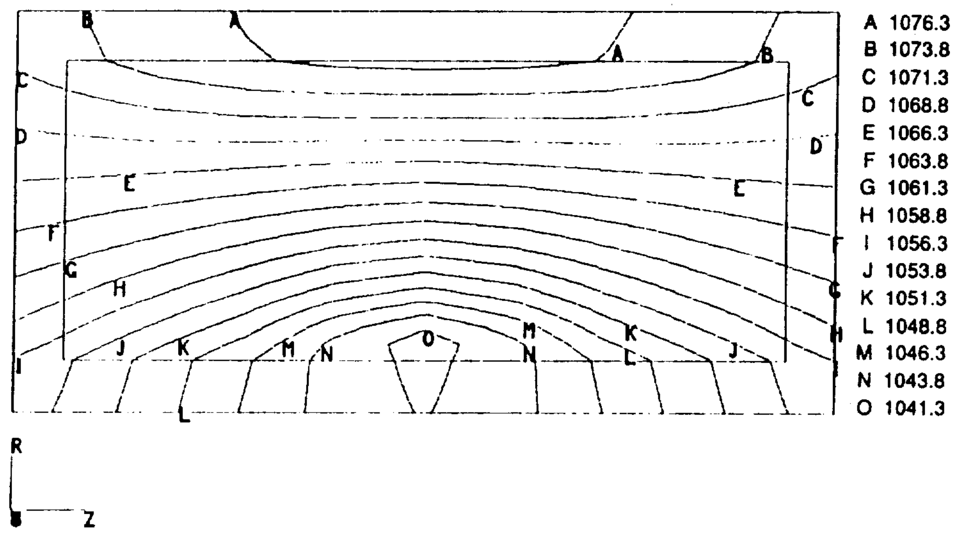

(b) Time = 54.63 min.

Figure 5.11. Canister Temperature Contour Maps, K.

(a) Time=24.28 min.
(b) Time=54.63 min.

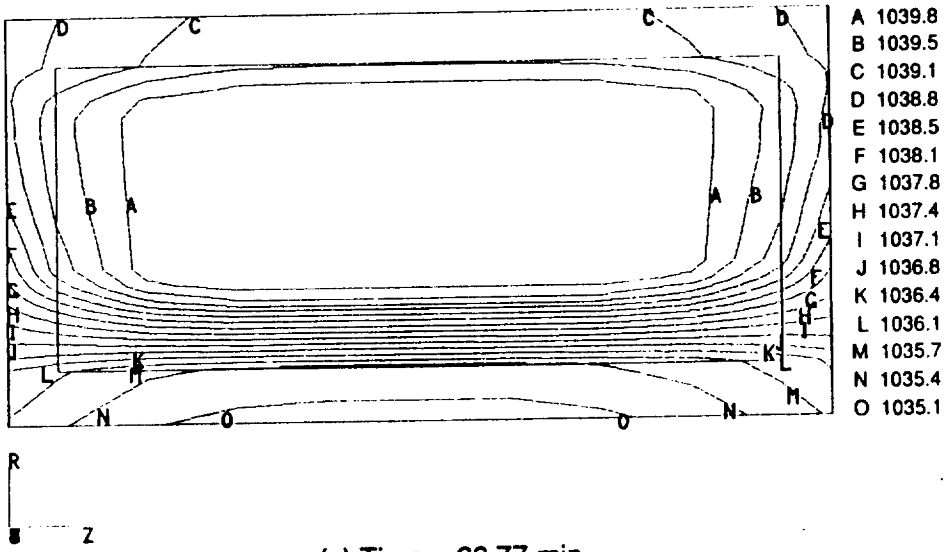

(c) Time = 66.77 min.

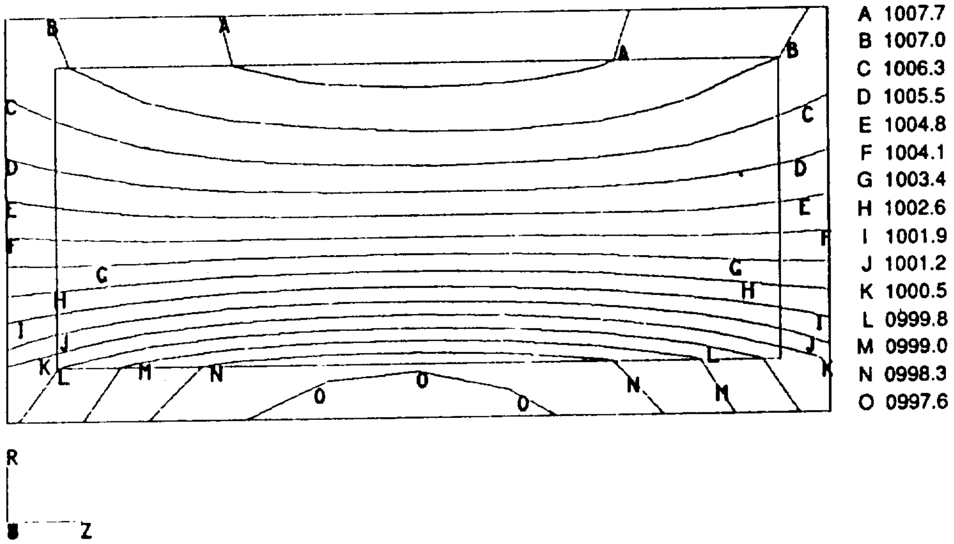

(d) Time = 91.05 min.

Figure 5.11. Canister Temperature Contour Maps, K.

(c) Time=66.77 min.
(d) Time=91.05 min.

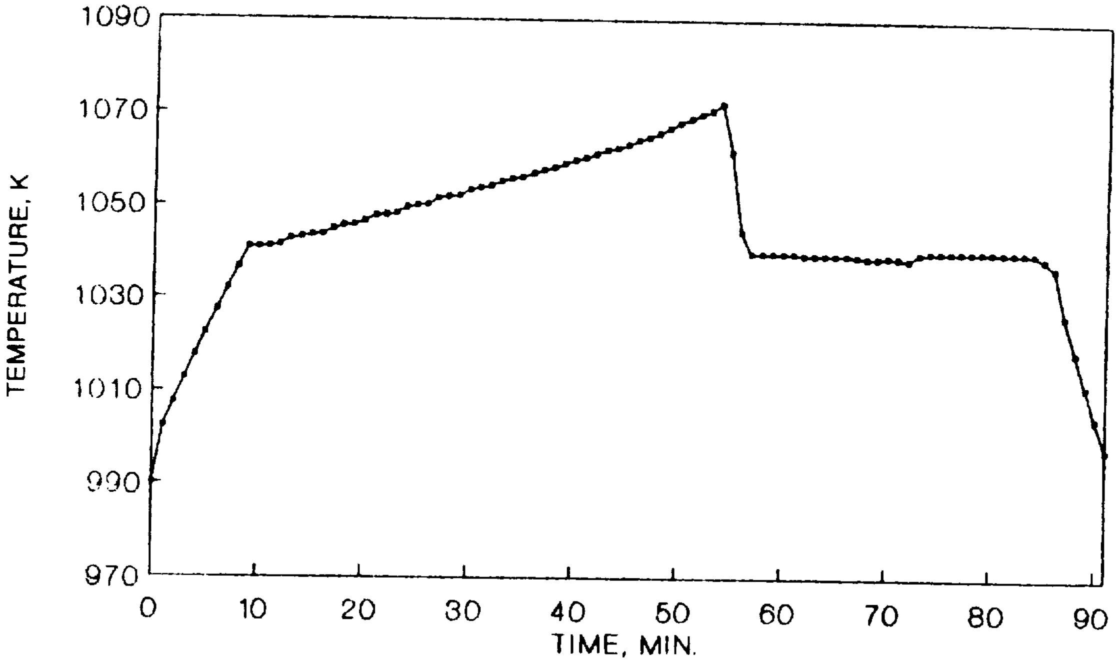

(a) Maximum canister wall temperature.

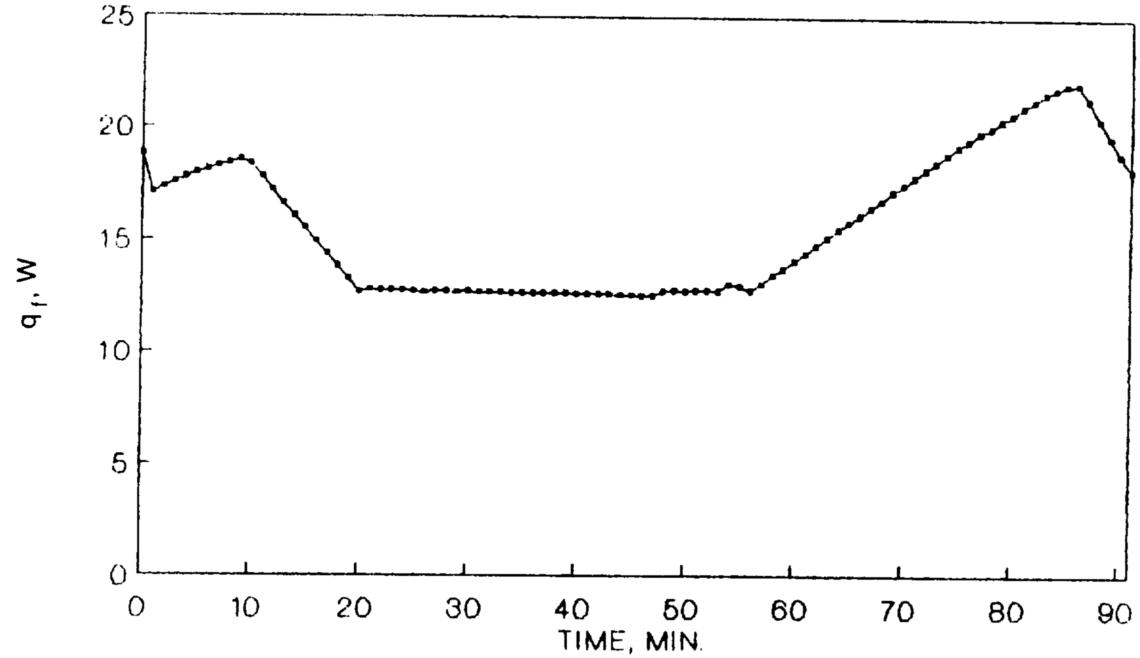

(b) Heat transfer to cooling fluid.

Figure 5.12. Cyclic Variations In Maximum Canister Wall Temperature And Heat Transfer To The Cooling Fluid.

(a) Maximum Canister Wall Temperature
(b) Heat Transfer To Cooling Fluid

wall temperature occurs at the axial midpoint of the outer wall. This temperature is a strong function of the phase change process (see Figure 5.12a). As long as liquid and solid PCM coexist (in this case from 9-86 minutes), absorbed canister energy manifests itself as latent heat and hence, temperatures will not strongly deviate from the PCM melting temperature, T_m=1040 K. Finite temperature deviations from 1040 K are required to transfer heat to and from the solid-liquid interface. However, these deviations are held to acceptable levels by choosing a reasonably high canister conductance, i.e. by limiting canister size and selecting adequate wall thicknesses. Once a single PCM phase exists, large temperature transients result as a consequence of sensible energy change.

Variation in cooling fluid heat transfer can generally be ascribed to variation in cooling fluid inlet temperature, $T_f(0,t)$ (see Figure 5.12b). Heat transfer to the fluid is proportional to the temperature difference between the cooling fluid tube wall (i.e., the canister inner wall) and the fluid. Since for most of the cycle time, two-phase PCM exists, tube wall temperatures remain fairly constant near T_m. Thus during this period, the temporal change in cooling fluid heat transfer is inversely proportional to the temporal change in $T_f(0,t)$: hence, an increase in $T_f(0,t)$ leads to a corresponding decrease in cooling fluid heat transfer. The exception to this behavior occurs at the beginning and at the end of the 91 minute cycle when only solid PCM exists. During these periods, tube wall temperature transients are larger than transients in $T_f(0,t)$. Thus at the beginning of the cycle, for example, this behavior results in increasing cooling fluid heat transfer with increasing $T_f(0,t)$.

5.3.1.4 Side Wall Heat Transfer Fractions

Since the LiF-CaF$_2$ PCM is a poor thermal conductor, highly conducting canister walls are necessary to distribute energy absorbed at the canister outer surface to the PCM and to the cooling fluid (heat engine working fluid) without excessive temperature gradients. One measure of the effectiveness in which the canister walls redistribute absorbed energy is the fraction of total canister radial heat transfer which occurs via the canister side walls. This "side wall fraction" is plotted versus time in Figure 5.13 for three radial locations: r_i^+, r_o^-, and $(r_i + r_o)/2$. Side wall fractions generally run between 40 and 60 percent during the heat input period. Three distinctive dips in the curves are evident at times 12 minutes, 32 minutes, and 53 minutes for locations r_o^-, $(r_i + r_o)/2$, r_i^+, respectively. These dips are associated with the passage of the PCM melt front at which time radial PCM heat flow increases (thereby decreasing the side wall fraction) to support the melt front advancement.

During the heat removal period, side wall fractions are

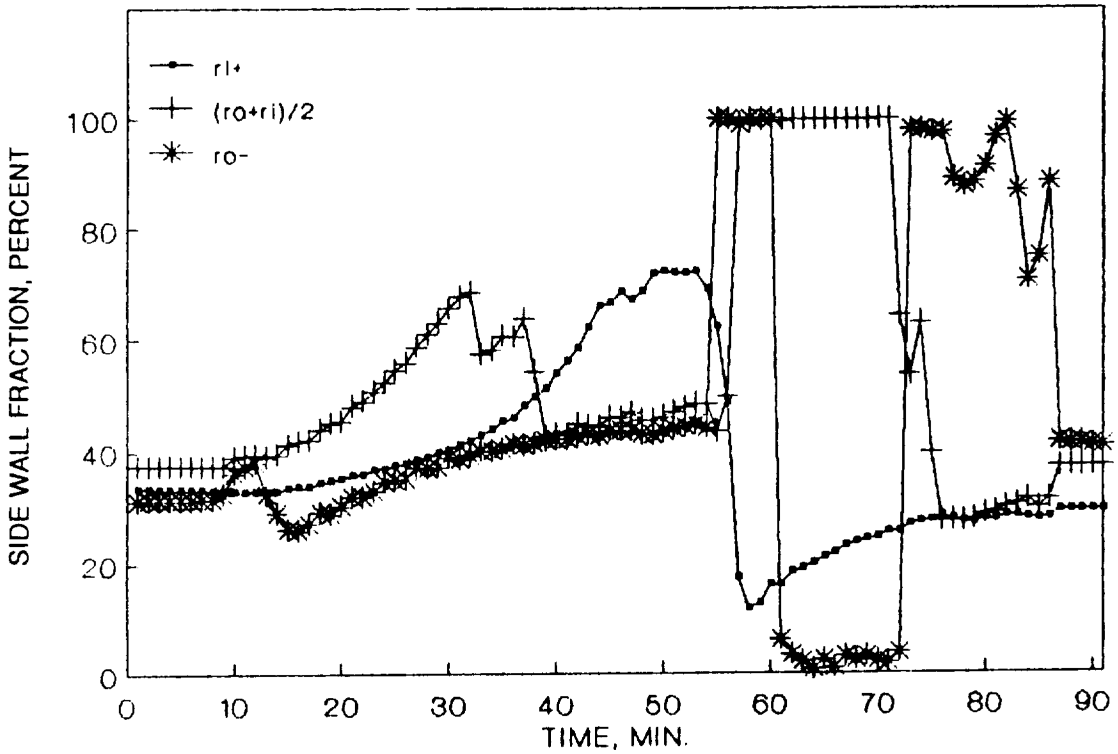

Figure 5.13. Fraction Of Total Canister Radial Heat Transfer Through Side Walls.

widely varying. The side wall fraction at r_o^- closely follows the variation in boundary heat flux, q(t). Initially, q(t) is negative which freezes a thin, isothermal PCM layer on the canister outer wall while a small, but finite, side wall temperature gradient exists. Thus, a side wall fraction in the 100 percent range is achieved. At ~62 minutes, the thin PCM layer has completely solidified creating relatively large PCM temperature gradients. At the same time, the negative outer wall absorbed heat flux, q(t), combined with inner wall convective cooling effectively flattens canister side wall radial temperature gradients near the outer radius. Thus, the side wall fraction approaches zero during this period. At 73 minutes, q(t) becomes positive and quickly re-establishes side wall temperature gradients forcing the side wall fraction up into the 70 to 100 percent range.

The opposite behavior occurs at the canister mean radius, $(r_i + r_o)/2$, during the heat removal period. As shown by Figure 5.10c, a small liquid PCM zone surrounded by solid and mushy PCM exists in the central portion of the canister volume. Radial temperature gradients through this liquid zone are essentially zero giving rise to 99 percent side wall fractions through the 71 minute point in the cycle. Thereafter, the PCM freeze front advances radially outward beyond $(r_i + r_o)/2$ establishing larger solid PCM temperature gradients in response to cooling fluid heat extraction at r_i. This forces side wall fractions back into the 30 to 40 percent range for the remaining portion of the cycle.

5.3.1.5 Limiting Effects of a Void

The effect of a void on transient canister wall temperatures has not been quantified with the two-dimensional analyses described in this section. However, to derive a preliminary estimate of how a void could potentially increase predicted wall temperatures, the extreme case of a canister filled with PCM of zero thermal conductivity was analyzed. For this case, peak canister wall temperatures run between 20 K and 135 K higher than what is predicted for the canister with finite conductivity PCM. The likely peak wall temperature for a canister containing PCM with a void will be somewhere between the predictions of these two cases. Results from this analysis provide an upper limit of canister wall temperatures which are useful in developing the two-dimensional void heat transfer model. Canister thermal performance predictions with a void are discussed in the next section.

5.3.2 Canister With Void Model

5.3.2.1 Temperature and PCM Phase Distributions

Figure 5.14 illustrates canister temperature contour and

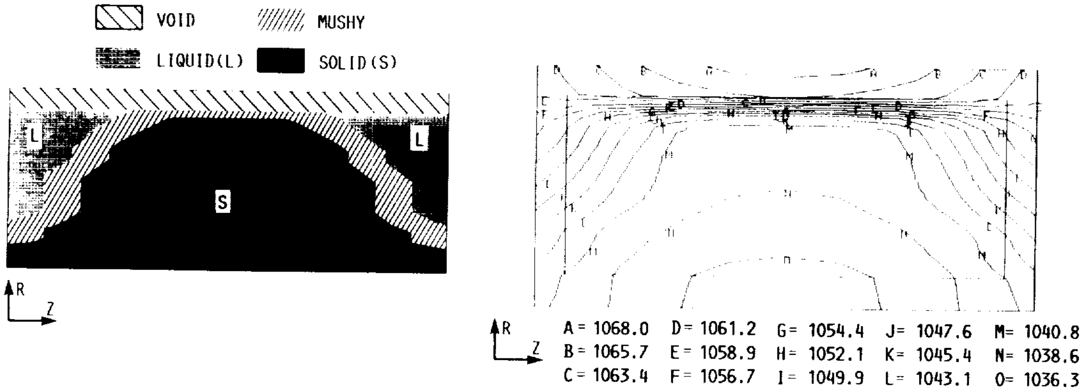

(a) TIME = 24.28 MIN MFL=0.3244 VVF=0.1507 NU=1.000

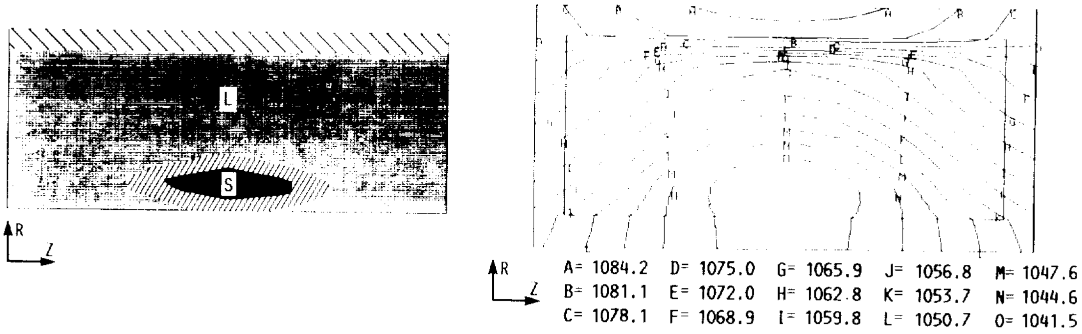

(b) TIME = 48.56 MIN MFL=0.9097 VVF=0.1507 NU=1.000

Figure 5.14. Canister Temperature Contour (Deg K) And PCM Phase Maps With Void.

(a) Time=24.28 min., MFL=0.3244, VVF=0.1507, Nu=1.000
(b) Time=48.56 min., MFL=0.9097, VVF=0.1507, Nu=1.000

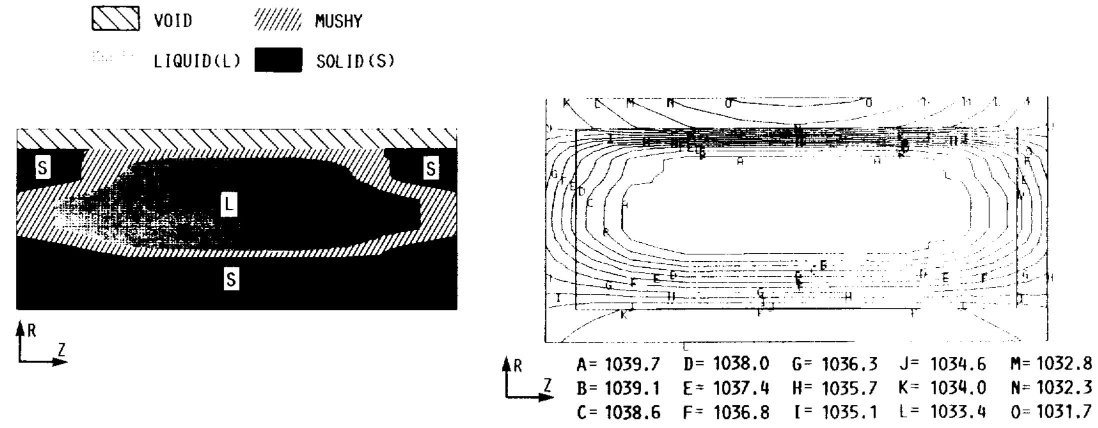

(c) TIME = 69.80 MIN MFL=0.5137 VVF=0.1507 NU=1.000

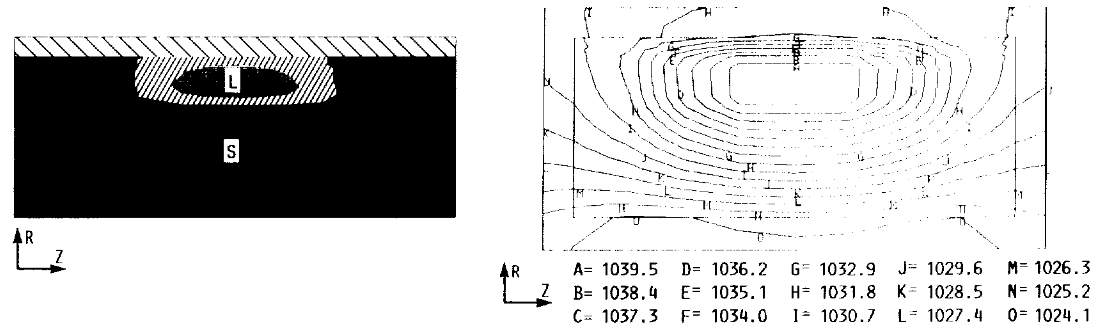

(d) TIME = 81.94 MIN MFL=0.0933 VVF=0.1507 NU=1.000

Figure 5.14. Canister Temperature Contour (Deg K) And PCM Phase Maps With Void.

(c) Time=69.80 min., MFL=0.5137, VVF=0.1507, Nu=1.000
(d) Time=81.94 min., MFL=0.0933, VVF=0.1507, Nu=1.000

PCM phase maps at four times (24.28, 48.56, 69.80, and 81.94 minutes) during a 91 minute orbital melt-freeze cycle. The PCM melting portion of the cycle occurs from time = 0 to ~55 minutes while PCM freezing occurs for the remaining portion of the cycle from time = ~55 to ~91 minutes. Initially, all PCM is solid at time = 0 minutes. During the PCM melting period, the large void thermal resistance forces a large percentage of canister heat transfer to occur via canister walls. This is illustrated in Figure 5.14a which shows high temperature gradients in the void region and isotherm normals (i.e., the direction of heat flow) generally aligned parallel to canister walls. Thus, energy absorbed in the canister outer wall diffuses around the void, down the side walls, and then into the PCM. As a consequence of this heat flow pattern, PCM melting occurs axially inward from both side walls. By time = 48.56 minutes when ~90 percent of the PCM is liquid (see Figure 5.14b), heat transfer axially along the canister inner wall initiates PCM melting radially outward until all the PCM is liquified at time = ~55 minutes.

PCM melting along the container walls is an extremely beneficial attribute of this TES canister design from a long-term structural integrity point of view. The two primary benefits include 1) structurally decoupling the solid PCM from the canister side walls and 2) providing a means through which expanding liquid PCM can flow into the void during the melting process. Decoupling the PCM from the metal reduces canister thermal stresses created by differential thermal expansion between the PCM and metallic containment structure. PCM liquid flow paths to the void are highly desirable to preclude pressurizing entrapped liquid regions and the concomitant build-up of potentially large canister wall stresses. The importance of providing pressure relief flow paths is underscored by one experimental study involving a large volume of PCM (i.e., a cube with 30 cm long sides), see Sparrow et al. (1978). For this experiment, the apparatus was constructed with a so-called vent heater installed in the PCM to guarantee a liquid flow path from the primary heated PCM region to the container void space.

During PCM freezing, the heat of fusion energy liberated is transferred to the engine working fluid that cools the canister inner wall and to the canister outer wall where radiative heat loss to the receiver cavity occurs. Because the void acts as a thermal insulator, much of the heat loss from the liquid PCM to the canister outer wall occurs via conduction in canister side walls. As a consequence of this heat flow pattern, PCM freezing occurs along the canister inner wall and along the void surface. In addition, the maximum side wall temperature exists at about the radial midpoint (see Figure 5.14c). Near the end of the orbital cycle at time = 81.94 minutes, ~90 percent of the PCM is frozen and the last remaining liquid PCM exists adjacent to void (see Figure 5.14d). Side wall radial temperature profiles have been reestablished with temperature increasing in the positive radial direction. This is due to a small radiative heat input to the canister outer wall from the receiver cavity during the last ~18 minutes of the orbital cycle (see Figure 3.3).

5.3.2.2 Void Heat Transfer

Figure 5.15 illustrates void radial heat transfer, Q_{void}, as a function of time during the orbital melt-freeze cycle. Q_{void} is comprised of vapor conduction and surface-to-surface radiation components. By convention, these components are taken as positive if the resulting heat transfer is radially inward. During PCM melting, void heat transfer via radiation is about 3 times greater than that by vapor conduction and both components are positive and remain fairly constant. During PCM freezing, radiation is about 2 times greater than vapor conduction and both components remain negative until ~85 minutes into the cycle when all the PCM has frozen. The jump in the curves at ~72 minutes is associated with the outer wall radiative heat flux boundary condition going from negative to positive.

The fact that both components of void heat transfer remain negative from ~72 to ~85 minutes has interesting implications for the canister heat flow pattern. For this time period, relatively warm PCM transfers heat radially outward across the void to the canister outer wall where it

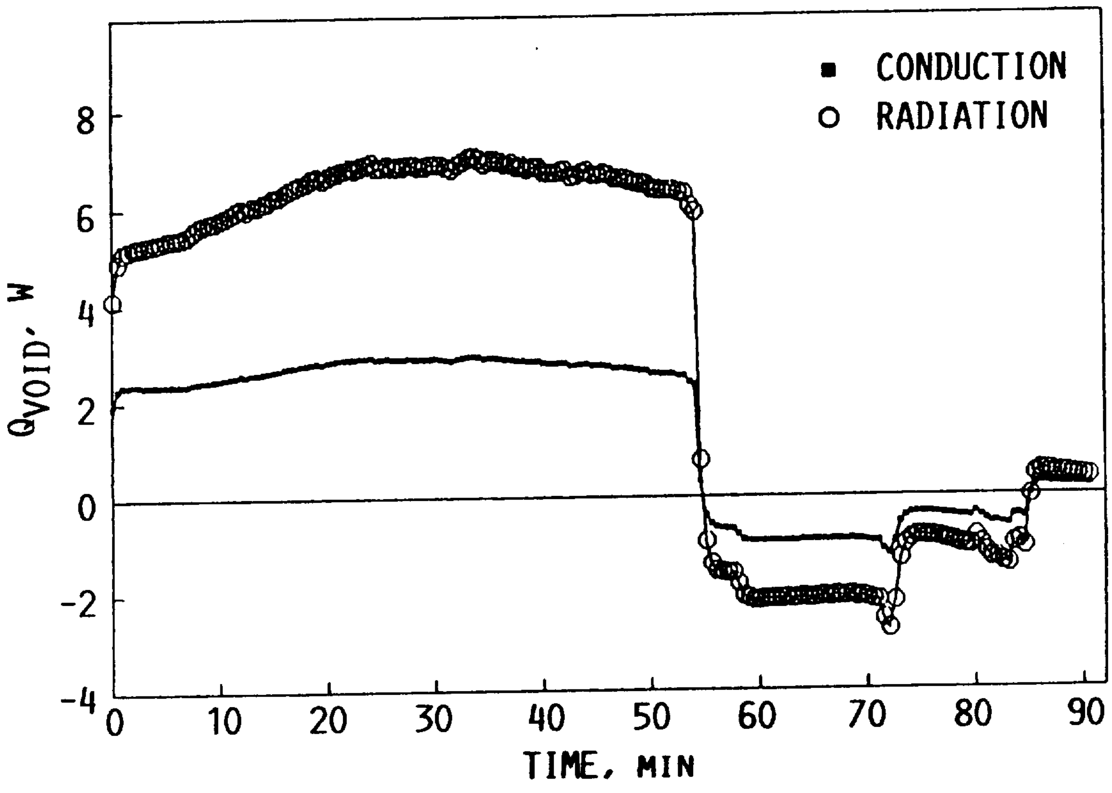

Figure 5.15. Void Radial Heat Transfer.

is then transferred back down the canister side wall and into the engine working fluid coolant (see Figure 5.14d).

The conservative placement of a vapor-filled void volume adjacent to the canister outer wall generates the two negative effects of increased wall temperatures and increased wall temperature gradients (when compared to the case without void) during PCM melting. These effects increase canister thermal stresses and decrease canister design life predictions based on cumulative creep damage theory. Introduction of a void also reverses the sign of the side wall temperature gradient during the first half of PCM freezing period which does not occur in the case without a void. The resulting change in the canister side wall thermal stress distribution and the resulting impact (good, bad or indifferent) on canister life prediction is not easily determined without detailed structural analysis.

A potentially beneficial effect of a void placed at the canister outer wall is a reduction in canister heat loss (more precisely, canister heat exchange with other canisters in the receiver cavity and heat loss out the cavity aperture) during PCM freezing due to the insulating quality of the void. The greatest canister heat loss occurs in the hottest canisters located near the aperture end of the receiver cavity (see Figure 2.2). These canisters are also located on the coolant tube near the inlet manifold and are thus cooled by relatively low temperature heat engine working fluid. Reduction of heat loss from these hottest canisters permits greater heat transfer to the relatively cool working fluid near the inlet end of the coolant tube thereby decreasing the required working fluid heat transfer of canisters further down-stream. This, in turn, reduces the required temperature of down-stream canisters which must transfer heat to the highest temperature working fluid.

5.3.3 Canister With Void and Free Convection Models

5.3.3.1 Temperature and PCM Phase Distributions

Figure 5.16 illustrates the corresponding canister temperature contour and PCM phase maps for a 91 minute melt-freeze cycle which includes free convection in the liquid PCM. Figure 5.16a is identical to Figure 5.14a since the liquid PCM Rayleigh number (Ra) is below the critical Ra number and liquid PCM heat transfer is still controlled by conduction. Thus, no convective heat transfer enhancement takes place during the early part of the orbital cycle. At about 30 minutes into the cycle, the critical Ra number is exceeded and the Nu number begins steadily increasing from 1.0 to a value of 4.5 at the end of the melting period (~55 minutes). Free convection in the liquid increases the rate of PCM melting and decreases canister temperature gradients as shown in Figure 5.16b where Nu = 3.047. During the PCM freezing portion of the cycle, liquid convective effects quickly die out and the Nu number falls back to 1.0 by ~60

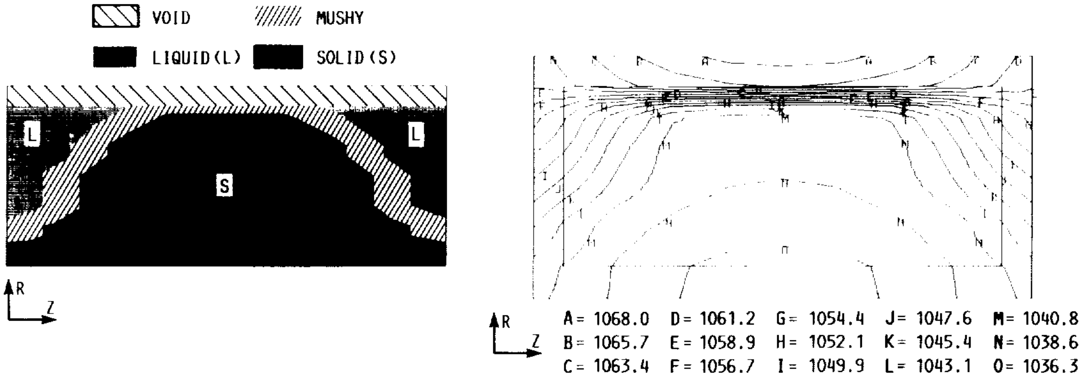

(a) TIME = 24.28 MIN MFL=0.3244 VVF=0.1507 NU=1.000

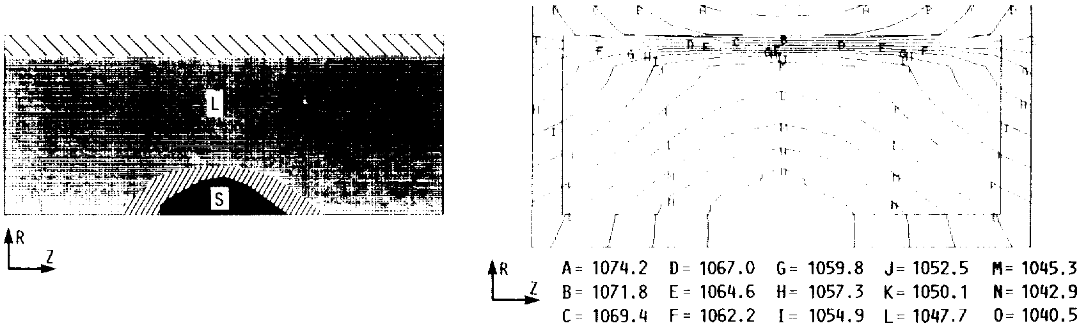

(b) TIME = 48.55 MIN MFL=0.9397 VVF=0.1507 NU=3.047

Figure 5.16. Canister Temperature Contour (Deg K) And PCM Phase Maps With Void And Free Convection.

(a) Time=24.28 min., MFL=0.3244, VVF=0.1507, Nu=1.000
(b) Time=48.55 min., MFL=0.9397, VVF=0.1507, Nu=3.047

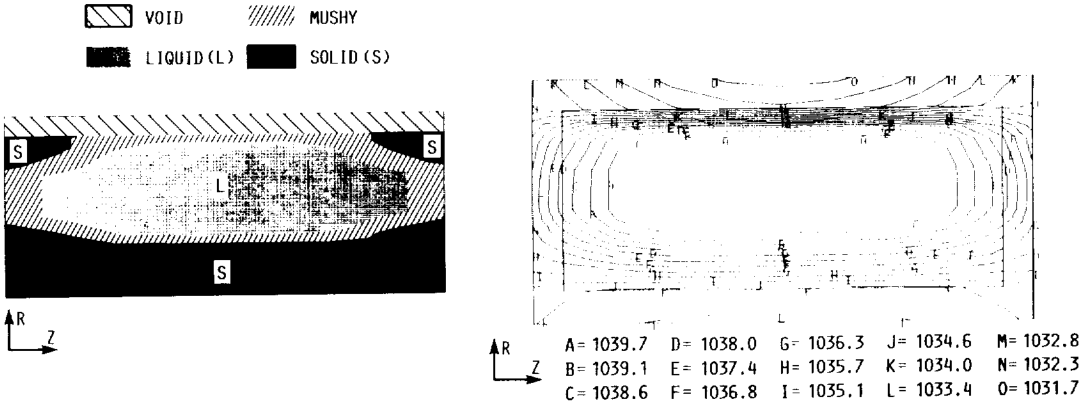

(c) TIME = 69.80 MIN MFL=0.5305 VVF=0.1507 NU=1.000

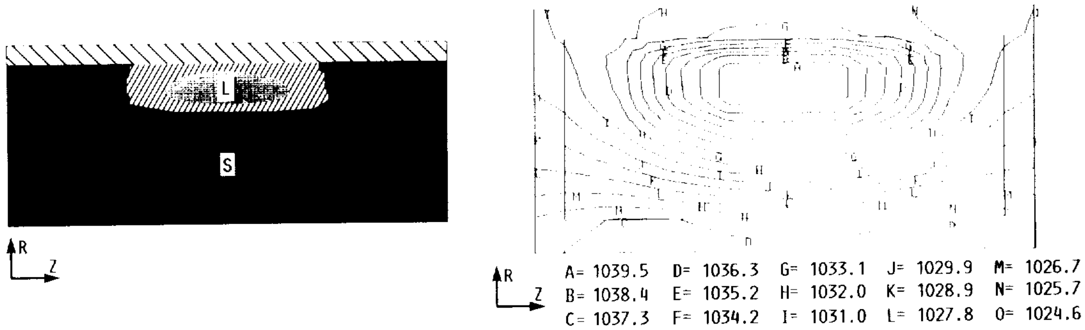

(d) TIME = 81.94 MIN MFL=0.1074 VVF=0.1507 NU=1.000

Figure 5.16. Canister Temperature Contour (Deg K) And PCM Phase Maps With Void And Free Convection.

(c) Time=69.80 min., MFL=0.5305, VVF=0.1507, Nu=1.000
(d) Time=81.94 min., MFL=0.1074, VVF=0.1507, Nu=1.000

minutes into the cycle. Thus, for the majority of the PCM freezing period, liquid PCM heat transfer is again controlled by conduction. Hence, Figures 5.16c and 5.16d are nearly identical to Figures 5.14c and 5.14d with the exception that slightly more liquid PCM exists at the times of comparison for the case with free convection, i.e. the values of MFL (PCM mass fraction liquid) are slightly greater.

5.3.3.2 Effects of Free Convection

Although relatively large Nu numbers exist during the PCM melting period, the length of time in which they occur is short. Thus over this short period of time, canister thermal performance in a 1-g environment, defined in terms of maximum wall temperature, canister temperature gradients, and PCM melting rate and/or PCM utilization, is not greatly different from that expected in a micro-g environment. For roughly 25 percent of canisters in the receiver cavity that contain high quality two-phase PCM (i.e., $0.5 < \text{MFL} < 1.0$), a small reduction in maximum wall temperature and a small increase in PCM utilization would be expected during 1-g operation as a consequence of liquid PCM convection. For roughly 50 percent of the canisters that contain completely liquified PCM, approximately the same cyclic temperature range during 1-g and micro-g operation would be experienced. However, these canisters would experience a slightly lower "time-at-maximum-temperature" history. For the remaining 25 percent of canisters containing low quality two-phase PCM (i.e., $0.0 < MFL < 0.5$), thermal performance would be essentially unaffected. Therefore, within the scope of this analysis, results indicate that canister thermal performance during ground tests should not be significantly different than that expected on-orbit.

5.3.3.3 Free Convection Model Assumptions

These results must be interpreted in light of the assumptions of 1) axisymmetry (which requires alignment of the gravity vector and the canister axis of symmetry), 2) constant radiative flux input conditions at the canister outer wall in each case considered, 3) a prescribed void shape and location, and 4) axial-averaged liquid PCM characteristic length and radial temperature difference. Assumption 1 restricts the validity of analytical results to a ground test configuration with the canister axis vertical and with circumferentially uniform outer wall heating. Assumption 2 limits the available latitude for direct case-to-case comparison of results since large differences in canister temperature predictions invalidates the assumption of identical outer wall heat flux conditions in each case. This holds true since the canister outer wall boundary condition is a function of the radiation environment in the receiver cavity as well as canister outer wall temperature.

Assumption 3 removes the possibility of different void shapes and locations that are likely to occur between 1-g canister tests and micro-g canister operation. However, the canister performance differences associated with void shape and more importantly, void location, are bounded by results from two cases considered herein, i.e. a canister without a void and a canister with a void conservatively located adjacent to the outer wall. This assumption is further discussed in section 5.3.4.

5.3.3.4 Free Convection Model With Local Nu Numbers

The validity of assumption 4) was checked by incorporating a local Nu number calculation into the two-dimensional canister computer program. For this calculation, the liquid PCM region characteristic length and radial temperature difference were determined for each PCM axial element group along the canister length from which a "z-dependent" Nusselt number, Nu(z), was calculated. Thus, the possibility for greater liquid PCM conductivity enhancement is permitted in locations adjacent to canister side walls where PCM liquifies first over centrally located PCM which liquifies last.

Figure 5.17 shows Nu(z) as a function of time for the first 4 out of 8 PCM axial element groups. Nu(z) for the last 4 element groups are not shown since near longitudinal symmetry exists. The local Nu number first exceeds 1.0 at

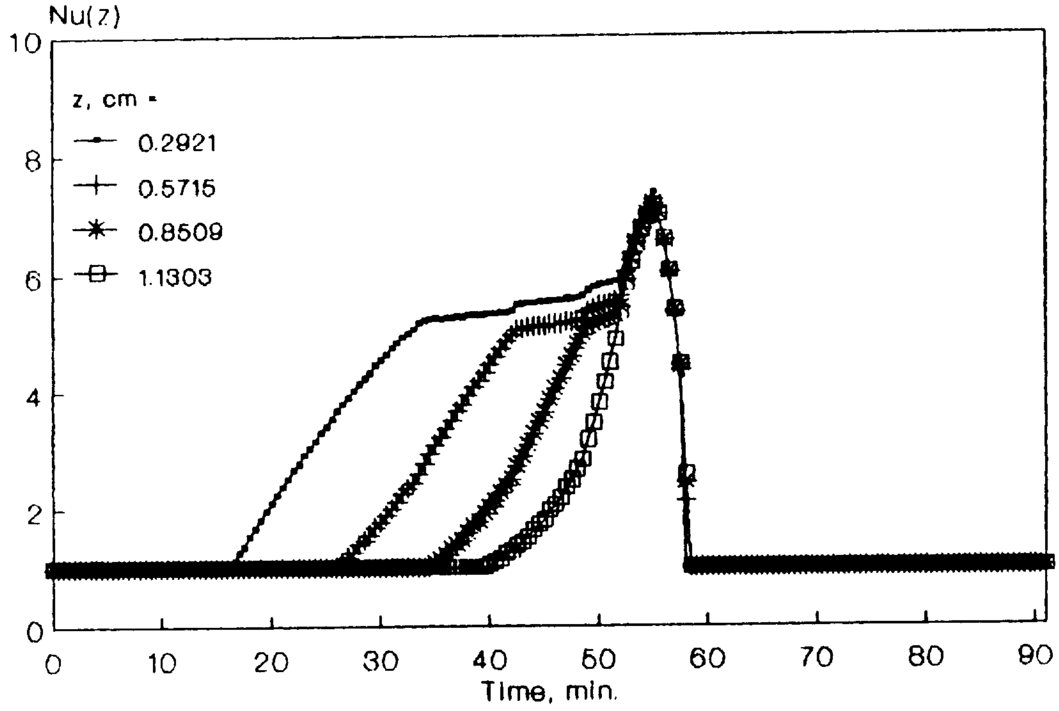

Figure 5.17. Liquid PCM Nu Axial Variation.

z=0.2921 cm which is the coordinate of the PCM element group adjacent to the canister side wall at z=0. Further into the TES charging period, local Nu numbers exceed 1.0 at progressively larger z values until the last Nu(z) exceeds 1.0 for the centrally located PCM element group at z=1.1303 cm. The local Nu numbers individually increase to a plateau of about 5.5. This value corresponds to conditions of maximum characteristic length and moderated temperature difference due to the presence of two-phase PCM. At about 52 minutes into the TES charging period, the 4 Nu(z) curves coalesce which corresponds to the time when complete PCM liquefication has occurred. Nu(z) values then increase to a maximum value of about 7.5 at the end of the TES charging period in response to higher outer wall temperatures.

Figure 5.18 shows a comparison of the previously calculated overall Nu number and the arithmetic mean of local Nu numbers calculated for one PCM charge-discharge cycle. The mean value of Nu(z), at any given instant, is about 60 to 70 percent higher than the overall Nu number calculated. This increase is attributed to the smaller effective convective cell aspect ratio, i.e. the PCM liquid height-to-width ratio. Yet the resulting impact on canister thermal performance is minimal. The predicted temperature and PCM phase distributions are nearly identical to those in Figure 5.16 in which the overall Nu number calculation was used. The predicted maximum canister wall temperature at any given time is not more than 5 K lower and the PCM mass

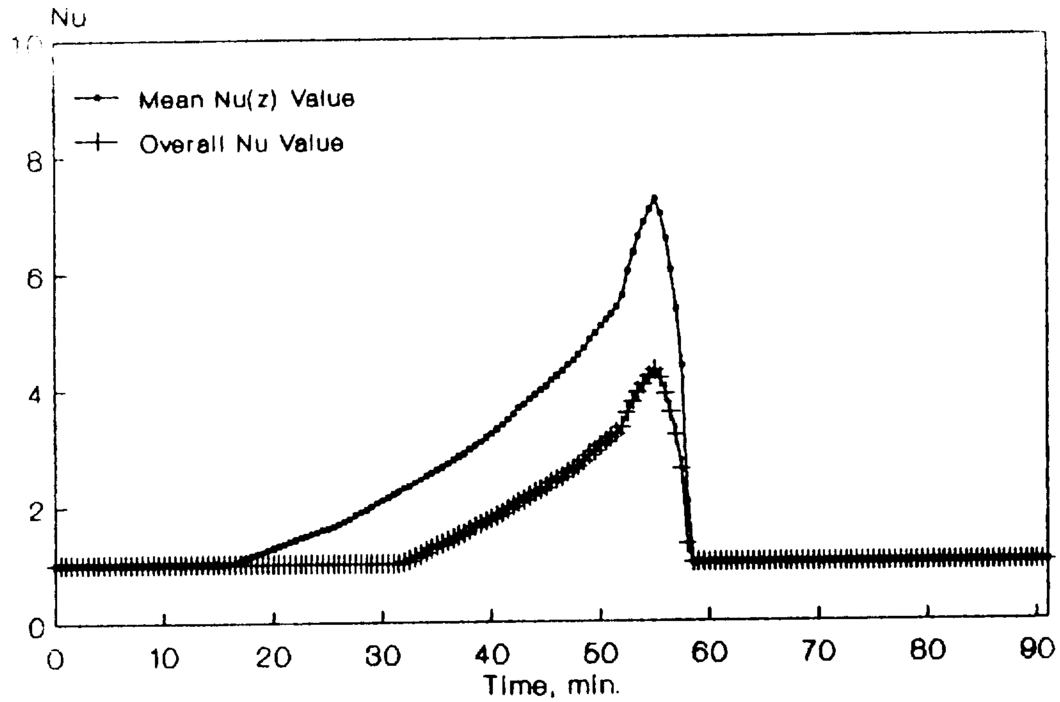

Figure 5.18. Liquid PCM Nu Comparison.

fraction liquid increases by only 1 to 2 percent. Therefore, the overall Nu number calculation method, which uses an averaged liquid PCM characteristic length and radial temperature difference, appears to be a satisfactory approach to further simplify modeling of convection effects in the liquid PCM region whose geometry is axially dependent.

5.3.4 Performance Comparison

In this section, results from three canister analytical cases are compared: 1) without a void, 2) with a void, and 3) with a void and liquid PCM free convection (axial-averaged). Comparison of results from cases 1 and 2 is intended to isolate the impacts of a void on canister heat transfer performance. Comparison of results from cases 2 and 3 is intended to show likely canister performance differences during ground testing (in 1-g) and flight operation (in micro-g).

5.3.4.1 Maximum Wall Temperatures

Figure 5.19 illustrates the maximum canister wall temperature, $T(r,z)_{max}$, throughout the 91 minute orbital cycle for cases 1, 2, and 3. $T(r,z)_{max}$ occurs at the axial midpoint of the outer wall and does not vary in position for the majority of the cycle. The introduction of a void

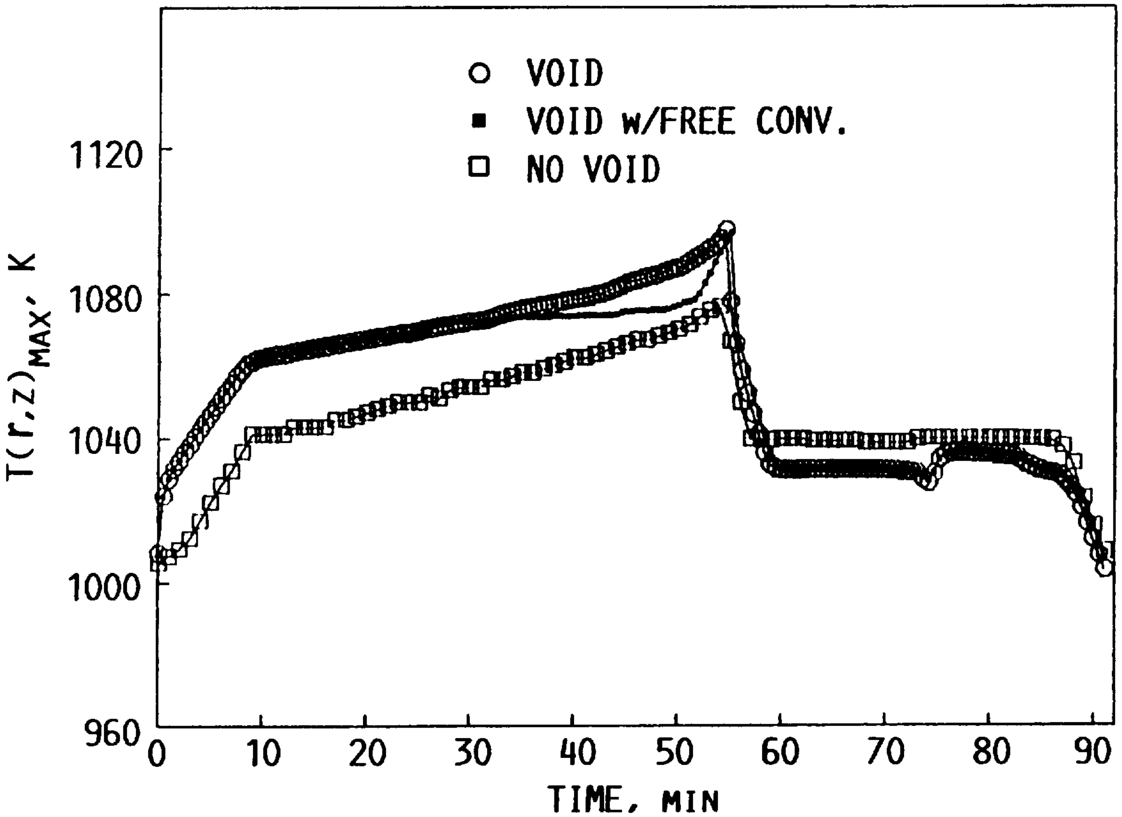

Figure 5.19. Maximum Canister Wall Temperature.

increases $T(r,z)_{max}$ about 20 K during the PCM melting period (0 to ~55 minutes) and decreases $T(r,z)_{max}$ about 10 K during the PCM freezing period (~55 to ~91 minutes). These changes are associated with the large void thermal resistance which increases outer wall axial temperature gradients by ~100 percent and increases side wall radial temperature gradients by ~80 percent during the PCM melting period.

The inclusion of liquid PCM free convection reduces $T(r,z)_{max}$ 0 to 10 K for the time between ~30 and ~55 minutes and has essentially no impact during other time periods (see Figure 5.19). During the same period, canister wall temperature gradients are ~20 percent lower and the MFL is about 2 percent greater than for the case without free convection. Note that a further temperature reduction of up to 5 K is predicted when a local Nu is incorporated into the analysis. It is also interesting to note that although convective effects moderate the increase in $T(r,z)_{max}$ during PCM melting, total PCM liquefication occurs earlier than for the case without free convection. Thus, sensible heating of the liquid PCM occurs and quickly increases $T(r,z)_{max}$ to about the same value that is predicted for the case without free convection.

5.3.4.2 Side Wall Heat Transfer Fractions

Figure 5.20 illustrates the fraction of total canister radial heat transfer (comprised of void conduction, void

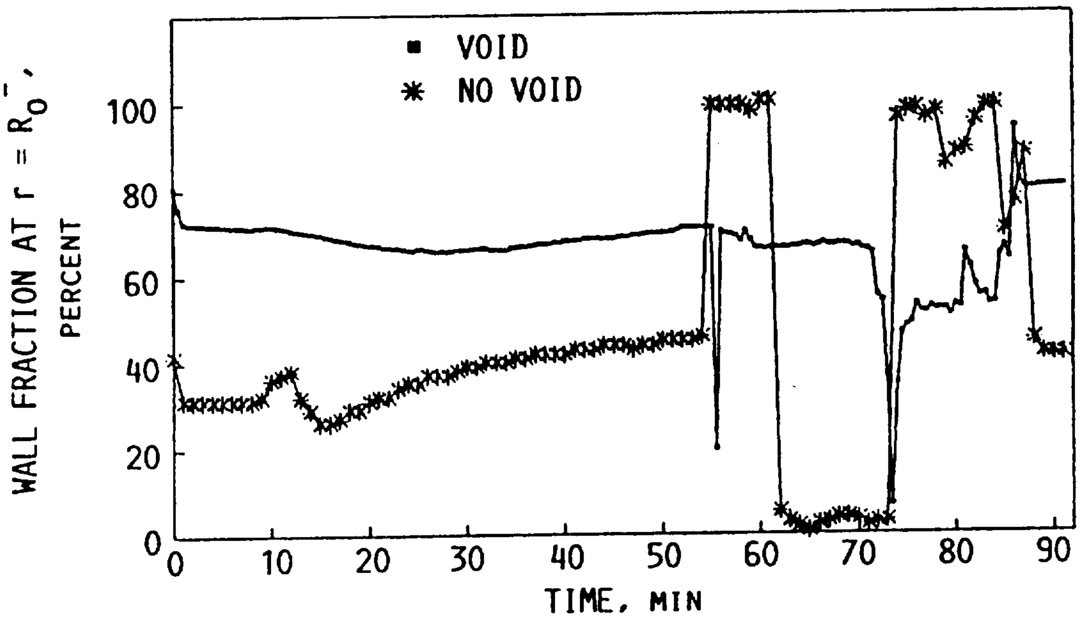

Figure 5.20. Radial Heat Transfer Side Wall Fraction.

radiation, and canister wall conduction) that occurs by conduction in the two canister side walls. This "side wall fraction" was evaluated at the radial location corresponding to the inner surface of the outer canister wall, R_o^-. The side wall fraction is a quantitative measure of how effectively canister walls redistribute energy absorbed in the outer wall and also provides a qualitative indication of wall temperature sensitivity to void location.

The side wall fraction is relatively constant at ~70 percent for the case with a void (see Figure 5.20, "void" curve). Large perturbations in side wall fraction occur for brief periods of time at ~55, ~72, and ~85 minutes. The three perturbations are associated with two step changes in the outer wall heat flux boundary condition and the point of complete PCM solidification, respectively. For the case without a void, the side wall fraction is considerably lower, i.e. 30 to 50 percent, due to the relatively high thermal conductance of the PCM when compared to the void. The same three perturbations exist as in the case with the void in addition to another perturbation at ~62 minutes. This last perturbation is associated with a ~7 minute period (from ~55 to ~62 minutes) during which a thin layer of PCM freezes along the outer wall. Once frozen, relatively large temperature gradients exist within the PCM layer which reduces the side wall fraction to only a couple percent at 62^+ minutes.

5.3.4.3 Relationship Between Void Characteristics, Side Wall Fractions, and Wall Temperatures

The prescribed void shape and location were chosen to permit a relatively straight-forward numerical analysis and to generate conservative predictions of canister wall temperatures. To confirm that void heat transfer and void placement are conservative, consider the relationship between maximum canister wall temperature and the radial heat transfer side wall fraction. As shown in Figures 5.19 and 5.20, the canister wall radial heat transfer contribution can double (i.e., side wall fraction increases by ~2 times) with only a 20 K increase in maximum wall temperature during PCM melting. Since the side wall fraction, by definition, is bounded by a 100 percent value, further increases in canister wall heat transfer are limited to ~40 percent. Thus, regardless of the nature of void heat transfer, the increase in maximum canister wall temperature from introduction of a void is bounded by ~28 K or a $T(r,z)_{max}$ of 1105 K for these case runs. This $T(r,z)_{max}$ value is just slightly higher than that predicted for the canister with void case (see Figure 5.19). Additionally, for any other viable void shape and location, PCM would be placed in contact with the outer wall thereby lowering the side wall fraction (see Figure 5.20, "no void" curve) and hence, lowering the maximum wall temperature. Therefore, differences in void shape and location between canister 1-g ground tests and micro-g operation lead to relatively small changes in predicted canister thermal performance which are essentially bounded by the void cases considered herein.

Results from two-dimensional canister analyses show that the largest changes in $T(r,z)_{max}$ due to free convection and the introduction of a void are ~-15 K and ~+20 K, respectively. These changes are an order-of-magnitude lower than the changes predicted from one-dimensional analyses in section 5.2.2 and the wall temperature increases from a void are 100 K lower than the preliminary estimates of section 5.3.1. Therefore, this confirms the assertions from sections 5.2.2 and 5.3.1 that the effects of free convection and a void on canister thermal performance are much less pronounced in two-dimensional analyses than in a one-dimensional analyses. This result is attributed to the large heat transfer contribution of conduction within canister side walls.

CHAPTER VI

CONCLUSIONS

6.1 One-Dimensional Analyses

1. The present numerical solution methods accurately predict PCM canister thermal performance with and without the inclusion of a void (on the basis of comparisons with exact solutions).

2. For a given thermal energy storage requirement, a constant charge/discharge boundary temperature results in lower boundary temperature variations from T_m than with a constant flux boundary condition.

3. Modes of void heat transfer must be selected to be consistent with the void size, void thermophysical properties, and the anticipated thermal environment. For the problems considered herein, void heat transfer from canister wall to PCM is best analyzed as a combined conduction-radiation process.

4. The presence of a one-dimensional void reduces material phase change rate under constant temperature boundary conditions by a factor of 4 to 5 and increases canister wall temperatures under constant flux input conditions by 50 to 200 K.

5. The presence of liquid PCM free convection lowers canister wall temperatures by as much as 150 K and slightly enhances the PCM melting process during the heat input portion of the charge/discharge cycle. Free convection effects are essentially nonexistent during the TES discharge period.

6. Ground-based receiver and canister performance in 1-g will be improved over on-orbit, micro-g performance. Therefore, ground test configurations which minimize free convective effects are suggested. The recommended test configuration places the canister and receiver axes of symmetry parallel to the gravity vector and the direction of heat input normal to the gravity vector.

6.2 Two-Dimensional Analyses

1. Based on the PCM freezing pattern from analyses without a void, a central core void location completely surrounded by solid PCM is anticipated at the end of the discharge period if PCM density change is taken into account.

2. Canister walls effectively redistribute energy absorbed in the outer wall to the PCM and cooling fluid. Between 30 and 70 percent of the total canister radial heat transfer occurs by conduction within the canister side walls.

3. Introduction of a void at the canister outer diameter: a) increases peak wall temperatures by 20 K, b) doubles canister wall temperature gradients during PCM melting, and c) transforms a predominately radial melting process into a predominately axial melting process.

4. The void reduces radiative heat losses from the hottest canisters within the receiver cavity during the eclipse portion of the orbit. This beneficial effect improves the overall heat transfer to the engine working fluid and lowers canister temperatures during this period.

5. Void placement at the canister outer diameter is conservative and canister performance with any other viable void distribution is bounded by the performance predicted for the cases with and without a void considered herein.

6. The presence of free convection in the liquid PCM: a) lowers peak wall temperatures by 0 to 15 K during the second half of the PCM melting period, b) lowers canister wall temperature gradients by 20 percent, c) increases the mass fraction of liquid PCM by ~2 percent, and d) does not significantly alter the PCM melting/freezing process.

7. An axial-averaged Nu number approach for modeling liquid PCM free convection heat transfer effects is an acceptable engineering approximation to a more detailed, local Nu number approach.

8. One-dimensional analyses, that neglect canister side wall conduction, greatly over predict canister wall temperature changes associated with a void and free convection in the liquid PCM.

9. The differences in predicted canister performance between ground-based tests, in 1-g, and flight operation, in micro-g, are small on the basis of free convection heat transfer enhancement and void distribution effects.

6.3 Future Work

There are several options for extending the TES canister analytical work documented herein. Three particularly important options include: 1) further verification of analytical predictions, 2) extension of analytical methods to a three-dimensional canister geometry, and 3) parametric sensitivity and optimization studies.

Analysis verification is a planned activity which will quantify the validity of the many engineering assumptions used to analyze canister heat transfer. This activity will utilize ground-based test data currently being generated at NASA Lewis Research Center, flight test data to be available in mid-1993 (see Namkoong (1989)), numerical predictions from the computer program developed by Wilson and Flanery (1988), and other numerical solutions available in the literature for idealized phase change problems.

Extension to a three-dimensional geometry is necessary to predict non-axisymmetric canister thermal performance. The asymmetries are associated with: a) a non-uniform outer wall flux boundary condition (i.e., one half of the canister circumference is exposed to direct concentrated solar energy and thermal radiation exchange with the receiver cavity while the other half of the circumference is exposed to reflected and reradiated energy from the receiver internal cavity wall) and b) ground testing in an orientation that does not maintain the canister axis of symmetry aligned parallel with the gravity vector.

Parametric sensitivity studies are necessary to quantify the presumably small influence of uncertainties on analytical predictions. Uncertainties associated with the following items require consideration: material properties, boundary conditions, and the effective thermal conductance of the braze joint that attaches the canisters to cooling fluid tubes. Lastly, optimization studies could be performed to further refine the canister design. Variables on which to optimize include canister mass, PCM utilization, wall temperatures, and wall temperature gradients (i.e., thermal stresses).

BIBLIOGRAPHY

Bathelt, A. G., et al.,[1979],"An Experimental Investigation of Natural Convection in the Melted Region Around a Heated Horizontal Cylinder," J. Fluid Mech., vol. 90, pp. 227.

Bathelt, A. G., et al.,[1979],"Latent Heat-of-Fusion Energy Storage: Experiments on Heat Transfer from Cylinders During Melting," J. Heat Transfer, vol. 101, pp. 453-458.

Blumenberg, J., and Weingartner, S.,[1988],"Preparation of a D2-Experiment for Analyzing the Thermal Properties of Relevant High-Temperature Storage Media Under Microgravity," IAF-88-211, 39th Congress of the International Astronautical Federation, Bangalore, India, October 8-15.

Borucka, Alina,[1975],"Survey and Selection of Inorganic Salts for Application to Thermal Energy Storage," Report to U.S. Energy Research and Development Administration.

Carslaw, H. S., and Jaeger, J. C.,[1959],Conduction of Heat in Solids: 2nd Edition, Oxford University Press, pp. 282-296.

Chiesa, F. M., and Guthrie, R. I. L.,[1974],"Natural Convection Heat Transfer Rates During Solidification and Melting of Metal and Alloy Systems," J. Heat Transfer, vol. 96, pp. 377-384.

Concus, Paul, and Finn, Robert,[1990],"Dichotomous Behavior Of Capillary Surfaces In Zero Gravity," LBL-29225.

Deal, R., and Solomon, A. D.,[1981],"The Simulation of Four Pure Conduction Paraffin-wax Freezing Experiments," ORNL/CSD-74.

El-Sherbiny, S. M., et al.,[1982],"Heat Transfer By Natural Convection Across Vertical and Inclined Air Layers," J. Heat Transfer, vol. 104, pp. 96-102.

Flemings, Merton C.,[1974],Solidification Processing, McGraw-Hill.

Goldstein, R. J.,and Ramsey, J. W.,[1979],"Heat Transfer to a Melting Solid With Application to Thermal Energy Storage Systems," Heat Transfer Studies: Festschrift for E. R. G. Eckert, Hemisphere Publishing Corp., New York.

Grodzka, P. G. and Fan, C.,[1968],"Thermal Control by Freezing and Melting," NASA-CR-120641.

Hale, N. W., Jr., and Viskanta, R.,[1980],"Solid-liquid Phase-change Heat Transfer and Interface Motion in Materials Cooled or Heated From Above or Below," Int. J. Heat Mass Transfer, vol. 23, pp. 283.

Hollands, K. G. T., et al.,[1976],"Free Convection Heat Transfer Across Inclined Air Layers," J. Heat Transfer, vol. 98, pp. 189-193.

Humphries, William R.,[1974],"Performance of Finned Thermal Capacitors," NASA-TN-D-7690.

Kemink, R. G. and Sparrow, E. M.,[1981],"Heat Transfer Coefficients For Melting About a Vertical Cylinder With or Without Subcooling and For Open or Closed Containment," Int. J. Heat Mass Transfer, vol.24, pp. 1699.

Kerslake, Thomas W. and Ibrahim, Mounir B.,[1990],"Analysis of Thermal Energy Storage Material with Change-of-Phase Volumetric Effects," Proceedings of the 12th Annual ASME International Solar Energy Conference, ASME, New York, pp. 315-325. (see also, NASA TM-102457).

Kerslake, Thomas W. and Ibrahim, Mounir B.,[1990],"Two-Dimensional Model of a Space Station Freedom Thermal Energy Storage Canister," Proceedings of the 25th Intersociety Energy Conversion Engineering Conference, vol. 2, pp 151-159. (see also, NASA TM-103124).

Langbein, D., et al.,[1990],"Parabolic Flight Experiments on Fluid Surfaces and Wetting," Appl. Microgravity Tech. II, pp. 198-211.

Leuenberger, H., and Person, R. A.,[1956],"Compilation of Radiation Shape Factors For Cylindrical Assemblies," ASME, paper no. 56-A-144.

Minning, C. P.,[1979],"Shape Factors between Coaxial Annular Disks Separated by a Solid Cylinder," AIAA J., vol. 17, no. 3, pp. 318-320.

Namkoong, David,[1989],"Flight Experiment of Thermal Energy Storage," NASA TM-102081.

Özisik, M. Necati,[1985],Heat Transfer: A Basic Approach, McGraw-Hill, pp. 452-455.

Raithby, G. D., and Hollands, K. G. T.,[1975],"A General Method For Obtaining Approximate Solutions to Laminar and Turbulent Free Convection Problems," in T.F. Irvine and J. P. Hartnett (eds.), Advances in Heat Transfer, vol.11, Academic, New York, pp. 265-315.

Rea, Samuel N.,[1975],"Rapid Method for Determining Concentric Cylindrical Radiation View Factors," AIAA J., vol. 13, no. 8, pp. 1122-1123.

Sedgwick, L. M.,et al.,[1989],"A Brayton Cycle Solar Dynamic Heat Receiver For Space," Proceedings of the 24th Intersociety Energy Conversion Engineering Conference, vol.2, pp. 905-909.

Sheffield, J. W.,[1981],"Solidification of High Temperature Molten Salts for Thermal Energy Storage," AIAA 81-1049.

Siegel, Robert,[1967],"Effects of Reduced Gravity on Heat Transfer," Advances in Heat Transfer, vol. 4, edited by James P. Hartnett and Thomas F. Irvine, Jr., Academic Press, pp. 143-228.

Siegel, Robert, and Howell, John R.,[1981],Thermal Radiation Heat Transfer: 2nd Edition, Hemisphere Publishing Corporation, pp. 243.

Siegel, R.,[1982],"Analysis of Solidification Interface Shape Resulting From Applied Sinusoidal Heating," Journal of Heat Transfer, vol. 104, pp. 13-18.

Siegel, Robert,[1985],"Analysis of Three-dimensional Solidification Interface Shape," Int. J. of Heat Mass Transfer, vol. 28, no. 3, pp. 701-705.

Solomon, A. D.,[1979],"Mathematical Modeling of Phase Change Processes for Latent Heat Thermal Energy Storage," ORNL/CSD-39.

Solomon, Alan,[1981],"A Note on the Stefan Number in Slab Melting and Solidification," Letters in Heat and Mass Transfer, Vol. 8, pp. 229-235.

Solomon, A. D. and Wilson, D. G.,[1986],"A Stefan-Type Problem With Void Formation and Its Explicit Solution," ORNL-6277.

Solomon, A. D., et al.,[1986],"The Development of a Simulation Code for a Latent Heat Thermal Energy Storage System in a Space Station," ORNL-6213.

Sparrow, E. M., et al.,[1962],"Radiative Effectiveness of Annular-Finned Space Radiators, Including Mutual Irradiation Between Radiator Elements," J. Aerospace Sci., vol. 29, no. 11, pp. 1291-1299.

Sparrow, E. M., et al.,[1977],"Analysis of Melting in the Presence of Natural Convection in the Melt Region," J. Heat Transfer, vol. 99, pp. 520.

Sparrow, E. M., et al.,[1978],"Experiments on the Role of Natural Convection in the Melting of Solids," J. Heat Transfer, vol. 100, pp. 11.

Springer, George S. and Olson, Donald R.,[1962],"Method of Solution of Axisymmetric Solidification and Melting Problems," Transactions of the ASME, 62-WA-246.

Strumpf, Hal J. and Coombs, Murray G.,[1987],"Solar Receiver for the Space Station Brayton Engine," Transactions of the ASME, 87-GT-252.

Strumpf, Hal J., and Coombs, Murray G.,[1989],"Solar Receiver Experiment for the Hybrid Space Station Brayton Engine," ASME Solar Energy Division Conference, San Diego, California.

Szekeley, J., and Chhabra, P. S.,[1970],"The Effect of Natural Convection on the Shape and Movement of the Melt-Solid Interface in the Controlled Solidification of Lead," Metallurgical Trans., vol.1, pp. 1195-1203.

Tanaka, Kotaro, et al.,[1989],"Advanced Concepts for Latent Thermal Energy Storage for Solar Dynamic Receivers," Space Power, vol. 8, no. 4, pp. 425-434.

Taylor, M. F., et al.,[1988],"Internal Forced Convection to Low-Prandtl-Number Gas Mixtures," Int. J. Heat Mass Transfer, Vol. 31, No. 1, pp. 13-25.

Thibault, Jules,[1985],"Comparison of Nine Three-Dimensional Numerical Methods for the Solution of the Heat Diffusion Equation," Numerical Heat Transfer, Vol. 8, pp. 281-298.

Tong, M. T., Kerslake, T. W. and Thompson, R. L.,[1988], "Structural Assessment of a Space Station Solar Dynamic Heat Receiver Thermal Energy Storage Canister," AIAA SDM Issues of the International Space Station, Williamsburg Virginia, April 21-22, pp. 162-172.

Torab, Hamid,[1989],"Optimal Design of Thermal Energy Storage for Space Power," Space Power, vol. 8, no. 4, pp. 415-423.

Viterna, Larry Alan,[1989],"A Finite Element Model Of Conduction, Convection, and Phase Change Near A Solid/Melt Interface," Ph.D. dissertation, The University of Michigan, Ann Arbor, Michigan.

Wichner, R. P., et al.,[1988],"Thermal Analysis of Heat Storage Canisters for a Solar Dynamic, Space Power System," ORNL/TM-10665.

Wilson, D. G., and Flanery, R. E.,[1988],"Modeling Cyclic Melting and Refreezing in a Hollow Metal Canister," ORNL-6497.

Yao, L. S., and Prusa, J.,[1989], "Melting and Freezing," Advances in Heat Transfer, edited by James P. Hartnett and Thomas F. Irvine, Jr., Academic Press Inc., pp. 12.

APPENDICES

Appendix A1. Finite-Difference Equations

The finite-difference energy balance equations for six canister model elements is given in Appendix A1. The six elements are located in the following positions: 1) in the central PCM (1<i<ivl, 1<j<jj), 2) in the PCM at the PCM-void interface (i=ivl, 1<j<jj), 3) in the canister outer wall (i=ii, 1<j<jj), 4) in the canister side wall adjacent to the void (ivl<i<ii, j=1), 5) in the canister side wall adjacent to PCM (1<i<ivl, j=jj), and 6) in the canister inner wall (i=1, 1<j<jj). The element numbering system is shown in Figure 4.1 and the symbols used in the following equations are defined in the nomenclature and/or in Appendix A2, section A2.2.

Element 1

$$\begin{aligned} E_{i,j}^{n+1}=E_{i,j}^{n} &+C1_{i,j}*kip_{i,j}^{n}*[T_{i+1,j}^{n}-T_{i,j}^{n}] \\ &+C2_{i,j}*kim_{i,j}^{n}*[T_{i-1,j}^{n}-T_{i,j}^{n}] \\ &+C3_{i,j}*kjp_{i,j}^{n}*[T_{i,j+1}^{n}-T_{i,j}^{n}] \\ &+C4_{i,j}*kjm_{i,j}^{n}*[T_{i,j-1}^{n}-T_{i,j}^{n}] \;. \end{aligned} \tag{A.1}$$

Element 2

$$\begin{aligned} E_{i,j}^{n+1}=E_{i,j}^{n} &+C2_{i,j}*kim_{i,j}^{n}*[T_{i-1,j}^{n}-T_{i,j}^{n}] \\ &+C3_{i,j}*kjp_{i,j}^{n}*[T_{i,j+1}^{n}-T_{i,j}^{n}] \\ &+C4_{i,j}*kjm_{i,j}^{n}*[T_{i,j-1}^{n}-T_{i,j}^{n}] \\ &-econ_{j}^{n}-qrad_{j-1}^{n}*\Delta t \;. \end{aligned} \tag{A.2}$$

Element 3

$$\begin{aligned}E_{ii,j}^{n+1}=E_{ii,j}^{n} &+C3_{ii,j}*kjp_{ii,j}^{n}*[T_{ii,j+1}^{n}-T_{ii,j}^{n}]\\ &+C4_{ii,j}*kjm_{ii,j}^{n}*[T_{ii,j-1}^{n}-T_{ii,j}^{n}]\\ &+econ_{j}^{n}+q*C10-qrad_{j+jj-3}^{n}*\Delta t\ .\end{aligned}\tag{A.3}$$

Element 4

$$\begin{aligned}E_{i,j}^{n+1}=E_{i,j}^{n} &+C1_{i,j}*kip_{i,j}^{n}*[T_{i+1,j}^{n}-T_{i,j}^{n}]\\ &+C2_{i,j}*kim_{i,j}^{n}*[T_{i-1,j}^{n}-T_{i,j}^{n}]\\ &+C3_{i,j}*kjp_{i,j}^{n}*[T_{i,j+1}^{n}-T_{i,j}^{n}]\\ &-qrad_{2*jj-3}^{n}*\Delta t\ .\end{aligned}\tag{A.4}$$

Element 5

$$\begin{aligned}E_{i,j}^{n+1}=E_{i,j}^{n} &+C1_{i,j}*kip_{i,j}^{n}*[T_{i+1,j}^{n}-T_{i,j}^{n}]\\ &+C2_{i,j}*kim_{i,j}^{n}*[T_{i-1,j}^{n}-T_{i,j}^{n}]\\ &+C4_{i,j}*kjm_{i,j}^{n}*[T_{i,j-1}^{n}-T_{i,j}^{n}]\ .\end{aligned}\tag{A.5}$$

Element 6

$$\begin{aligned}E_{i,j}^{n+1}=E_{i,j}^{n} &+C1_{i,j}*kip_{i,j}^{n}*[T_{i+1,j}^{n}-T_{i,j}^{n}]\\ &+C3_{i,j}*kjp_{i,j}^{n}*[T_{i,j+1}^{n}-T_{i,j}^{n}]\\ &+C4_{i,j}*kjm_{i,j}^{n}*[T_{i,j-1}^{n}-T_{i,j}^{n}]\\ &+C8*[T_{f\ j}^{n}-T_{i,j}^{n}]\ .\end{aligned}\tag{A.6}$$

In the above equations, the coefficient terms and the conductor terms are defined by:

$$C1_{i,j}=2*\pi*\Delta z_{j}*\Delta t/\ln[r_{i+1}/r_{i}]\ ,\tag{A.7}$$

$$C2_{i,j}=2*\pi*\Delta z_{j}*\Delta t/\ln[r_{i}/r_{i-1}]\ ,\tag{A.8}$$

$$C3_{i,j}=4*\pi*r_{i}*\Delta r_{i}*\Delta t/[\Delta z_{j+1}+\Delta z_{j}]\ ,\tag{A.9}$$

$$C4_{i,j}=4*\pi*r_i*\Delta r_i*\Delta t/[\Delta z_j+\Delta z_{j-1}] \quad , \tag{A.10}$$

$$kip_{i,j}{}^n=k_{i+1,j}{}^n*k_{i,j}{}^n*[\Delta r_{i+1}+\Delta r_i]/[k_{i+1,j}{}^n*\Delta r_i+k_{i,j}{}^n*\Delta r_{i+1}] \quad , \tag{A.11}$$

$$kim_{i,j}{}^n=k_{i-1,j}{}^n*k_{i,j}{}^n*[\Delta r_{i-1}+\Delta r_i]/[k_{i-1,j}{}^n*\Delta r_i+k_{i,j}{}^n*\Delta r_{i-1}] \quad , \tag{A.12}$$

$$kjp_{i,j}{}^n=k_{i,j+1}{}^n*k_{i,j}{}^n*[\Delta z_{j+1}+\Delta z_j]/[k_{i,j+1}{}^n*\Delta z_j+k_{i,j}{}^n*\Delta z_{j+1}] \quad , \tag{A.13}$$

$$kjm_{i,j}{}^n=k_{i,j-1}{}^n*k_{i,j}{}^n*[\Delta z_{j-1}+\Delta z_j]/[k_{i,j-1}{}^n*\Delta z_j+k_{i,j}{}^n*\Delta z_{j-1}] \quad , \tag{A.14}$$

and where,

$$C8=2*\pi*ri1*U*\Delta z_j*\Delta t \quad , \tag{A.15}$$

$$C10=2*\pi*ro2*\Delta z_j*\Delta t \quad . \tag{A.16}$$

Appendix A2. FORTRAN Program Description and Listing

FORTRAN 77 computer programs were written to analyze one- and two-dimensional containment canister heat transfer. Appendix A2 contains the listing and variable definitions for the two-dimensional computer program called NUCAM2DV which is an abbreviation for Numerical Canister Model: Two-dimensional with Void. A block diagram showing the main program and subroutines of NUCAM2DV is given in Figure A.1. The main program, MAIN, reads input data and executes a "time-marching" analysis via calls to various subroutines which are briefly described in the following paragraph.

The subroutine INIT is called once at the beginning of program execution to read initial canister temperatures and initialize all program variables. Once in the time loop, calls are made at each time step to five subroutines. VOIDCON calculates steady state void vapor conduction heat transfer and temperature distributions. VOIDRAD calculates void surface element net radiation heat loss terms assuming that the void is a diffuse, gray, and opaque enclosure with a non-participating void vapor. SHELL performs an energy balance on the containment canister shell and determines canister wall temperature distributions. FLUID calculates he/xe cooling fluid pseudo-steady state temperature distributions and total heat transfer to the cooling fluid. SALT performs an energy balance on the LiF-CaF$_2$ salt PCM and determines PCM temperatures, phase distributions, and up-

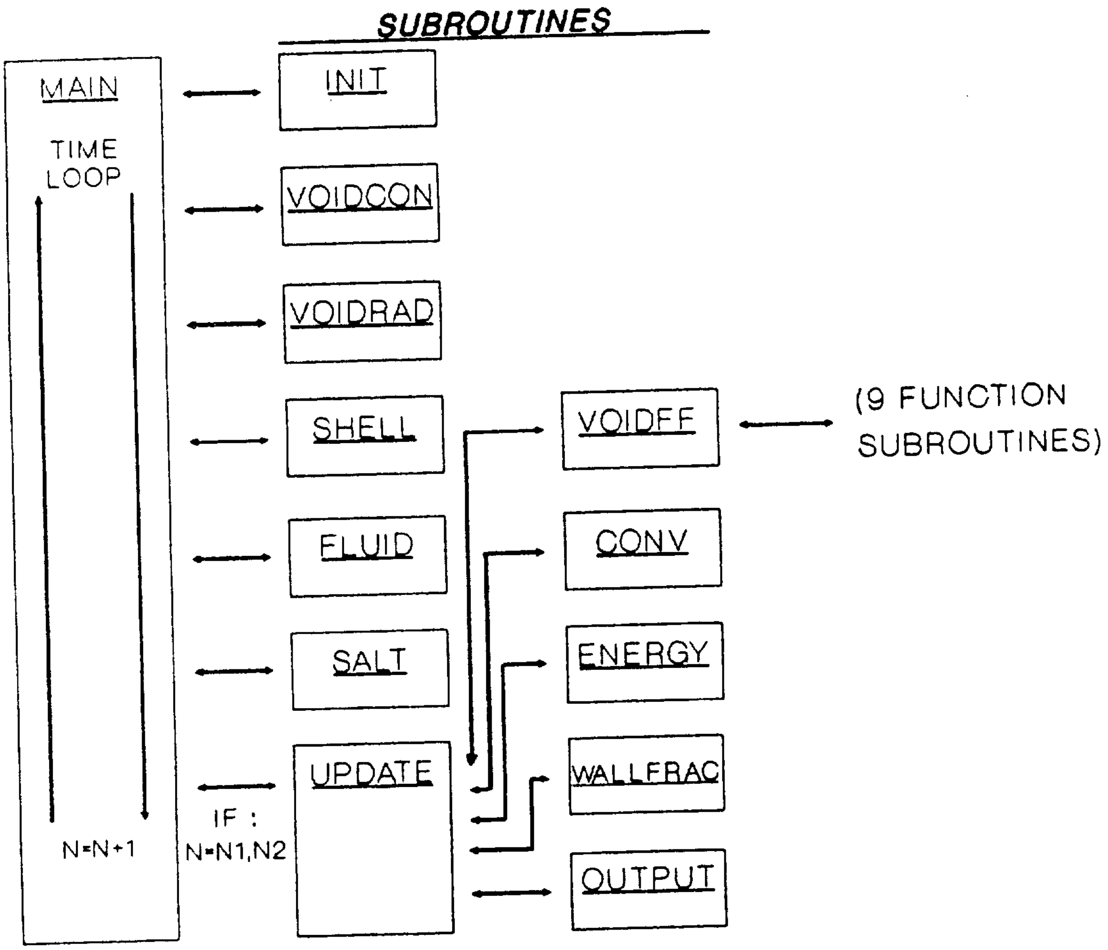

Figure A.1. NUCAM2DV Computer Program Block Diagram dated material properties. The last subroutine, UPDATE, is called by MAIN at two different time increments during program execution (typically, 1.0 min. and 3.035 min.). UPDATE, in turn, makes calls to five subroutines which are briefly described below.

VOIDFF calculates void surface element view factors (using closed-form solutions and view factor algebra) and inverts the "view factor - emittance" matrix. From VOIDFF, "calls" to nine different function subroutines are made. Function subroutines are needed to evaluate view factor algebra equations which employ multiple calls from the same line of code. CONV calculates liquid PCM Rayleigh numbers, Nusselt numbers, and enhanced conductivity values. ENERGY evaluates the global canister energy balance. WALLFRAC calculates side wall radial heat transfer fractions near the inner, mean, and outer canister radial locations. The last subroutine, OUTPUT, creates files for numerical data output.

A2.1 Two-Dimensional Analysis Program Listing

```
C
C    2-D (R,Z), TRANSIENT TES CANISTER MODEL:  NUCAM2DV
C
C    INCLUDES VOID AND FREE CONVECTION AS FUNCTION OF Z
C
C    THOMAS W. KERSLAKE   NASA-LEWIS RESEARCH CENTER  CLEVELAND, OHIO
C                  SOLAR DYNAMIC POWER SYSTEM BRANCH
C
C    ADVISER : DR. MOUNIR B. IBRAHIM    CSU DEPT. OF MECH. ENG.
C
C    START DATE:20 NOV 89   REV. DATE:23 JULY 90
C
C    SIMPLE EXPLICIT NUMERICAL FORMULATION / ENTHALPY METHOD
C
C    UNITS :  LENGTH       CENTIMETER
C             MASS         GRAM
C             ENERGY       JOULE
C             TIME         SECOND
C             TEMPERATURE  DEG K
C
      CHARACTER*4 PHASE(40,20),NC
      REAL MDOT,KW,KS,KL,KLE,MT,MS,ML,K(40,20),KIP(40,20),
     &KIM(40,20),KJP(40,20),KJM(40,20),MFL,MUF,NU,NUL,KF
      COMMON DT,DRR,DZZ,DELWO,DELWI,DELWS,RI1,KIP,BBINV(18,18),QRAD(18),
     &RI2,RO1,RO2,Q,TFI,MDOT,CPF,KW,CPW,RHOW,KS,CPS,RHOS,FF(18,18),
     &KL,CPL,RHOL,TM,HM,KLE,Z2,Z3,Z4,PI,VOLT,Q1,Q2,VOL(40,20),RCML(20),
     &MT,MS,VOLS,ML,VOLL,ESHSUM,EFSUM,RA,NU,CHARL,C7,C12,ECON(20),
     &TV,TO(40,20),T(40,20),K,RHO(40,20),XF(40,20),TFIN(20),AREAOLD(3),
     &YF(40,20),DR(40),DZ(20),Z(20),R(40),EO(40,20),E(40,20),AREA(30),
     &TFO(20),TF(20),C1(40,20),C2(40,20),C3(40,20),C4(40,20),RCMLO(20),
     &TFOUT,EE(40,20),TIMEPR1,TIMEPR2,TIMEP,TIMEF,TFP,TFF,RV,RM,
     &TIME2,TIME3,TIME4,TF2,TF3,TF4,EINIT,ECAN,EBAL,EEL(40,20),
     &EELO(40,20),EELO2(40,20),PR,EML(40,20),
     &MFL,QF,II,IV1,IV2,JJ,N,PHASE,NC,
     &ZKLE(10),ZNU(10),ZRA(10),ZCHARL(10),ZNUAVG
C
C     INPUT DATA
C
      READ (1,1000) DT,NN,DRR,II,DZZ,JJ,DELWO,DELWI,DELWS,RI1,
     &     NC,MT,MDOT,PRF,MUF,CPF,KF,RHOF,KW,CPW,RHOW,EW,
     &     KS,CPS,RHOS,ES,KL,CPL,RHOL,TM,HM,NUL,BETA,RAC,
     &     G,TIMEPR1,TIMEPR2,
     &     TIME1,TIME2,TIME3,TIME4,TF1,TF2,TF3,TF4,
     &     Q1,Q2,Q3
C
C     CALCULATE PROGRAM CONSTANTS
C
```

```
      AS=KS/(RHOS*CPS)
      AL=KL/(RHOL*CPL)
      PR=NUL/AL
      GAMMAO=1.D00-RHOL/RHOS
      KLE=KL
      RI2=RI1+DELWI
      RO1=RI2+DRR*(II-2)
      RO2=RO1+DELWO
      Z2=DELWS
      Z3=DELWS+DZZ*(JJ-2)
      Z4=Z3+DELWS
      JJ2=JJ/2
      TIMEP=TIME1
      TIMEF=TIME2
      TFP=TF1
      TFF=TF2
      PI=2.0D00*DARSIN(1.0D00)
      V=MDOT/(RHOF*PI*RI1**2)
      RE=2.0D00*MDOT/(PI*MUF*RI1)
C
C     CONSTANT PROPERTY, FULLY DEVELOPED FLOW CORRELATION (KAYS 1966)
C
      H=KF*0.022D00*RE**0.8D00*PRF**0.6D00/(2.0D00*RI1)
      U=1.D00/(1.D00/H+DLOG((RI1+DELWI/2.D00)/RI1)*RI1/KW)
      DUM=PI
      TFI=TF1
      Q=Q1
C
C     INITIALIZE ARRAYS AND VARIABLES TO AN "ALL SOLID SALT" STATE
C     FOR WHICH ALL CANISTER TEMPERATURES ARE < TM AND DEFINE
C     GEOMETRY ARRAYS
C
      CALL INIT(VVF,VOLV)
      IF (RV.LT.RO1) CALL VOIDFF(ES,EW)
      C7=G*BETA/(AL*NUL)
      C8=2.0D00*PI*RI1*U*DT*DZZ
      C9=2.0D00*PI*RI1*U*DT*DELWS
      C10=2.0D00*PI*RO2*DT*DZZ
      C11=2.0D00*PI*RO2*DT*DELWS
      C12=2.0D00*PI*RO2*Z4
      C13=U*PI*RI1*DELWS
      C14=MDOT*CPF
      C15=C13+C14
      C16=U*PI*RI1*DZZ
      C17=C16+C14
      MS=MT
      VOLS=MS/RHOS
      QSHELL=Q*C12
      TTUBE=0.0D00
```

```
      DO 11 J=1,JJ
        TTUBE=TTUBE+TO(1,J)
11    CONTINUE
      TTUBE=TTUBE/JJ
      QF=U*2.D00*PI*RI1*Z4*(TTUBE-TFI)
      QSALT=QSHELL-QF
      TV=TO(IV1,JJ2)
      NU=1.0D00
      ZNUAVG=1.0D00
      QVOIDCON=0.0D00
      QVOIDRAD=0.0D00
      QVOIDTOT=0.0D00
C
C     ECHO INPUT AND INITIALIZED VARIABLES
C
      WRITE(7,1000) DT,NN,DRR,II,DZZ,JJ,DELWO,DELWI,DELWS,RI1,
     &     NC,MT,MDOT,PRF,MUF,CPF,KF,RHOF,KW,CPW,RHOW,EW,
     &     KS,CPS,RHOS,ES,KL,CPL,RHOL,TM,HM,NUL,BETA,RAC,G,TIMEPR1,
     &     TIMEPR2,TIME1,TIME2,TIME3,TIME4,TF1,TF2,TF3,TF4,
     &     Q1,Q2,Q3
      WRITE(7,2000) AS,AL,PI,GAMMAO,PR,RI2,RV,RO1,RO2,Z2,Z3,Z4,
     &     VOLT,VOLS,VOLL,VOLV,MT,MS,ML,V,RE,H,U
      WRITE (8,2100) DT,NN,DRR,II,DZZ,JJ,DELWO,DELWI,DELWS,RI1,RO2,Z4,
     &      MT,MDOT,H,NC,Q1,Q2,Q3
      WRITE (8,2200) TIMEM,MFL,T(II,JJ2),VVF,
     &TFI,TFOUT,QF,EBAL,EBALP,QVOIDCON,QVOIDRAD,QVOIDTOT
      WRITE (11,2410)
      WRITE (11,2420) TIMEM,WALLFR1,WALLFR2,WALLFR3
      IF(NC.EQ.'ON  ') WRITE(9,2300) DT,NN,DRR,II,DZZ,JJ,DELWO,
     &      DELWI,DELWS,MT,TFI,MDOT,H,NC,RAC,Q1,Q2,Q3
      IF(NC.EQ.'ON  ') WRITE (9,2400) TIMEM,CHARL,TSHELL,RA,NU
      IF(NC.EQ.'ON  ') WRITE (17,3600)
      IF(NC.EQ.'ON  ') WRITE (18,3605)
      IF(NC.EQ.'ON  ') WRITE (17,3650) TIMEM,ZNUAVG,(ZNU(J),J=2,JJ-1),
     &               (ZCHARL(J),J=2,JJ-1)
      IF(NC.EQ.'ON  ') WRITE (18,3655) TIMEM,ZRAAVG,(ZRA(J),J=2,JJ-1)
      N=2
      CALL OUTPUT(TIMEM,N1,N2,WALLFR1,WALLFR2,WALLFR3,EBALP,VVF)
C
C     START SIMULATION
C
      N1=(TIMEPR1/DT)+1.0
      N2=(TIMEPR2/DT)+1.0
      N4=2
      DO 20 N=2,NN
C
C     STEADY STATE VOID CONDUCTION HEAT TRANSFER IN RADIAL DIRECTION
C
      CALL VOIDCON(DUM)
```

```
C
C     DIFFUSE, OPAQUE, AND GRAY VOID RADIATION HEAT TRANSFER
C
      CALL VOIDRAD(DUM)
C
C     ENERGY BALANCE ON SHELL (CONTAINMENT CANISTER) ELEMENTS
C
      CALL SHELL(C8,C9,C10,C11)
C
C     ENERGY BALANCE ON HE/XE GASEOUS COOLING FLUID ELEMENTS
C
      CALL FLUID(C13,C14,C15,C16,C17)
C
C     ENERGY BALANCE ON EUTECTIC LIF-CAF2 SALT PCM
C
      CALL SALT(DUM)
C
C     "ADVANCE" TIME-DEPENDENT VARIABLES TO THE "N+1" TIME STEP
C
      DO 25 J=1,JJ
      TFO(J)=TF(J)
      DO 30 I=1,II
        TO(I,J)=T(I,J)
        EO(I,J)=E(I,J)
 30   CONTINUE
 25   CONTINUE
C
C     UP-DATE VOID EFFECTS, FREE CONVECTION EFFECTS, ENERGY BALANCE
C     TALLY, WALL FRACTION CALCULATION, AND OUTPUT RESULTS
C
      IF(N.EQ.N1.OR.N.EQ.N2) CALL UPDATE(N1,N2,VVF)
C
C     OUTPUT TEMPERATURE DATA FOR VIDEO ANIMATION
C
      IF (N.NE.N4) GO TO 20
      TIME=(N-1)*DT
      WRITE (16,2450) TIME,MFL,VVF,ZNUAVG,(Z(J),J=1,JJ)
      WRITE (16,2050)
      DO 855 I=1,II
       III1=II+1-I
       WRITE(16,2500) R(III1),(T(III1,J),J=1,JJ)
855   CONTINUE
      N4=N4+6.0D00/DT
 20   CONTINUE
C
1000  FORMAT(F9.7,1X,I6,2(1X,F7.5,1X,I3),4(1X,F7.5)/
     & A4,1X,F6.3,1X,F6.3,1X,F7.5/
     & 4(D9.3,1X)/4(F7.5,1X)/4(F7.5,1X)/3(F7.5,1X),F6.1,1X,
     & F5.1,1X,F6.4,1X,D8.2,1X,F7.1,1X,F5.1/F6.1,1X,F6.1/
```

```
   & 4(F6.2,1X)/4(F6.1,1X)/3(F6.3,1X))
2000 FORMAT(6(5(D12.5,1X)/))
2100 FORMAT('DT=',F9.7,'  NN=',I6,'  DR=',F7.5,'  II=',I3,'  DZ=',F7.5,
   &'  JJ=',I3/'DELWO=',F7.5,'  DELWI=',F7.5,'  DELWS=',F7.5,'  RI=',
   &F7.5,'  RO=',F7.5/'L= ',F7.5,'  MT=',
   &F6.3,'  MDOT=',F6.3,'  H=',F7.5,'  NC=',A4/
   &'Q1=',F6.3,'  Q2=',F6.3,'  Q3=',F6.3/
   &/' TIME',T10,'MFL',T16,'TMAX',T23,' VVF ',T33,
   &'TFI',T40,'TFO',T49,'QF',T56,'EBAL',T63,'%EBAL',
   &2X,'QVOIDCON',2X,'QVOIDRAD',2X,'QVOIDTOT'//)
2200 FORMAT(F6.2,2X,F5.3,1X,F6.1,2X,F6.4,2(2X,F6.1),1X,F7.2,
   &      2X,F7.0,2X,F5.2,2X,3(F8.3,2X))
2300 FORMAT('DT=',F9.7,'  NN=',I6,'  DR=',F7.5,'  II=',I3,'  DZ=',F7.5,
   &' JJ=',I3/'DELWO=',F7.5,'  DELWI=',F7.5,'  DELWS=',F7.5,'   MT  ='
   &,F6.3/' TFI(0 MIN)=',F6.1,'  MDOT=',F6.3,'  H=',F7.5,'  NC=',A4,
   &1X,'  RAC=',F7.1/'Q1=',F6.3,'  Q2=',F6.3,'  Q3=',F6.3//
   &' TIME',T8,'CHARL',T14,'  TV ',T26,'RA',T36,'NU'/)
2400 FORMAT(F6.2,1X,F5.3,2X,F6.1,2X,F9.0,2X,F6.3)
2410 FORMAT('  WALL HEAT TRANSFER FRACTIONS, %'//' TIME ',5X,
   &'WALLFR1',3X,'WALLFR2',3X,'WALLFR3'/)
2420 FORMAT(F7.3,3(3X,F7.3))
2050 FORMAT('R, CM')
2450 FORMAT(/' TIME=',F6.1,'  MFL=',F6.4,'  VVF=',F6.4,'  NU=',F6.3
   &//'  Z, CM =',20(2X,F6.4))
2500 FORMAT(F6.4,6X,20(F6.1,2X))
3600 FORMAT(' TIME',T8,'ZNUAVG',T30,'NU(Z)',T80,'CHARL(Z)')
3605 FORMAT(' TIME',T11,'ZRAAVG',T30,'RA(Z)')
3650 FORMAT(F6.2,2X,F5.3,2X,8(F5.3,1X),1X,8(F5.3,1X))
3655 FORMAT(F6.2,2X,F9.0,2X,8(F9.0,1X))
    STOP
    END
C
    SUBROUTINE INIT(VVF,VOLV)
    CHARACTER*4 PHASE(40,20),NC
    REAL MDOT,KW,KS,KL,KLE,MT,MS,ML,K(40,20),KIP(40,20),
   &KIM(40,20),KJP(40,20),KJM(40,20),MFL,MUF,NU,NUL,KF
    COMMON DT,DRR,DZZ,DELWO,DELWI,DELWS,RI1,KIP,BBINV(18,18),QRAD(18),
   &RI2,RO1,RO2,Q,TFI,MDOT,CPF,KW,CPW,RHOW,KS,CPS,RHOS,FF(18,18),
   &KL,CPL,RHOL,TM,HM,KLE,Z2,Z3,Z4,PI,VOLT,Q1,Q2,VOL(40,20),RCML(20),
   &MT,MS,VOLS,ML,VOLL,ESHSUM,EFSUM,RA,NU,CHARL,C7,C12,ECON(20),
   &TV,TO(40,20),T(40,20),K,RHO(40,20),XF(40,20),TFIN(20),AREAOLD(3),
   &YF(40,20),DR(40),DZ(20),Z(20),R(40),EO(40,20),E(40,20),AREA(30),
   &TFO(20),TF(20),C1(40,20),C2(40,20),C3(40,20),C4(40,20),RCMLO(20),
   &TFOUT,EE(40,20),TIMEPR1,TIMEPR2,TIMEP,TIMEF,TFP,TFF,RV,RM,
   &TIME2,TIME3,TIME4,TF2,TF3,TF4,EINIT,ECAN,EBAL,EEL(40,20),
   &EELO(40,20),EELO2(40,20),PR,EML(40,20),
   &MFL,QF,II,IV1,IV2,JJ,N,PHASE,NC,
   &ZKLE(10),ZNU(10),ZRA(10),ZCHARL(10),ZNUAVG
C
```

```
C     READ IN INITIAL ELEMENT TEMPERATURES AND DETERMINE INITIAL ELEMENT
C     DIMENSIONS, MATERIAL PROPERTIES, AND GEOMETRY COEFFICIENT MATRICES
C
      DO 41 I=1,II
        II1=II+1-I
        READ (2,1100) (TO(II1,J),J=1,JJ)
 41   CONTINUE
      DO 25 I=2,II-1
      DR(I)=DRR
      R(I)=RI2+DRR/2.D00+(I-2)*DRR
      DO 30 J=2,JJ-1
        ZKLE(J)=KL
        ZNU(J)=1.0D00
        K(I,J)=KS
        RHO(I,J)=RHOS
        PHASE(I,J)='SOL'
        XF(I,J)=0.0D00
        YF(I,J)=0.0D00
        DZ(J)=DZZ
        VOL(I,J)=2.0D00*PI*R(I)*DR(I)*DZ(J)
        EO(I,J)=(TO(I,J)-TM)*CPS*RHO(I,J)*VOL(I,J)
 30   CONTINUE
 25   CONTINUE
      R(1)=RI1+DELWI/2.D00
      R(II)=RO1+DELWO/2.D00
      DR(1)=DELWI
      DR(II)=DELWO
      DO 35 J=2,JJ-1
        Z(J)=DELWS+DZZ/2.D00+(J-2)*DZZ
        K(1,J)=KW
        K(II,J)=KW
        TFO(J)=TFI
        TFIN(J)=TFI
        VOL(1,J)=2.0D00*PI*R(1)*DR(1)*DZ(J)
        VOL(II,J)=2.0D00*PI*R(II)*DR(II)*DZ(J)
        EO(1,J)=(TO(1,J)-TM)*CPW*RHOW*VOL(1,J)
        EO(II,J)=(TO(II,J)-TM)*CPW*RHOW*VOL(II,J)
 35   CONTINUE
      DZ(1)=DELWS
      DZ(JJ)=DELWS
      Z(1)=DELWS/2.D00
      Z(JJ)=DELWS/2.D00+Z3
      DO 40 I=2,II-1
        K(I,1)=KW
        K(I,JJ)=KW
        VOL(I,1)=2.0D00*PI*R(I)*DR(I)*DZ(1)
        VOL(I,JJ)=2.0D00*PI*R(I)*DR(I)*DZ(JJ)
        EO(I,1)=(TO(I,1)-TM)*CPW*RHOW*VOL(I,1)
        EO(I,JJ)=(TO(I,JJ)-TM)*CPW*RHOW*VOL(I,JJ)
```

```
40  CONTINUE
    TFO(1)=TFI
    TFO(JJ)=TFI
    TFOUT=TFI
    TFIN(JJ)=TFI
    VOL(1,1)=2.0D00*PI*R(1)*DR(1)*DZ(1)
    VOL(1,JJ)=2.0D00*PI*R(1)*DR(1)*DZ(JJ)
    VOL(II,1)=2.0D00*PI*R(II)*DR(II)*DZ(1)
    VOL(II,JJ)=2.0D00*PI*R(II)*DR(II)*DZ(JJ)
    EO(1,1)=(TO(1,1)-TM)*CPW*RHOW*VOL(1,1)
    EO(1,JJ)=(TO(1,JJ)-TM)*CPW*RHOW*VOL(1,JJ)
    EO(II,1)=(TO(II,1)-TM)*CPW*RHOW*VOL(II,1)
    EO(II,JJ)=(TO(II,JJ)-TM)*CPW*RHOW*VOL(II,JJ)
    K(1,1)=KW
    K(1,JJ)=KW
    K(II,1)=KW
    K(II,JJ)=KW
C
C    RECALCULATE VOID AFFECTED VARIABLES
C
    IV1=II-1
    IV2=IV1
    RV=DSQRT(1.0D00*RI2*RI2+MT/(RHOS*PI*(Z3-Z2)))
    IF (RV.EQ.RO1) GO TO 44
    II=II-1
    IV1=(RV-RI2)/DRR+1.0D00
    IV2=IV1+1
    DR(IV1)=RV-(R(IV1-1)+DRR/2.D00)
    DR(IV2)=(R(IV2+2)-DRR/2.D00)-RV
    DR(II)=DELWO
    R(IV1)=RV-DR(IV1)/2.0D00
    R(IV2)=RV+DR(IV2)/2.0D00
    DO 37 J=2,JJ-1
      K(II,J)=KW
      DO 36 I=IV2,II-1
        K(I,J)=4.6D-04*DSQRT(TO(I,J)/1000.0D00)
        PHASE(I,J)='VOID'
        EO(I,J)=0.0D00
        E(I,J)=0.0D00
36    CONTINUE
      VOL(IV1,J)=2.0D00*PI*R(IV1)*DR(IV1)*DZ(J)
      EO(IV1,J)=(TO(IV1,J)-TM)*CPS*RHOS*VOL(IV1,J)
37  CONTINUE
    DO 38 I=IV1,II
      R(I)=R(I-1)+(DR(I)+DR(I-1))/2.0D00
      VOL(I,1)=2.0D00*PI*R(I)*DR(I)*DZ(1)
      EO(I,1)=(TO(I,1)-TM)*CPW*RHOW*VOL(I,1)
      VOL(I,JJ)=2.0D00*PI*R(I)*DR(I)*DZ(JJ)
      EO(I,JJ)=(TO(I,JJ)-TM)*CPW*RHOW*VOL(I,JJ)
```

```
38   CONTINUE
     DO 39 J=2,JJ-1
       VOL(II,J)=2.0D00*PI*R(II)*DR(II)*DZ(J)
       EO(II,J)=(TO(II,J)-TM)*CPW*RHOW*VOL(II,J)
39   CONTINUE
     RO1=R(II)-DR(II)/2.0D00
     RO2=R(II)+DR(II)/2.0D00
44   DO 45 I=2,II-1
     DO 50 J=2,JJ-1
       C1(I,J)=2.D00*PI*DZ(J)*DT/DLOG(1.0D00*R(I+1)/R(I))
       C2(I,J)=2.D00*PI*DZ(J)*DT/DLOG(1.0D00*R(I)/R(I-1))
       C3(I,J)=4.D00*PI*R(I)*DR(I)*DT/(DZ(J+1)+DZ(J))
       C4(I,J)=4.D00*PI*R(I)*DR(I)*DT/(DZ(J-1)+DZ(J))
50   CONTINUE
45   CONTINUE
     DO 55 I=2,II-1
       C1(I,1)=2.D00*PI*DZ(1)*DT/DLOG(1.0D00*R(I+1)/R(I))
       C2(I,1)=2.D00*PI*DZ(1)*DT/DLOG(1.0D00*R(I)/R(I-1))
       C3(I,1)=4.D00*PI*R(I)*DR(I)*DT/(DZ(2)+DZ(1))
       C1(I,JJ)=2.D00*PI*DZ(JJ)*DT/DLOG(1.0D00*R(I+1)/R(I))
       C2(I,JJ)=2.D00*PI*DZ(JJ)*DT/DLOG(1.0D00*R(I)/R(I-1))
       C4(I,JJ)=4.D00*PI*R(I)*DR(I)*DT/(DZ(JJ-1)+DZ(JJ))
55   CONTINUE
     DO 60 J=2,JJ-1
       C1(1,J)=2.D00*PI*DZ(J)*DT/DLOG(1.0D00*R(2)/R(1))
       C3(1,J)=4.D00*PI*R(1)*DR(1)*DT/(DZ(J+1)+DZ(J))
       C4(1,J)=4.D00*PI*R(1)*DR(1)*DT/(DZ(J-1)+DZ(J))
       C2(II,J)=2.D00*PI*DZ(J)*DT/DLOG(1.0D00*R(II)/R(II-1))
       C3(II,J)=4.D00*PI*R(II)*DR(II)*DT/(DZ(J+1)+DZ(J))
       C4(II,J)=4.D00*PI*R(II)*DR(II)*DT/(DZ(J-1)+DZ(J))
60   CONTINUE
     C1(1,1)=2.D00*PI*DZ(1)*DT/DLOG(1.0D00*R(2)/R(1))
     C3(1,1)=4.D00*PI*R(1)*DR(1)*DT/(DZ(2)+DZ(1))
     C1(1,JJ)=2.D00*PI*DZ(JJ)*DT/DLOG(1.0D00*R(2)/R(1))
     C4(1,JJ)=4.D00*PI*R(1)*DR(1)*DT/(DZ(JJ-1)+DZ(JJ))
     C2(II,1)=2.D00*PI*DZ(1)*DT/DLOG(1.0D00*R(II)/R(II-1))
     C3(II,1)=4.D00*PI*R(II)*DR(II)*DT/(DZ(2)+DZ(1))
     C2(II,JJ)=2.D00*PI*DZ(JJ)*DT/DLOG(1.0D00*R(II)/R(II-1))
     C4(II,JJ)=4.D00*PI*R(II)*DR(II)*DT/(DZ(JJ-1)+DZ(JJ))
     VOLV=PI*(RO1*RO1-RV*RV)*(Z3-Z2)
     VOLT=PI*(RO1**2-RI2**2)*(Z3-Z2)
     VVF=VOLV/VOLT
     EINIT=0.0D00
     DO 65 I=1,II
     DO 70 J=1,JJ
       EINIT=EINIT+EO(I,J)
70   CONTINUE
65   CONTINUE
     ECAN=EINIT
```

```
1100 FORMAT(12X,20(F6.1,2X))
      RETURN
      END
C
      SUBROUTINE VOIDCON(DUM)
      CHARACTER*4 PHASE(40,20),NC
      REAL MDOT,KW,KS,KL,KLE,MT,MS,ML,K(40,20),KIP(40,20),
     &KIM(40,20),KJP(40,20),KJM(40,20),MFL,MUF,NU,NUL,KF
      COMMON DT,DRR,DZZ,DELWO,DELWI,DELWS,RI1,KIP,BBINV(18,18),QRAD(18),
     &RI2,RO1,RO2,Q,TFI,MDOT,CPF,KW,CPW,RHOW,KS,CPS,RHOS,FF(18,18),
     &KL,CPL,RHOL,TM,HM,KLE,Z2,Z3,Z4,PI,VOLT,Q1,Q2,VOL(40,20),RCML(20),
     &MT,MS,VOLS,ML,VOLL,ESHSUM,EFSUM,RA,NU,CHARL,C7,C12,ECON(20),
     &TV,TO(40,20),T(40,20),K,RHO(40,20),XF(40,20),TFIN(20),AREAOLD(3),
     &YF(40,20),DR(40),DZ(20),Z(20),R(40),EO(40,20),E(40,20),AREA(30),
     &TFO(20),TF(20),C1(40,20),C2(40,20),C3(40,20),C4(40,20),RCMLO(20),
     &TFOUT,EE(40,20),TIMEPR1,TIMEPR2,TIMEP,TIMEF,TFP,TFF,RV,RM,
     &TIME2,TIME3,TIME4,TF2,TF3,TF4,EINIT,ECAN,EBAL,EEL(40,20),
     &EELO(40,20),EELO2(40,20),PR,EML(40,20),
     &MFL,QF,II,IV1,IV2,JJ,N,PHASE,NC,
     &ZKLE(10),ZNU(10),ZRA(10),ZCHARL(10),ZNUAVG
      DO 10 J=2,JJ-1
        C=(TO(II,J)-TO(IV1,J))/DLOG(RO1/RV)
        D=TO(IV1,J)-DLOG(RV)*(TO(II,J)-TO(IV1,J))/DLOG(RO1/RV)
        DO 20 I=IV2,II-1
          T(I,J)=C*DLOG(R(I))+D
          TO(I,J)=T(I,J)
          K(I,J)=4.6D-04*DSQRT(T(I,J)/1000.0D00)
 20     CONTINUE
 10   CONTINUE
      RETURN
      END
C
      SUBROUTINE VOIDRAD(DUM)
      CHARACTER*4 PHASE(40,20),NC
      REAL MDOT,KW,KS,KL,KLE,MT,MS,ML,K(40,20),KIP(40,20),TTO(18),
     &KIM(40,20),KJP(40,20),KJM(40,20),MFL,MUF,NU,NUL,KF,DD(18)
      COMMON DT,DRR,DZZ,DELWO,DELWI,DELWS,RI1,KIP,BBINV(18,18),QRAD(18),
     &RI2,RO1,RO2,Q,TFI,MDOT,CPF,KW,CPW,RHOW,KS,CPS,RHOS,FF(18,18),
     &KL,CPL,RHOL,TM,HM,KLE,Z2,Z3,Z4,PI,VOLT,Q1,Q2,VOL(40,20),RCML(20),
     &MT,MS,VOLS,ML,VOLL,ESHSUM,EFSUM,RA,NU,CHARL,C7,C12,ECON(20),
     &TV,TO(40,20),T(40,20),K,RHO(40,20),XF(40,20),TFIN(20),AREAOLD(3),
     &YF(40,20),DR(40),DZ(20),Z(20),R(40),EO(40,20),E(40,20),AREA(30),
     &TFO(20),TF(20),C1(40,20),C2(40,20),C3(40,20),C4(40,20),RCMLO(20),
     &TFOUT,EE(40,20),TIMEPR1,TIMEPR2,TIMEP,TIMEF,TFP,TFF,RV,RM,
     &TIME2,TIME3,TIME4,TF2,TF3,TF4,EINIT,ECAN,EBAL,EEL(40,20),
     &EELO(40,20),EELO2(40,20),PR,EML(40,20),
     &MFL,QF,II,IV1,IV2,JJ,N,PHASE,NC,
     &ZKLE(10),ZNU(10),ZRA(10),ZCHARL(10),ZNUAVG
      SIGMA=5.67D-12
```

```
      NRS=2*(JJ-2)+2
      DO 5 KK=1,JJ-2
        TTO(KK)=TO(IV1,KK+1)
        TTO(KK+JJ-2)=TO(II,KK+1)
 5    CONTINUE
      I=IV2
      JRANGE=2*(JJ-2)+1
      TTO(JRANGE)=0.0D00
      TTO(JRANGE+1)=0.0D00
      DO 6 KK=JRANGE,NRS-1,2
      DO 7 I=IV2,II-1
        TTO(KK)=TTO(KK)+TO(I,1)
        TTO(KK+1)=TTO(KK+1)+TO(I,JJ)
 7    CONTINUE
      TTO(KK)=TTO(KK)/(II-IV2)
      TTO(KK+1)=TTO(KK+1)/(II-IV2)
 6    CONTINUE
C
C     DEFINE "DD" MATRIX SUCH THAT {BB}{QRAD}={DD} WHERE {BB} IS
C     THE "VIEW FACTOR-EMITTANCE" MATRIX AND {DD} IS THE
C     "TEMPERATURE-TO-THE-FOURTH-POWER DIFFERENCE" MATRIX
C
      DO 10 KK=1,NRS
      SUM=0.0D00
      DO 20 J=1,NRS
        SUM=SUM+FF(KK,J)*(TTO(KK)**4-TTO(J)**4)
 20   CONTINUE
      DD(KK)=SIGMA*SUM
 10   CONTINUE
C
C     DETERMINE ELEMENT NET HEAT LOSS TERMS
C
      QRADSUM=0.0D00
      DO 30 KK=1,NRS
      QRAD(KK)=0.0D00
      DO 40 J=1,NRS
        QRAD(KK)=QRAD(KK)+BBINV(KK,J)*DD(J)
 40   CONTINUE
      QRADSUM=QRADSUM+QRAD(KK)
 30   CONTINUE
      RETURN
      END
C
      SUBROUTINE SHELL(C8,C9,C10,C11)
      CHARACTER*4 PHASE(40,20),NC
      REAL MDOT,KW,KS,KL,KLE,MT,MS,ML,K(40,20),KIP(40,20),
     &KIM(40,20),KJP(40,20),KJM(40,20),MFL,MUF,NU,NUL,KF
      COMMON DT,DRR,DZZ,DELWO,DELWI,DELWS,RI1,KIP,BBINV(18,18),QRAD(18),
     &RI2,RO1,RO2,Q,TFI,MDOT,CPF,KW,CPW,RHOW,KS,CPS,RHOS,FF(18,18),
```

```
     &KL,CPL,RHOL,TM,HM,KLE,Z2,Z3,Z4,PI,VOLT,Q1,Q2,VOL(40,20),RCML(20),
     &MT,MS,VOLS,ML,VOLL,ESHSUM,EFSUM,RA,NU,CHARL,C7,C12,ECON(20),
     &TV,TO(40,20),T(40,20),K,RHO(40,20),XF(40,20),TFIN(20),AREAOLD(3),
     &YF(40,20),DR(40),DZ(20),Z(20),R(40),EO(40,20),E(40,20),AREA(30),
     &TFO(20),TF(20),C1(40,20),C2(40,20),C3(40,20),C4(40,20),RCMLO(20),
     &TFOUT,EE(40,20),TIMEPR1,TIMEPR2,TIMEP,TIMEF,TFP,TFF,RV,RM,
     &TIME2,TIME3,TIME4,TF2,TF3,TF4,EINIT,ECAN,EBAL,EEL(40,20),
     &EELO(40,20),EELO2(40,20),PR,EML(40,20),
     &MFL,QF,II,IV1,IV2,JJ,N,PHASE,NC,
     &ZKLE(10),ZNU(10),ZRA(10),ZCHARL(10),ZNUAVG
C
C     UP-DATE CONDUCTORS AND DETERMINE ENERGY TRANSFER
C
      DO 100 J=2,JJ-1
        KIP(1,J)=K(2,J)*K(1,J)*(DR(2)+DR(1))/(K(2,J)*DR(1)
     &          +K(1,J)*DR(2))
        KJP(1,J)=K(1,J+1)*K(1,J)*(DZ(J+1)+DZ(J))/(K(1,J+1)*DZ(J)
     &          +K(1,J)*DZ(J+1))
        KJM(1,J)=K(1,J-1)*K(1,J)*(DZ(J-1)+DZ(J))/(K(1,J-1)*DZ(J)
     &          +K(1,J)*DZ(J-1))
        E(1,J)=EO(1,J)+C1(1,J)*KIP(1,J)*(TO(2,J)-TO(1,J))
     &                +C8*(TFO(J)-TO(1,J))
     &                +C3(1,J)*KJP(1,J)*(TO(1,J+1)-TO(1,J))
     &                +C4(1,J)*KJM(1,J)*(TO(1,J-1)-TO(1,J))
        KIM(II,J)=K(II-1,J)*K(II,J)*(DR(II-1)+DR(II))/(K(II-1,J)*DR(II)
     &          +K(II,J)*DR(II-1))
        KJP(II,J)=K(II,J+1)*K(II,J)*(DZ(J+1)+DZ(J))/(K(II,J+1)*DZ(J)
     &          +K(II,J)*DZ(J+1))
        KJM(II,J)=K(II,J-1)*K(II,J)*(DZ(J-1)+DZ(J))/(K(II,J-1)*DZ(J)
     &          +K(II,J)*DZ(J-1))
        E(II,J)=EO(II,J)+Q*C10-QRAD(J-1+JJ-2)*DT
     &                +C2(II,J)*KIM(II,J)*(TO(II-1,J)-TO(II,J))
     &                +C3(II,J)*KJP(II,J)*(TO(II,J+1)-TO(II,J))
     &                +C4(II,J)*KJM(II,J)*(TO(II,J-1)-TO(II,J))
        ECON(J)=C2(II,J)*KIM(II,J)*(TO(II-1,J)-TO(II,J))
  100 CONTINUE
      DO 105 I=2,IV1
        KIP(I,1)=K(I+1,1)*K(I,1)*(DR(I+1)+DR(I))/(K(I+1,1)*DR(I)
     &          +K(I,1)*DR(I+1))
        KIM(I,1)=K(I-1,1)*K(I,1)*(DR(I-1)+DR(I))/(K(I-1,1)*DR(I)
     &          +K(I,1)*DR(I-1))
        KJP(I,1)=K(I,2)*K(I,1)*(DZ(2)+DZ(1))/(K(I,2)*DZ(1)
     &          +K(I,1)*DZ(2))
        E(I,1)=EO(I,1)+C1(I,1)*KIP(I,1)*(TO(I+1,1)-TO(I,1))
     &                +C2(I,1)*KIM(I,1)*(TO(I-1,1)-TO(I,1))
     &                +C3(I,1)*KJP(I,1)*(TO(I,2)-TO(I,1))
        KIP(I,JJ)=K(I+1,JJ)*K(I,JJ)*(DR(I+1)+DR(I))/(K(I+1,JJ)*DR(I)
     &          +K(I,JJ)*DR(I+1))
        KIM(I,JJ)=K(I-1,JJ)*K(I,JJ)*(DR(I-1)+DR(I))/(K(I-1,JJ)*DR(I)
```

```
  &         +K(I,JJ)*DR(I-1))
    KJM(I,JJ)=K(I,JJ-1)*K(I,JJ)*(DZ(JJ-1)+DZ(JJ))/(K(I,JJ-1)*DZ(JJ)
  &         +K(I,JJ)*DZ(JJ-1))
    E(I,JJ)=EO(I,JJ)+C1(I,JJ)*KIP(I,JJ)*(TO(I+1,JJ)-TO(I,JJ))
  &              +C2(I,JJ)*KIM(I,JJ)*(TO(I-1,JJ)-TO(I,JJ))
  &              +C4(I,JJ)*KJM(I,JJ)*(TO(I,JJ-1)-TO(I,JJ))
105 CONTINUE
    JRANGE=2*(JJ-2)+1
    JJJ=1
    DO 106 I=IV2,II-1
     KIP(I,1)=K(I+1,1)*K(I,1)*(DR(I+1)+DR(I))/(K(I+1,1)*DR(I)
  &         +K(I,1)*DR(I+1))
     KIM(I,1)=K(I-1,1)*K(I,1)*(DR(I-1)+DR(I))/(K(I-1,1)*DR(I)
  &         +K(I,1)*DR(I-1))
     KJP(I,1)=0.0D00
     E(I,1)=EO(I,1)+C1(I,1)*KIP(I,1)*(TO(I+1,1)-TO(I,1))
  &              +C2(I,1)*KIM(I,1)*(TO(I-1,1)-TO(I,1))
  &              +C3(I,1)*KJP(I,1)*(TO(I,2)-TO(I,1))
  &              -QRAD(JRANGE)*DT*AREAOLD(JJJ)/AREA(JRANGE)
     KIP(I,JJ)=K(I+1,JJ)*K(I,JJ)*(DR(I+1)+DR(I))/(K(I+1,JJ)*DR(I)
  &         +K(I,JJ)*DR(I+1))
     KIM(I,JJ)=K(I-1,JJ)*K(I,JJ)*(DR(I-1)+DR(I))/(K(I-1,JJ)*DR(I)
  &         +K(I,JJ)*DR(I-1))
     KJM(I,JJ)=0.0D00
     E(I,JJ)=EO(I,JJ)+C1(I,JJ)*KIP(I,JJ)*(TO(I+1,JJ)-TO(I,JJ))
  &              +C2(I,JJ)*KIM(I,JJ)*(TO(I-1,JJ)-TO(I,JJ))
  &              +C4(I,JJ)*KJM(I,JJ)*(TO(I,JJ-1)-TO(I,JJ))
  &              -QRAD(JRANGE+1)*DT*AREAOLD(JJJ)/AREA(JRANGE+1)
    JJJ=JJJ+1
106 CONTINUE
    KIP(1,1)=K(2,1)*K(1,1)*(DR(2)+DR(1))/(K(2,1)*DR(1)
  &         +K(1,1)*DR(2))
    KJP(1,1)=K(1,2)*K(1,1)*(DZ(2)+DZ(1))/(K(1,2)*DZ(1)
  &         +K(1,1)*DZ(2))
    E(1,1)=EO(1,1)+C1(1,1)*KIP(1,1)*(TO(2,1)-TO(1,1))
  &              +C9*(TFO(1)-TO(1,1))
  &              +C3(1,1)*KJP(1,1)*(TO(1,2)-TO(1,1))
    KIP(1,JJ)=K(2,JJ)*K(1,JJ)*(DR(2)+DR(1))/(K(2,JJ)*DR(1)
  &         +K(1,JJ)*DR(2))
    KJM(1,JJ)=K(1,JJ-1)*K(1,JJ)*(DZ(JJ-1)+DZ(JJ))/(K(1,JJ-1)*DZ(JJ)
  &         +K(1,JJ)*DZ(JJ-1))
    E(1,JJ)=EO(1,JJ)+C1(1,JJ)*KIP(1,JJ)*(TO(2,JJ)-TO(1,JJ))
  &              +C9*(TFO(JJ)-TO(1,JJ))
  &              +C4(1,JJ)*KJM(1,JJ)*(TO(1,JJ-1)-TO(1,JJ))
    KIM(II,1)=K(II-1,1)*K(II,1)*(DR(II-1)+DR(II))/(K(II-1,1)*DR(II)
  &         +K(II,1)*DR(II-1))
    KJP(II,1)=K(II,2)*K(II,1)*(DZ(2)+DZ(1))/(K(II,2)*DZ(1)
  &         +K(II,1)*DZ(2))
    E(II,1)=EO(II,1)+Q*C11
```

```
     &           +C2(II,1)*KIM(II,1)*(TO(II-1,1)-TO(II,1))
     &           +C3(II,1)*KJP(II,1)*(TO(II,2)-TO(II,1))
      KIM(II,JJ)=K(II-1,JJ)*K(II,JJ)*(DR(II-1)+DR(II))/(K(II-1,JJ)*
     &         DR(II)+K(II,JJ)*DR(II-1))
      KJM(II,JJ)=K(II,JJ-1)*K(II,JJ)*(DZ(JJ-1)+DZ(JJ))/(K(II,JJ-1)*
     &         DZ(JJ)+K(II,JJ)*DZ(JJ-1))
      E(II,JJ)=EO(II,JJ)+Q*C11
     &           +C2(II,JJ)*KIM(II,JJ)*(TO(II-1,JJ)-TO(II,JJ))
     &           +C4(II,JJ)*KJM(II,JJ)*(TO(II,JJ-1)-TO(II,JJ))
C
C     DETERMINE ELEMENT TEMPERATURES
C
      DO 110 J=1,JJ
       EE(1,J)=E(1,J)/(RHOW*VOL(1,J))
       T(1,J)=(EE(1,J)/CPW)+TM
       EE(II,J)=E(II,J)/(RHOW*VOL(II,J))
       T(II,J)=(EE(II,J)/CPW)+TM
 110  CONTINUE
      DO 115 I=2,II-1
       EE(I,1)=E(I,1)/(RHOW*VOL(I,1))
       T(I,1)=(EE(I,1)/CPW)+TM
       EE(I,JJ)=E(I,JJ)/(RHOW*VOL(I,JJ))
       T(I,JJ)=(EE(I,JJ)/CPW)+TM
 115  CONTINUE
      RETURN
      END
C
      SUBROUTINE FLUID(C13,C14,C15,C16,C17)
      CHARACTER*4 PHASE(40,20),NC
      REAL MDOT,KW,KS,KL,KLE,MT,MS,ML,K(40,20),KIP(40,20),
     &KIM(40,20),KJP(40,20),KJM(40,20),MFL,MUF,NU,NUL,KF
      COMMON DT,DRR,DZZ,DELWO,DELWI,DELWS,RI1,KIP,BBINV(18,18),QRAD(18),
     &RI2,RO1,RO2,Q,TFI,MDOT,CPF,KW,CPW,RHOW,KS,CPS,RHOS,FF(18,18),
     &KL,CPL,RHOL,TM,HM,KLE,Z2,Z3,Z4,PI,VOLT,Q1,Q2,VOL(40,20),RCML(20),
     &MT,MS,VOLS,ML,VOLL,ESHSUM,EFSUM,RA,NU,CHARL,C7,C12,ECON(20),
     &TV,TO(40,20),T(40,20),K,RHO(40,20),XF(40,20),TFIN(20),AREAOLD(3),
     &YF(40,20),DR(40),DZ(20),Z(20),R(40),EO(40,20),E(40,20),AREA(30),
     &TFO(20),TF(20),C1(40,20),C2(40,20),C3(40,20),C4(40,20),RCMLO(20),
     &TFOUT,EE(40,20),TIMEPR1,TIMEPR2,TIMEP,TIMEF,TFP,TFF,RV,RM,
     &TIME2,TIME3,TIME4,TF2,TF3,TF4,EINIT,ECAN,EBAL,EEL(40,20),
     &EELO(40,20),EELO2(40,20),PR,EML(40,20),
     &MFL,QF,II,IV1,IV2,JJ,N,PHASE,NC,
     &ZKLE(10),ZNU(10),ZRA(10),ZCHARL(10),ZNUAVG
C
C     DETERMINE FLUID TEMPERATURE DISTRIBUTION BASED ON
C     A "PSEUDO-STEADY STATE" ASSUMPTION
C
      TF(1)=(C13*T(1,1)+C14*TFI)/C15
      TFIN(2)=2.0D00*TF(1)-TFI
```

```
      DO 200 J=2,JJ-1
        TF(J)=(C16*T(1,J)+C14*TFIN(J))/C17
        TFIN(J+1)=2.0D00*TF(J)-TFIN(J)
  200 CONTINUE
      TF(JJ)=(C13*T(1,JJ)+C14*TFIN(JJ))/C15
      TFOUT=2.0D00*TF(JJ)-TFIN(JJ)
      QF=MDOT*CPF*(TFOUT-TFI)
      EFSUM=EFSUM+QF*DT
      RETURN
      END
C
      SUBROUTINE SALT(DUM)
      CHARACTER*4 PHASE(40,20),NC
      REAL MDOT,KW,KS,KL,KLE,MT,MS,ML,K(40,20),KIP(40,20),
     &KIM(40,20),KJP(40,20),KJM(40,20),MFL,MUF,NU,NUL,KF,EEO(40,20)
      COMMON DT,DRR,DZZ,DELWO,DELWI,DELWS,RI1,KIP,BBINV(18,18),QRAD(18),
     &RI2,RO1,RO2,Q,TFI,MDOT,CPF,KW,CPW,RHOW,KS,CPS,RHOS,FF(18,18),
     &KL,CPL,RHOL,TM,HM,KLE,Z2,Z3,Z4,PI,VOLT,Q1,Q2,VOL(40,20),RCML(20),
     &MT,MS,VOLS,ML,VOLL,ESHSUM,EFSUM,RA,NU,CHARL,C7,C12,ECON(20),
     &TV,TO(40,20),T(40,20),K,RHO(40,20),XF(40,20),TFIN(20),AREAOLD(3),
     &YF(40,20),DR(40),DZ(20),Z(20),R(40),EO(40,20),E(40,20),AREA(30),
     &TFO(20),TF(20),C1(40,20),C2(40,20),C3(40,20),C4(40,20),RCMLO(20),
     &TFOUT,EE(40,20),TIMEPR1,TIMEPR2,TIMEP,TIMEF,TFP,TFF,RV,RM,
     &TIME2,TIME3,TIME4,TF2,TF3,TF4,EINIT,ECAN,EBAL,EEL(40,20),
     &EELO(40,20),EELO2(40,20),PR,EML(40,20),
     &MFL,QF,II,IV1,IV2,JJ,N,PHASE,NC,
     &ZKLE(10),ZNU(10),ZRA(10),ZCHARL(10),ZNUAVG
C
C     UP-DATE CONDUCTORS, DETERMINE ENERGY TRANSFER, AND
C     UP-DATE PCM ELEMENT TEMPERATURES AND PROPERTIES
C
      ML=0.0D00
      DO 300 I=2,IV1-1
      DO 305 J=2,JJ-1
        KIP(I,J)=K(I+1,J)*K(I,J)*(DR(I+1)+DR(I))/(K(I+1,J)*DR(I)
     &           +K(I,J)*DR(I+1))
        KIM(I,J)=K(I-1,J)*K(I,J)*(DR(I-1)+DR(I))/(K(I-1,J)*DR(I)
     &           +K(I,J)*DR(I-1))
        KJP(I,J)=K(I,J+1)*K(I,J)*(DZ(J+1)+DZ(J))/(K(I,J+1)*DZ(J)
     &           +K(I,J)*DZ(J+1))
        KJM(I,J)=K(I,J-1)*K(I,J)*(DZ(J-1)+DZ(J))/(K(I,J-1)*DZ(J)
     &           +K(I,J)*DZ(J-1))
        E(I,J)=EO(I,J)+C1(I,J)*KIP(I,J)*(TO(I+1,J)-TO(I,J))
     &                +C2(I,J)*KIM(I,J)*(TO(I-1,J)-TO(I,J))
     &                +C3(I,J)*KJP(I,J)*(TO(I,J+1)-TO(I,J))
     &                +C4(I,J)*KJM(I,J)*(TO(I,J-1)-TO(I,J))
        EE(I,J)=E(I,J)/(RHO(I,J)*VOL(I,J))
        IF (EE(I,J).GT.HM) GO TO 310
        IF (EE(I,J).LT.0.D00) GO TO 315
```

```
      T(I,J)=TM
      XF(I,J)=EE(I,J)/HM
      YF(I,J)=1.D00/(1.D00+(RHOL/RHOS)*(1.D00/XF(I,J)-1.D00))
      K(I,J)=(1.D00-XF(I,J))*KS+XF(I,J)*ZKLE(J)
      RHO(I,J)=(1.D00-YF(I,J))*RHOS+YF(I,J)*RHOL
      PHASE(I,J)='MUSH'
      GO TO 304
310    T(I,J)=(EE(I,J)-HM)/CPL+TM
      K(I,J)=ZKLE(J)
      RHO(I,J)=RHOL
      XF(I,J)=1.0D00
      PHASE(I,J)='LIQ'
      GO TO 304
315    T(I,J)=(EE(I,J)/CPS)+TM
      K(I,J)=KS
      RHO(I,J)=RHOS
      XF(I,J)=0.0D00
      PHASE(I,J)='SOL'
304    ML=ML+XF(I,J)*RHOL*VOL(I,J)
305   CONTINUE
300   CONTINUE
    I=IV1
    DO 320 J=2,JJ-1
      KIM(I,J)=K(I-1,J)*K(I,J)*(DR(I-1)+DR(I))/(K(I-1,J)*DR(I)
   &          +K(I,J)*DR(I-1))
      KJP(I,J)=K(I,J+1)*K(I,J)*(DZ(J+1)+DZ(J))/(K(I,J+1)*DZ(J)
   &          +K(I,J)*DZ(J+1))
      KJM(I,J)=K(I,J-1)*K(I,J)*(DZ(J-1)+DZ(J))/(K(I,J-1)*DZ(J)
   &          +K(I,J)*DZ(J-1))
      E(I,J)=EO(I,J)-ECON(J)
   &                +C2(I,J)*KIM(I,J)*(TO(I-1,J)-TO(I,J))
   &                +C3(I,J)*KJP(I,J)*(TO(I,J+1)-TO(I,J))
   &                +C4(I,J)*KJM(I,J)*(TO(I,J-1)-TO(I,J))
   &                -QRAD(J-1)*DT
      EE(I,J)=E(I,J)/(RHO(I,J)*VOL(I,J))
      IF (EE(I,J).GT.HM) GO TO 330
      IF (EE(I,J).LT.0.D00) GO TO 335
      T(I,J)=TM
      XF(I,J)=EE(I,J)/HM
      YF(I,J)=1.D00/(1.D00+(RHOL/RHOS)*(1.D00/XF(I,J)-1.D00))
      K(I,J)=(1.D00-XF(I,J))*KS+XF(I,J)*ZKLE(J)
      RHO(I,J)=(1.D00-YF(I,J))*RHOS+YF(I,J)*RHOL
      PHASE(I,J)='MUSH'
      GO TO 324
330    T(I,J)=(EE(I,J)-HM)/CPL+TM
      K(I,J)=ZKLE(J)
      RHO(I,J)=RHOL
      XF(I,J)=1.0D00
      PHASE(I,J)='LIQ'
```

```
      GO TO 324
 335   T(I,J)=(EE(I,J)/CPS)+TM
      K(I,J)=KS
      RHO(I,J)=RHOS
      XF(I,J)=0.0D00
      PHASE(I,J)='SOL'
 324   ML=ML+XF(I,J)*RHOL*VOL(I,J)
 320  CONTINUE
      MFL=ML/MT
      RETURN
      END
C
      SUBROUTINE UPDATE(N1,N2,N3,VVF)
      CHARACTER*4 PHASE(40,20),NC
      REAL MDOT,KW,KS,KL,KLE,MT,MS,ML,K(40,20),KIP(40,20),
     &KIM(40,20),KJP(40,20),KJM(40,20),MFL,MUF,NU,NUL,KF
      COMMON DT,DRR,DZZ,DELWO,DELWI,DELWS,RI1,KIP,BBINV(18,18),QRAD(18),
     &RI2,RO1,RO2,Q,TFI,MDOT,CPF,KW,CPW,RHOW,KS,CPS,RHOS,FF(18,18),
     &KL,CPL,RHOL,TM,HM,KLE,Z2,Z3,Z4,PI,VOLT,Q1,Q2,VOL(40,20),RCML(20),
     &MT,MS,VOLS,ML,VOLL,ESHSUM,EFSUM,RA,NU,CHARL,C7,C12,ECON(20),
     &TV,TO(40,20),T(40,20),K,RHO(40,20),XF(40,20),TFIN(20),AREAOLD(3),
     &YF(40,20),DR(40),DZ(20),Z(20),R(40),EO(40,20),E(40,20),AREA(30),
     &TFO(20),TF(20),C1(40,20),C2(40,20),C3(40,20),C4(40,20),RCMLO(20),
     &TFOUT,EE(40,20),TIMEPR1,TIMEPR2,TIMEP,TIMEF,TFP,TFF,RV,RM,
     &TIME2,TIME3,TIME4,TF2,TF3,TF4,EINIT,ECAN,EBAL,EEL(40,20),
     &EELO(40,20),EELO2(40,20),PR,EML(40,20),
     &MFL,QF,II,IV1,IV2,JJ,N,PHASE,NC,
     &ZKLE(10),ZNU(10),ZRA(10),ZCHARL(10),ZNUAVG
      TIMEM=(N-1)*DT/60.0D00
      IDIFFO=(II-1)-IV1
      IDIFFN=(II-1)-IV1
C
C      VOID VIEW FACTORS
C
      IF (IDIFFN.NE.IDIFFO) CALL VOIDFF(ES,EW)
C
C      SALT NATURAL CONVECTION CORRELATION
C
      IF(NC.EQ.'ON  ') CALL CONV(DUM)
C
C      GLOBAL HEAT TRANSFER AND ENERGY BALANCE
C
      CALL ENERGY(EBALP,TIMEM)
C
C      DETERMINE SIDE WALL HEAT TRANSFER FRACTIONS
C
      CALL WALLFRAC(WALLFR1,WALLFR2,WALLFR3)
C
C      PRINT RESULTS TO OUTPUT FILES
```

```
C
      CALL OUTPUT(TIMEM,N1,N2,WALLFR1,WALLFR2,WALLFR3,EBALP,VVF)
C
C      UP-DATE INPUT HEAT FLUX
C
      IF(TIMEM.GE.54.63) Q=Q2
      IF(TIMEM.GE.72.8) Q=Q3
C
C      UP-DATE INPUT COOLING FLUID INLET TEMPERATURE
C
      IF(TIMEM.GE.TIME2.AND.TIMEM.LT.TIME3) GO TO 920
      IF(TIMEM.GE.TIME3) GO TO 930
      GO TO 905
 920  TIMEP=TIME2
      TIMEF=TIME3
      TFP=TF2
      TFF=TF3
      GO TO 905
 930  TIMEP=TIME3
      TIMEF=TIME4
      TFP=TF3
      TFF=TF4
 905  TFI=TFP+(TIMEM-TIMEP)*((TFF-TFP)/(TIMEF-TIMEP))
 950  RETURN
      END
C
      SUBROUTINE VOIDFF(ES,EW)
      CHARACTER*4 PHASE(40,20),NC
      REAL MDOT,KW,KS,KL,KLE,MT,MS,ML,K(40,20),KIP(40,20),
     &KIM(40,20),KJP(40,20),KJM(40,20),MFL,MUF,NU,NUL,KF,
     &BB(18,18),EPS(30),FFSUM(18),F12(18),F13(18),
     &F23(18),F34(18)
      COMMON DT,DRR,DZZ,DELWO,DELWI,DELWS,RI1,KIP,BBINV(18,18),QRAD(18),
     &RI2,RO1,RO2,Q,TFI,MDOT,CPF,KW,CPW,RHOW,KS,CPS,RHOS,FF(18,18),
     &KL,CPL,RHOL,TM,HM,KLE,Z2,Z3,Z4,PI,VOLT,Q1,Q2,VOL(40,20),RCML(20),
     &MT,MS,VOLS,ML,VOLL,ESHSUM,EFSUM,RA,NU,CHARL,C7,C12,ECON(20),
     &TV,TO(40,20),T(40,20),K,RHO(40,20),XF(40,20),TFIN(20),AREAOLD(3),
     &YF(40,20),DR(40),DZ(20),Z(20),R(40),EO(40,20),E(40,20),AREA(30),
     &TFO(20),TF(20),C1(40,20),C2(40,20),C3(40,20),C4(40,20),RCMLO(20),
     &TFOUT,EE(40,20),TIMEPR1,TIMEPR2,TIMEP,TIMEF,TFP,TFF,RV,RM,
     &TIME2,TIME3,TIME4,TF2,TF3,TF4,EINIT,ECAN,EBAL,EEL(40,20),
     &EELO(40,20),EELO2(40,20),PR,EML(40,20),
     &MFL,QF,II,IV1,IV2,JJ,N,PHASE,NC,
     &ZKLE(10),ZNU(10),ZRA(10),ZCHARL(10),ZNUAVG
      NRS=2*(JJ-2)+2*(II-1-IV1)
      DO 10 J=1,JJ-2
        EPS(J)=ES
 10   CONTINUE
      DO 20 J=JJ-1,NRS
```

```
        EPS(J)=EW
 20   CONTINUE
      DO 30 J=1,JJ-2
        AREA(J)=2.0D00*PI*RV*DZZ
        AREA(J+JJ-2)=2.0D00*PI*RO1*DZZ
 30   CONTINUE
      JRANGE=2*(JJ-2)+1
      I=IV2
      JJJ=1
      DO 40 J=JRANGE,NRS-1,2
        AREA(J)=2.0D00*PI*R(I)*DR(I)
        AREAOLD(JJJ)=AREA(J)
        AREA(J+1)=AREA(J)
        I=I+1
        JJJ=JJJ+1
 40   CONTINUE
      DO 11 KK=2*(JJ-2)+3,NRS-1,2
        AREA(JRANGE)=AREA(JRANGE)+AREA(KK)
        AREA(JRANGE+1)=AREA(JRANGE)
 11   CONTINUE
      NRS=2*(JJ-2)+2
      LDBBINV=NRS
      LDBB=NRS
C
C     DEFINE THE FF(KK,J) VIEW FACTOR MATRIX FOR SURFACE
C     ELEMENTS COMPRISING THE ANNULAR GEOMETRY VOID WITH
C     AN INNER SURFACE "1", AN OUTER SURFACE "2", AND
C     SIDE SURFACES "3" AND "4"
C
      DZZ1=DZZ
      DO 41 KK=1,JJ-2
      DO 42 J=JJ-1,2*(JJ-2)
        ZKJ=DZZ1*(ABS(J-(JJ-2)-KK)-1)
        IF (ZKJ.LT.0.0D00) GO TO 42
        FF(KK,J)=FF1K2J(RV,RO1,DZZ1,DZZ1,ZKJ,PI)
        FF(J,KK)=FF(KK,J)*AREA(KK)/AREA(J)
 42   CONTINUE
      FF(KK+JJ-2,KK)=FF21(RV,RO1,DZZ1,PI)
      FF(KK,KK+JJ-2)=FF(KK+JJ-2,KK)*AREA(KK+JJ-2)/AREA(KK)
 41   CONTINUE
      DO 43 KK=1,JJ-2
      I=IV2
      ZKJ=DZZ1*KK
      DO 44 J=2*(JJ-2)+1,NRS-1,2
        DR2=RO1-RV
        R2=(RO1+RV)/2.D00
        FF(KK,J)=FF1K3J(RV,R2,DZZ1,DR2,ZKJ,PI)
        FF(J,KK)=FF(KK,J)*AREA(KK)/AREA(J)
        FF(JJ-1-KK,J+1)=FF(KK,J)
```

```
        FF(J+1,JJ-1-KK)=FF(J,KK)
        I=I+1
44    CONTINUE
43    CONTINUE
      DZZ1=DZZ
      FF(JJ-1,JJ-1)=FF22(RV,RO1,DZZ1,PI)
      FFJJ1=FF(JJ,1)
      DO 45 KK=JJ-1,2*(JJ-2)
      DO 46 J=JJ-1,2*(JJ-2)
        IF(KK.EQ.J) GO TO 46
        FF(KK,J)=FF2K2J(RV,RO1,DZZ1,KK,J,PI,FFJJ1)
46    CONTINUE
      FF(KK,KK)=FF(JJ-1,JJ-1)
45    CONTINUE
      DO 47 KK=JJ-1,2*(JJ-2)
      I=IV2
      DO 48 J=2*(JJ-2)+1,NRS-1,2
        ZKJ=DZZ1*(KK-(JJ-2))
        R1=(RV+RO1)/2.D00
        DR1=RO1-RV
        FF(KK,J)=FF2K3J(R1,RO1,DZZ1,DR1,ZKJ,PI)
        FF(J,KK)=FF(KK,J)*AREA(KK)/AREA(J)
        FF(3*(JJ-2)+1-KK,J+1)=FF(KK,J)
        FF(J+1,3*(JJ-2)+1-KK)=FF(J,KK)
        I=I+1
48    CONTINUE
47    CONTINUE
      ZKJ=Z3-Z2
      I3=IV2
      I=I3
      JJJ=2*(JJ-2)+2
      KKK=2*(JJ-2)+1
      DO 49 KK=KKK,NRS-1,2
      R1=(RO1+RV)/2.D00
      DR1=RO1-RV
      DO 50 J=JJJ,NRS,2
        DR2=RO1-RV
        R2=(RO1+RV)/2.D00
        FF(KK,J)=FF3K4J(R1,R2,DR1,DR2,ZKJ,PI)
        FF(J,KK)=FF(KK,J)*AREA(KK)/AREA(J)
        I=I+1
50    CONTINUE
      I3=I3+1
      I=I3
      JJJ=JJJ+2
      KKK=KKK+2
49    CONTINUE
C
C     DEFINE "BB" MATRIX SUCH THAT {BB}{QRAD}={DD} WHERE {BB} IS
```

```
C     THE "VIEW FACTOR-EMITTANCE" MATRIX AND {DD} IS THE
C     "TEMPERATURE-TO-THE-FOURTH-POWER DIFFERENCE" MATRIX
C
      NRS=2*(JJ-2)+2
      DO 55 KK=1,NRS
      DO 60 J=1,NRS
        DELTA=0.0D00
        IF(KK.EQ.J) DELTA=1.0D00
        BB(KK,J)=(DELTA/EPS(J)-FF(KK,J)*(1.0D00-EPS(J))/EPS(J))/AREA(J)
 60   CONTINUE
 55   CONTINUE
C
C     INVERT {BB} MATRIX USING IMSL ROUTINE DLINRG
C
      CALL DLINRG(NRS,BB,LDBB,BBINV,LDBBINV)
      QRADSUM=0.0D00
      DO 70 KK=1,NRS
      FFSUM(KK)=0.0D00
      DO 80 J=1,NRS
        FFSUM(KK)=FFSUM(KK)+FF(KK,J)
 80   CONTINUE
      WRITE (14,1001) KK,FFSUM(KK),QRAD(KK)
      QRADSUM=QRADSUM+QRAD(KK)
 70   CONTINUE
      WRITE (14,1004) QRADSUM
      WRITE (14,1002) ((FF(KK,J),J=1,NRS),KK=1,NRS)
 1001 FORMAT(I4,2X,F8.6,2X,F9.5)
 1002 FORMAT(18(F6.4,1X))
 1004 FORMAT(16X,F9.5)
      RETURN
      END
C
      FUNCTION FF13(R113,R213,L13,PI)
      REAL L13
      RR=R213/R113
      A=L13**2+R213**2-R113**2
      B=L13**2-R213**2+R113**2
      C=L13**2+R213**2+R113**2
      FF13=(1.D00/(2.D00*PI))*(DARCOS(B/A)-(R113/(2.D00*L13))*
     &     (DSQRT(C**2/R113**4-4.D00*RR**2)*DARCOS(B/(RR*A))+
     &     (B/R113**2)*DARSIN(1.D00/RR)-(PI/2.D00)*(A/R113**2)))
      RETURN
      END
C
      FUNCTION FF21(R121,R221,L21F,PI)
      REAL L21,L21F
      RR=R221/R121
      L21=L21F/R121
      A=L21**2+RR**2-1.D00
```

```
      B=L21**2-RR**2+1.D00
      FF21=1.D00/RR-(1.D00/(PI*RR))*(DARCOS(B/A)-(1.D00/(2.D00*L21))*
     &   (DSQRT((A+2.D00)**2-4.D00*RR**2)*DARCOS(B/(RR*A))+
     &   B*DARSIN(1.D00/RR)-PI*A/2.D00))
      RETURN
      END
C
      FUNCTION FF22(R122,R222,L22F,PI)
      REAL L22,L22F
      RR=R222/R122
      L22=L22F/R122
      A=L22**2+RR**2-1.D00
      B=L22**2-RR**2+1.D00
      FF22=1.D00-1.D00/RR+(2.D00/(PI*RR))*DATAN(2.D00*DSQRT(RR**2-1.D00)
     &   /L22)-(L22/(2.D00*PI*RR))*((DSQRT(4.D00*RR**2+L22**2)/L22)*
     &   DARSIN((4.D00*(RR**2-1.D00)+(L22**2/RR**2)*(RR**2-2.D00))/
     &   (L22**2+4.D00*(RR**2-1.D00)))-DARSIN((RR**2-2.D00)/RR**2)+
     &   (PI/2.D00)*(DSQRT(4.D00*RR**2+L22**2)/L22-1.D00))
      RETURN
      END
C
      FUNCTION FF34(R134,R234,L34,PI)
      REAL L34
      FF34=1.D00-(2.D00*R134*L34/(R234**2-R134**2))*
     &   FF13(R134,R234,L34,PI)-
     &   (2.D00*R234*L34/(R234**2-R134**2))*(1.D00-
     &   FF22(R134,R234,L34,PI)-
     &   FF21(R134,R234,L34,PI))/2.D00
      RETURN
      END
C
      FUNCTION FF1K2J(R1,R2,L,Y,D,PI)
      REAL L
      IF (D.EQ.0.0D00) FF1K2J=((L+D)/L)*FF13(R1,R2,L+D,PI)+
     &   ((Y+D)/L)*FF13(R1,R2,Y+D,PI)-((L+D+Y)/L)*FF13(R1,R2,L+D+Y,PI)
      IF (D.EQ.0.0D00) GO TO 12
      FF1K2J=((L+D)/L)*FF13(R1,R2,L+D,PI)+((Y+D)/L)*FF13(R1,R2,Y+D,PI)-
     &      (D/L)*FF13(R1,R2,D,PI)-((L+D+Y)/L)*FF13(R1,R2,L+D+Y,PI)
 12   RETURN
      END
C
      FUNCTION FF1K3J(R1,R2,DZK,DRJ,ZKJ,PI)
      REAL L
      R2P=R2+DRJ/2.D00
      R2M=R2-DRJ/2.D00
      RDIFF=DABS(R2-R1)
      ZDIFF=DABS(ZKJ-DZK)
      IF (RDIFF.GT.DRJ) GO TO 39
      IF (ZDIFF.GT.0.01D00) GO TO 23
```

```
      FF1K3J=FF13(R1,R2P,ZKJ,PI)
      GO TO 19
 23   FF1K3J=(ZKJ/DZK)*FF13(R1,R2P,ZKJ,PI)-
     &     ((ZKJ-DZK)/DZK)*FF13(R1,R2P,ZKJ-DZK,PI)
      GO TO 19
 39   IF (ZDIFF.GT.0.01D00) GO TO 24
      FF1K3J=FF13(R1,R2P,ZKJ,PI)-FF13(R1,R2M,ZKJ,PI)
      GO TO 19
 24   FF1K3J=(ZKJ/DZK)*(FF13(R1,R2P,ZKJ,PI)-FF13(R1,
     &      R2M,ZKJ,PI))-((ZKJ-DZK)/DZK)*(FF13(R1,
     &      R2P,ZKJ-DZK,PI)-FF13(R1,R2M,ZKJ-DZK,PI))
 19   RETURN
      END
C
      FUNCTION FF2K2J(R1,R2,ZZZ22,KK,J,PI,FFJJ1)
      REAL L
      ZERO=0.0D00
      DIFFKJ=ABS(KK-J)+1.D00
      DIFFKJ1=ABS(KK-J)*1.D00
      DIFFKJ2=DIFFKJ1-1.D00
      DIFFKJ3=DIFFKJ2-1.D00
      IF (DIFFKJ1.EQ.1.D00) GO TO 15
      IF (DIFFKJ1.EQ.2.D00) GO TO 16
      FF2K2J=DIFFKJ1*(1.D00-FF22(R1,R2,DIFFKJ1*ZZZ22,PI)-FF21(R1,
     &      R2,DIFFKJ1*ZZZ22,PI))-
     &      DIFFKJ2*(1.D00-FF22(R1,R2,DIFFKJ2*ZZZ22,PI)-FF21(R1,
     &      R2,DIFFKJ2*ZZZ22,PI))/2.D00-
     &      DIFFKJ*(1.D00-FF22(R1,R2,DIFFKJ*ZZZ22,PI)-FF21(R1,
     &      R2,DIFFKJ*ZZZ22,PI))/2.D00-
     &      FF1K2J(R1,R2,DIFFKJ1*ZZZ22,ZZZ22,ZERO,PI)*
     &      DIFFKJ1*R1/R2+
     &      FF1K2J(R1,R2,DIFFKJ2*ZZZ22,ZZZ22,ZERO,PI)*
     &      DIFFKJ2*R1/R2
      GO TO 17
 15   FF2K2J=(1.D00-FF22(R1,R2,ZZZ22,PI)-FF21(R1,R2,ZZZ22,PI))-
     &      (1.D00-FF22(R1,R2,2.D00*ZZZ22,PI)-FF21(R1,
     &      R2,2.D00*ZZZ22,PI))-FFJJ1
      GO TO 17
 16   FF2K2J=DIFFKJ1*(1.D00-FF22(R1,R2,DIFFKJ1*ZZZ22,PI)-FF21(R1,
     &      R2,DIFFKJ1*ZZZ22,PI))-
     &      DIFFKJ2*(1.D00-FF22(R1,R2,DIFFKJ2*ZZZ22,PI)-FF21(R1,
     &      R2,DIFFKJ2*ZZZ22,PI))/2.D00-
     &      DIFFKJ*(1.D00-FF22(R1,R2,DIFFKJ*ZZZ22,PI)-FF21(R1,
     &      R2,DIFFKJ*ZZZ22,PI))/2.D00-
     &      FF1K2J(R1,R2,DIFFKJ1*ZZZ22,ZZZ22,DIFFKJ3*ZZZ22,PI)*
     &      DIFFKJ1*R1/R2+
     &      FF1K2J(R1,R2,DIFFKJ2*ZZZ22,ZZZ22,DIFFKJ3*ZZZ22,PI)*
     &      DIFFKJ2*R1/R2
 17   RETURN
```

```
      END
C
      FUNCTION FF2K3J(R1,R2,ZZZ,DR1,ZKJ,PI)
      REAL L
      R1P=R1+DR1/2.D00
      R1M=R1-DR1/2.D00
      RDIFF=DABS(R2-R1)
      DIFFKJ=ZKJ/ZZZ
      DIFFKJ1=DIFFKJ-1.D00
      IF (DIFFKJ.EQ.1.D00) GO TO 25
      IF (RDIFF.LT.DR1) GO TO 21
      FF2K3J=DIFFKJ*(1.D00-FF22(R1M,R2,DIFFKJ*ZZZ,PI)-
     &        FF21(R1M,R2,DIFFKJ*ZZZ,PI))/2.D00-
     &        DIFFKJ1*(1.D00-FF22(R1M,R2,DIFFKJ1*ZZZ,PI)-
     &        FF21(R1M,R2,DIFFKJ1*ZZZ,PI))/2.D00-
     &        DIFFKJ*(1.D00-FF22(R1P,R2,DIFFKJ*ZZZ,PI)-
     &        FF21(R1P,R2,DIFFKJ*ZZZ,PI))/2.D00+
     &        DIFFKJ1*(1.D00-FF22(R1P,R2,DIFFKJ1*ZZZ,PI)-
     &        FF21(R1P,R2,DIFFKJ1*ZZZ,PI))/2.D00
      GO TO 27
 21   FF2K3J=DIFFKJ*(1.D00-FF22(R1M,R2,DIFFKJ*ZZZ,PI)-
     &        FF21(R1M,R2,DIFFKJ*ZZZ,PI))/2.D00-
     &        DIFFKJ1*(1.D00-FF22(R1M,R2,DIFFKJ1*ZZZ,PI)-
     &        FF21(R1M,R2,DIFFKJ1*ZZZ,PI))/2.D00
      GO TO 27
 25   IF (RDIFF.LT.DR1) GO TO 22
      FF2K3J=(1.D00-FF22(R1M,R2,ZZZ,PI)-
     &        FF21(R1M,R2,ZZZ,PI))/2.D00-
     &        (1.D00-FF22(R1P,R2,ZZZ,PI)-
     &        FF21(R1P,R2,ZZZ,PI))/2.D00
      GO TO 27
 22   FF2K3J=(1.D00-FF22(R1M,R2,ZZZ,PI)-
     &        FF21(R1M,R2,ZZZ,PI))/2.D00
 27   RETURN
      END
C
      FUNCTION FF3K4J(R1,R2,DR1,DR2,L,PI)
      REAL L
      RJP=R2+DR2/2.D00
      RJM=R2-DR2/2.D00
      RKP=R1+DR1/2.D00
      RKM=R1-DR1/2.D00
      DIFFR1=DABS(R2-R1)
      DIFFR2=DABS(RJM-RKP)
      IF (DIFFR1.GT.1.0D-05) GO TO 11
      FF3K4J=FF34(RKM,RJP,L,PI)
      GO TO 337
 11   IF (DIFFR2.GT.1.0D-05) GO TO 12
      FF3K4J=(0.5D00)*(AJDAK*FF34(RKM,RJP,L,PI)-AAAK*
```

```
     &      FF34(RJM,RJP,L,PI)-FF34(RKM,RKP,L,PI))
      FDA=FF3K4J
      GO TO 337
 12   FF3K4J=(0.5D00)*(AJCDAK*FF34(RKM,RJP,L,PI)-AABAK*
     &      FF34(RKP,RJP,L,PI)-2.D00*FDA-FF34(RKM,RKP,L,PI))
 337  RETURN
      END
C
      SUBROUTINE CONV(DUM)
      CHARACTER*4 PHASE(40,20),NC
      REAL MDOT,KW,KS,KL,KLE,MT,MS,ML,K(40,20),KIP(40,20),
     &KIM(40,20),KJP(40,20),KJM(40,20),MFL,MUF,NU,NUL,KF,ZML(10)
      COMMON DT,DRR,DZZ,DELWO,DELWI,DELWS,RI1,KIP,BBINV(18,18),QRAD(18),
     &RI2,RO1,RO2,Q,TFI,MDOT,CPF,KW,CPW,RHOW,KS,CPS,RHOS,FF(18,18),
     &KL,CPL,RHOL,TM,HM,KLE,Z2,Z3,Z4,PI,VOLT,Q1,Q2,VOL(40,20),RCML(20),
     &MT,MS,VOLS,ML,VOLL,ESHSUM,EFSUM,RA,NU,CHARL,C7,C12,ECON(20),
     &TV,TO(40,20),T(40,20),K,RHO(40,20),XF(40,20),TFIN(20),AREAOLD(3),
     &YF(40,20),DR(40),DZ(20),Z(20),R(40),EO(40,20),E(40,20),AREA(30),
     &TFO(20),TF(20),C1(40,20),C2(40,20),C3(40,20),C4(40,20),RCMLO(20),
     &TFOUT,EE(40,20),TIMEPR1,TIMEPR2,TIMEP,TIMEF,TFP,TFF,RV,RM,
     &TIME2,TIME3,TIME4,TF2,TF3,TF4,EINIT,ECAN,EBAL,EEL(40,20),
     &EELO(40,20),EELO2(40,20),PR,EML(40,20),
     &MFL,QF,II,IV1,IV2,JJ,N,PHASE,NC,
     &ZKLE(10),ZNU(10),ZRA(10),ZCHARL(10),ZNUAVG
      MS=MT-ML
      RM=DSQRT(1.0D00*RI2*RI2+MS/(RHOS*PI*(Z3-Z2)))
      CHARL=RV-RM
      IF (CHARL.LE.0.0D00) GO TO 530
      C18=(Z3-Z2)/CHARL
      I=IV1
      IF (RV.EQ.RO1) I=II
      TV=0.0D00
      DO 500 J=2,JJ-1
        TV=TV+T(I,J)
 500  CONTINUE
      TV=TV/(JJ-2)
C
C     NOTE: FOR CASES WITHOUT VOID, I---> II AND TV=TSHELL @ O.D.
C
      RA=C7*(TV-TM)*CHARL**3
      IF (RA.LE.0.0D00) GO TO 530
      NU=0.42D00*PR**0.012D00*RA**0.25D00*C18**(-0.3D00)
      IF (C18.LT.10.0D00) NU=0.22D00*(RA*PR/(0.2D00+PR))**0.28D00
     &                 *C18**(-0.25D00)
      IF (NU.LT.1.0D00) GO TO 530
      GO TO 531
 530  NU=1.0D00
 531  KLE=KL*NU
C
```

```
C    FREE CONVECTION WITH AXIAL DEPENDENCE
C
     ZMT=MT/(JJ-2)
     DO 540 J=2,JJ-1
     ZML(J)=0.0D00
     DO 550 I=2,IV1
       ZML(J)=ZML(J)+XF(I,J)*RHOL*VOL(I,J)
 550 CONTINUE
     ZMS=ZMT-ZML(J)
     ZRM=DSQRT(1.0D00*RI2*RI2+ZMS/(RHOS*PI*DZZ))
     ZCHARL(J)=RV-ZRM
     IF (ZCHARL(J).LE.0.0D00) GO TO 560
     C18=DZZ/ZCHARL(J)
     I=IV1
     IF (RV.EQ.RO1) I=II
C
C    NOTE: FOR CASES WITHOUT VOID, I-->II AND T HOT = T SHELL @ O.D.
C
     ZRA(J)=C7*(T(I,J)-TM)*ZCHARL(J)**3
     IF (ZRA(J).LE.0.0D00) GO TO 560
     ZNU(J)=0.42D00*PR**0.012D00*ZRA(J)**0.25D00*C18**(-0.3D00)
     IF (C18.LT.10.0D00) ZNU(J)=0.22D00*(ZRA(J)*PR/(0.2D00+PR))
    &            **0.28D00*C18**(-0.25D00)
     IF (ZNU(J).LT.1.0D00) GO TO 560
     GO TO 561
 560 ZNU(J)=1.0D00
 561 ZKLE(J)=KL*ZNU(J)
 540 CONTINUE
     RETURN
     END
C
     SUBROUTINE ENERGY(EBALP,TIMEM)
     CHARACTER*4 PHASE(40,20),NC
     REAL MDOT,KW,KS,KL,KLE,MT,MS,ML,K(40,20),KIP(40,20),
    &KIM(40,20),KJP(40,20),KJM(40,20),MFL,MUF,NU,NUL,KF
     COMMON DT,DRR,DZZ,DELWO,DELWI,DELWS,RI1,KIP,BBINV(18,18),QRAD(18),
    &RI2,RO1,RO2,Q,TFI,MDOT,CPF,KW,CPW,RHOW,KS,CPS,RHOS,FF(18,18),
    &KL,CPL,RHOL,TM,HM,KLE,Z2,Z3,Z4,PI,VOLT,Q1,Q2,VOL(40,20),RCML(20),
    &MT,MS,VOLS,ML,VOLL,ESHSUM,EFSUM,RA,NU,CHARL,C7,C12,ECON(20),
    &TV,TO(40,20),T(40,20),K,RHO(40,20),XF(40,20),TFIN(20),AREAOLD(3),
    &YF(40,20),DR(40),DZ(20),Z(20),R(40),EO(40,20),E(40,20),AREA(30),
    &TFO(20),TF(20),C1(40,20),C2(40,20),C3(40,20),C4(40,20),RCMLO(20),
    &TFOUT,EE(40,20),TIMEPR1,TIMEPR2,TIMEP,TIMEF,TFP,TFF,RV,RM,
    &TIME2,TIME3,TIME4,TF2,TF3,TF4,EINIT,ECAN,EBAL,EEL(40,20),
    &EELO(40,20),EELO2(40,20),PR,EML(40,20),
    &MFL,QF,II,IV1,IV2,JJ,N,PHASE,NC,
    &ZKLE(10),ZNU(10),ZRA(10),ZCHARL(10),ZNUAVG
      QSHELL=Q*C12
      QSALT=QSHELL-QF
```

```
      ESHSUM=QSHELL*DT*(N-1)
      N546=3276.D00/DT
      ESH546=Q1*3276.D00*C12
      N728=4368.D00/DT
      ESH728=Q2*1092.D00*C12+ESH546
      IF(TIMEM.GT.54.7.AND.TIMEM.LT.72.7) ESHSUM=ESH546+QSHELL*DT*
     &                                   (N-N546)
      IF(TIMEM.GT.72.8) ESHSUM=ESH728+QSHELL*DT*(N-N728)
      ECAN=0.00D00
      DO 835 I=1,II
      DO 840 J=1,JJ
       ECAN=ECAN+E(I,J)
  840 CONTINUE
  835 CONTINUE
      EBAL=ESHSUM-EFSUM-(ECAN-EINIT)
      EBALP=100.*EBAL/ESHSUM
      RETURN
      END
C
      SUBROUTINE WALLFRAC(WALLFR1,WALLFR2,WALLFR3)
      CHARACTER*4 PHASE(40,20),NC
      REAL MDOT,KW,KS,KL,KLE,MT,MS,ML,K(40,20),KIP(40,20),
     &KIM(40,20),KJP(40,20),KJM(40,20),MFL,MUF,NU,NUL,KF
      COMMON DT,DRR,DZZ,DELWO,DELWI,DELWS,RI1,KIP,BBINV(18,18),QRAD(18),
     &RI2,RO1,RO2,Q,TFI,MDOT,CPF,KW,CPW,RHOW,KS,CPS,RHOS,FF(18,18),
     &KL,CPL,RHOL,TM,HM,KLE,Z2,Z3,Z4,PI,VOLT,Q1,Q2,VOL(40,20),RCML(20),
     &MT,MS,VOLS,ML,VOLL,ESHSUM,EFSUM,RA,NU,CHARL,C7,C12,ECON(20),
     &TV,TO(40,20),T(40,20),K,RHO(40,20),XF(40,20),TFIN(20),AREAOLD(3),
     &YF(40,20),DR(40),DZ(20),Z(20),R(40),EO(40,20),E(40,20),AREA(30),
     &TFO(20),TF(20),C1(40,20),C2(40,20),C3(40,20),C4(40,20),RCMLO(20),
     &TFOUT,EE(40,20),TIMEPR1,TIMEPR2,TIMEP,TIMEF,TFP,TFF,RV,RM,
     &TIME2,TIME3,TIME4,TF2,TF3,TF4,EINIT,ECAN,EBAL,EEL(40,20),
     &EELO(40,20),EELO2(40,20),PR,EML(40,20),
     &MFL,QF,II,IV1,IV2,JJ,N,PHASE,NC,
     &ZKLE(10),ZNU(10),ZRA(10),ZCHARL(10),ZNUAVG
      II2=II/2
      QW1=0.0D00
      QW2=0.0D00
      QW3=0.0D00
      QPCM1=0.0D00
      QPCM2=0.0D00
      QPCM3=0.0D00
      QW1=KW*2.0D00*PI*DELWS*(T(3,1)-T(2,1))/
     &  DLOG(1.00D00*R(3)/R(2))
      QW1=QW1+KW*2.0D00*PI*DELWS*(T(3,JJ)-T(2,JJ))/
     &  DLOG(1.00D00*R(3)/R(2))
      QW2=KW*2.0D00*PI*DELWS*(T(II2+1,1)-T(II2,1))/
     &  DLOG(1.00D00*R(II2+1)/R(II2))
      QW2=QW2+KW*2.0D00*PI*DELWS*(T(II2+1,JJ)-T(II2,JJ))/
```

```
     &  DLOG(1.00D00*R(II2+1)/R(II2))
      QW3=KW*2.0D00*PI*DELWS*(T(II,1)-T(II-1,1))/
     &  DLOG(1.00D00*R(II)/R(II-1))
      QW3=QW3+KW*2.0D00*PI*DELWS*(T(II,JJ)-T(II-1,JJ))/
     &  DLOG(1.00D00*R(II)/R(II-1))
      DO 701 J=2,JJ-1
      QPCM1=QPCM1+KIP(2,J)*2.0D00*PI*DZZ*(T(3,J)-T(2,J))/
     &    DLOG(1.00D00*R(3)/R(2))
      QPCM2=QPCM2+KIP(II2,J)*2.0D00*PI*DZZ*(T(II2+1,J)-T(II2,J))/
     &    DLOG(1.00D00*R(II2+1)/R(II2))
      QPCM3=QPCM3+DABS(ECON(J)/DT)+DABS(QRAD(J+7))
701   CONTINUE
      WALLFR1=100.D00*DABS(QW1)/(DABS(QW1)+DABS(QPCM1))
      WALLFR2=100.D00*DABS(QW2)/(DABS(QW2)+DABS(QPCM2))
      WALLFR3=100.D00*DABS(QW3)/(DABS(QW3)+DABS(QPCM3))
      RETURN
      END
C
      SUBROUTINE OUTPUT(TIMEM,N1,N2,WALLFR1,WALLFR2,WALLFR3,EBALP,VVF)
      CHARACTER*4 PHASE(40,20),NC
      REAL MDOT,KW,KS,KL,KLE,MT,MS,ML,K(40,20),KIP(40,20),
     &KIM(40,20),KJP(40,20),KJM(40,20),MFL,MUF,NU,NUL,KF
      COMMON DT,DRR,DZZ,DELWO,DELWI,DELWS,RI1,KIP,BBINV(18,18),QRAD(18),
     &RI2,RO1,RO2,Q,TFI,MDOT,CPF,KW,CPW,RHOW,KS,CPS,RHOS,FF(18,18),
     &KL,CPL,RHOL,TM,HM,KLE,Z2,Z3,Z4,PI,VOLT,Q1,Q2,VOL(40,20),RCML(20),
     &MT,MS,VOLS,ML,VOLL,ESHSUM,EFSUM,RA,NU,CHARL,C7,C12,ECON(20),
     &TV,TO(40,20),T(40,20),K,RHO(40,20),XF(40,20),TFIN(20),AREAOLD(3),
     &YF(40,20),DR(40),DZ(20),Z(20),R(40),EO(40,20),E(40,20),AREA(30),
     &TFO(20),TF(20),C1(40,20),C2(40,20),C3(40,20),C4(40,20),RCMLO(20),
     &TFOUT,EE(40,20),TIMEPR1,TIMEPR2,TIMEP,TIMEF,TFP,TFF,RV,RM,
     &TIME2,TIME3,TIME4,TF2,TF3,TF4,EINIT,ECAN,EBAL,EEL(40,20),
     &EELO(40,20),EELO2(40,20),PR,EML(40,20),
     &MFL,QF,II,IV1,IV2,JJ,N,PHASE,NC,
     &ZKLE(10),ZNU(10),ZRA(10),ZCHARL(10),ZNUAVG
       IF(N.NE.N1) GO TO 810
C
C      OUTPUT WALL FRACTION VALUES
C
       WRITE(11,3400) TIMEM,WALLFR1,WALLFR2,WALLFR3
       JJ2=JJ/2
       QVOIDCON=0.0D00
       QVOIDRAD=0.0D00
       QVOIDTOT=0.0D00
       ZNUAVG=0.0D00
       ZRAAVG=0.0D00
       DO 811 J=2,JJ-1
         QVOIDCON=QVOIDCON+(-ECON(J)/DT)
         QVOIDRAD=QVOIDRAD+(-QRAD(J-1))
         QVOIDTOT=QVOIDCON+QVOIDRAD
```

```
       ZNUAVG=ZNUAVG+ZNU(J)
       ZRAAVG=ZRAAVG+ZRA(J)
  811  CONTINUE
      ZRAAVG=ZRAAVG/(JJ-2)
      ZNUAVG=ZNUAVG/(JJ-2)
C
C     OUTPUT TIME-DEPENDENT TEMPERATURES AND HEAT FLUXES
C
      WRITE (8,2500) TIMEM,MFL,T(II,JJ2),VVF,
     &TFI,TFOUT,QF,EBAL,EBALP,QVOIDCON,QVOIDRAD,QVOIDTOT
C
C     OUTPUT FREE CONVECTION VALUES
C
      IF(NC.EQ.'ON  ') WRITE (9,2600) TIMEM,CHARL,TV,RA,NU
      IF(NC.EQ.'ON  ') WRITE (17,3750) TIMEM,ZNUAVG,(ZNU(J),J=2,JJ-1),
     &                (ZCHARL(J),J=2,JJ-1)
      IF(NC.EQ.'ON  ') WRITE (18,3755) TIMEM,ZRAAVG,(ZRA(J),J=2,JJ-1)
      N1=N1+(TIMEPR1/DT)
      GO TO 850
C
C     OUTPUT PCM PHASE DISTRIBUTIONS
C
 810  WRITE (13,3000) TIMEM,MFL,VVF,NU,(Z(J),J=2,JJ-1)
      WRITE (13,3050)
      DO 800 I=2,II-1
        II1=II+1-I
        WRITE(13,3100) R(II1),(PHASE(II1,J),J=2,JJ-1),K(II1,5)
 800  CONTINUE
C
C     OUTPUT CANISTER TEMPERATURE DISTRIBUTIONS
C
      WRITE (12,3450) TIMEM,MFL,VVF,NU,(Z(J),J=1,JJ)
      WRITE (12,3050)
      DO 855 I=1,II
        II1=II+1-I
        WRITE(12,3500) R(II1),(T(II1,J),J=1,JJ)
 855  CONTINUE
      N2=N2+TIMEPR2/DT
2500  FORMAT(F6.2,2X,F5.3,1X,F6.1,2X,F6.4,2(2X,F6.1),1X,F7.2,
     &        2X,F7.0,2X,F5.2,2X,3(F8.3,2X))
2600  FORMAT(F6.2,1X,F5.3,2X,F6.1,2X,F9.0,2X,F6.3)
3000  FORMAT(//' TIME=',F6.2,'  MFL=',F6.4,'  VVF=',F6.4,'  NU=',F6.3
     &//T25,' CANISTER PCM PHASE MAP'//'   Z, CM =',18(1X,F6.4))
3050  FORMAT('R, CM')
3100  FORMAT(F6.4,7X,8(A4,3X),D11.4)
3150  FORMAT(//'    SHELL TEMPERATURES AT TIME = ',F6.2,' MIN '//
     &' R, CM ',3X,' T(R,Z=0) ',3X,' T(R,Z=L) '/)
3200  FORMAT(F6.4,6X,F6.1,8X,F6.1)
3250  FORMAT(//'    SHELL TEMPERATURES AT TIME = ',F6.2,' MIN '//
```

```
   &' TFI=',F6.1,'  TFOUT=',F6.1//
   &' Z, CM ',3X,'T(R=RO,Z) ',4X,'T(R=RI,Z) ',5X,'  TF(Z)  '/)
3300 FORMAT(F6.4,6X,F6.1,8X,F6.1,8X,F6.1)
3400 FORMAT(F7.3,3(3X,F7.3),2X,2(I2,2X),6(F6.4,2X))
3450 FORMAT(//' TIME=',F6.2,'  MFL=',F6.4,'  VVF=',F6.4,'  NU=',F6.3
   &//T25,' CANISTER TEMPERATURE MAP'//'  Z, CM =',20(2X,F6.4))
3500 FORMAT(F6.4,6X,20(F6.1,2X))
3750 FORMAT(F6.2,2X,F5.3,2X,8(F5.3,1X),1X,8(F5.3,1X))
3755 FORMAT(F6.2,2X,F9.0,2X,8(F9.0,1X))
850  RETURN
     END
```

A2.2 Program Variable Definitions

NAME	VARIABLE TYPE	DEFINITION
AL	REAL*8	LIQUID PCM THERMAL DIFFUSIVITY, CM2/SEC
AREA	REAL*8	VOID SURFACE ELEMENT AREA ARRAY, CM2
AS	REAL*8	SOLID PCM THERMAL DIFFUSIVITY, CM2/SEC
BB	REAL*8	VOID "VIEW FACTOR – EMITTANCE" MATRIX
BETA	REAL*8	VOLUMETRIC COEFFICIENT OF THERMAL EXPANSION, 1/K
CHARL	REAL*8	LIQUID PCM CHARACTERISTIC LENGTH, CM
CPF	REAL*8	HE/XE COOLING FLUID SPECIFIC HEAT, J/G/K
CPL	REAL*8	LIQUID PCM SPECIFIC HEAT, J/G/K
CPS	REAL*8	SOLID PCM SPECIFIC HEAT, J/G/K
CPW	REAL*8	CONTAINMENT WALL SPECIFIC HEAT, J/G/K
C1	REAL*8	ELEMENT CONDUCTOR COEFFICIENT ARRAY
C2	REAL*8	ELEMENT CONDUCTOR COEFFICIENT ARRAY
C3	REAL*8	ELEMENT CONDUCTOR COEFFICIENT ARRAY
C4	REAL*8	ELEMENT CONDUCTOR COEFFICIENT ARRAY
C7–C18	REAL*8	MISCELLANEOUS CONSTANTS
DD	REAL*8	VOID "TEMPERATURE^4 DIFFERENCE" MATRIX
DEL	REAL*8	KRONECKER DELTA FUNCTION
DELWI	REAL*8	CANISTER INNER WALL THICKNESS, CM
DELWO	REAL*8	CANISTER OUTER WALL THICKNESS, CM
DELWS	REAL*8	CANISTER SIDE WALL THICKNESS, CM
DR	REAL*8	RADIAL GRID SIZE ARRAY, CM
DT	REAL*8	TIME STEP, SEC
DUM	REAL*8	DUMMY VARIABLE
DZ	REAL*8	AXIAL GRID SIZE ARRAY, CM
E	REAL*8	N+1 TIME STEP ELEMENT ENTHALPY, J
EBAL	REAL*8	GLOBAL ENERGY BALANCE, J
ECAN	REAL*8	CANISTER ENERGY CONTENT, J
ECON	REAL*8	VOID ELEMENT CONDUCTION ENERGY ARRAY, J
EE	REAL*8	ELEMENT SPECIFIC ENTHALPY, J/G
EFSUM	REAL*8	SUM OF ENERGY TRANSFER TO COOLING FLUID, J
EINIT	REAL*8	INITIAL CANISTER ENERGY CONTENT, J
EO	REAL*8	N TIME STEP ELEMENT ENTHALPY, J
EPS	REAL*8	VOID SURFACE ELEMENT EMITTANCE ARRAY
ES	REAL*8	PCM EMITTANCE
ESHSUM	REAL*8	ABSORBED CANISTER ENERGY, J
EW	REAL*8	CONTAINMENT WALL EMITTANCE
FF	REAL*8	VOID SURFACE ELEMENT VIEW FACTOR ARRAY
FFSUM	REAL*8	SUM OF VOID SURFACE ELEMENT VIEW FACTORS
G	REAL*8	GRAVITY ACCELERATION, CM/SEC2
GAMMAO	REAL*8	1–RHOL/RHOS
H	REAL*8	COOLING FLUID FILM COEFFICIENT, W/CM2/K
HM	REAL*8	PCM HEAT OF FUSION, J/G
I	INT*4	RADIAL DO LOOP INDEX
II	INT*4	TOTAL NUMBER OF RADIAL GRIDS

VARIABLE NAME	TYPE	DEFINITION
IV1	INT*4	RADIAL PCM GRIDS ADJACENT TO VOID
IV2	INT*4	RADIAL VOID GRIDS ADJACENT TO PCM
J	INT*4	AXIAL DO LOOP INDEX
JJ	INT*4	TOTAL NUMBER OF AXIAL GRIDS
K	REAL*8	ELEMENT THERMAL CONDUCTIVITY ARRAY, W/CM/K
KIM	REAL*8	"I-1" ELEMENT-TO-ELEMENT CONDUCTOR, W/CM/K
KIP	REAL*8	"I+1" ELEMENT-TO-ELEMENT CONDUCTOR, W/CM/K
KJM	REAL*8	"J-1" ELEMENT-TO-ELEMENT CONDUCTOR, W/CM/K
KJP	REAL*8	"J+1" ELEMENT-TO-ELEMENT CONDUCTOR, W/CM/K
KF	REAL*8	COOLING FLUID THERMAL CONDUCTIVITY, W/CM/K
KL	REAL*8	LIQUID PCM THERMAL CONDUCTIVITY, W/CM/K
KLE	REAL*8	ENHANCED LIQUID PCM THERMAL CONDUCTIVITY, W/CM/K
KS	REAL*8	SOLID PCM THERMAL CONDUCTIVITY, W/CM/K
KW	REAL*8	CONTAINMENT WALL THERMAL CONDUCTIVITY, W/CM/K
MDOT	REAL*8	COOLING FLUID MASS FLOW RATE, G/SEC
MFL	REAL*8	MASS FRACTION LIQUID PCM
ML	REAL*8	TOTAL LIQUID PCM MASS, G
MS	REAL*8	TOTAL SOLID PCM MASS, G
MT	REAL*8	TOTAL PCM MASS, G
MUF	REAL*8	COOLING FLUID VISCOSITY, G/SEC/CM
N	INT*4	TIME STEP DO LOOP INDEX
NC	CHAR	NATURAL CONVECTION ON/OFF FLAG
NN	INT*4	TOTAL NUMBER OF TIME STEPS
NRS	INT*4	NUMBER OF VOID SURFACE RADIATING ELEMENTS
NU	REAL*8	LIQUID PCM NUSSELT NUMBER
NUL	REAL*8	LIQUID PCM KINEMATIC VISCOSITY, CM2/SEC
N1,N2	INT*4	UPDATE AND/OR PRINTED OUTPUT TIME STEPS
PHASE	CHAR	PCM ELEMENT PHASE; LIQUID, MUSHY, SOLID, OR VOID
PI	REAL*8	PI CONSTANT
PR	REAL*8	LIQUID PCM PRANDTL NUMBER
PRF	REAL*8	COOLING FLUID PRANDTL NUMBER
Q	REAL*8	OUTER WALL ABSORBED HEAT FLUX, W/CM2
QF	REAL*8	HEAT TO COOLING FLUID, W
QPCM	REAL*8	RADIAL HEAT TRANSFER IN PCM, W
QRAD	REAL*8	VOID SURFACE ELEMENT NET HEAT LOSS ARRAY, W
QSALT	REAL*8	NET HEAT TO CANISTER, W
QSHELL	REAL*8	OUTER WALL ABSORBED HEAT, W
QVOIDCON	REAL*8	VOID CONDUCTION HEAT TRANSFER, W
QVOIDRAD	REAL*8	VOID RADIATION HEAT TRANSFER, W
QVOIDTOT	REAL*8	VOID TOTAL HEAT TRANSFER, W
QW	REAL*8	RADIAL HEAT TRANSFER IN CANISTER SIDE WALLS, W
R	REAL*8	RADIAL COORDINATE, CM
RA	REAL*8	LIQUID PCM RAYLEIGH NUMBER
RE	REAL*8	COOLING FLUID REYNOLDS NUMBER
RHO	REAL*8	ELEMENT DENSITY ARRAY, G/CM3
RHOF	REAL*8	COOLING FLUID DENSITY, G/CM3

NAME	VARIABLE TYPE	DEFINITION
RHOL	REAL*8	LIQUID PCM DENSITY, G/CM3
RHOS	REAL*8	SOLID PCM DENSITY, G/CM3
RHOW	REAL*8	CONTAINMENT WALL DENSITY, G/CM3
RI1	REAL*8	COOLING FLUID TUBE INNER RADIUS, CM
RI2	REAL*8	RI1+DELWI, CM
RM	REAL*8	AVERAGE PCM SOLID–LIQUID INTERFACE RADIUS, CM
RO1	REAL*8	RO2–DELWO, CM
RO2	REAL*8	CANISTER OUTER RADIUS, CM
RV	REAL*8	PCM–VOID INTERFACE RADIUS, CM
SIGMA	REAL*8	STEFAN–BOLTZMANN CONSTANT, W/CM2/K4
T	REAL*8	N+1 TIME STEP ELEMENT TEMPERATURE, K
TF	REAL*8	COOLING FLUID TEMPERATURE ARRAY, K
TFI	REAL*8	COOLING FLUID INLET TEMPERATURE, K
TFOUT	REAL*8	COOLING FLUID OUTLET TEMPERATURE, K
TIMEM	REAL*8	SIMULATION TIME, MIN
TM	REAL*8	PCM MELTING POINT, K
TO	REAL*8	N TIME STEP ELEMENT TEMPERATURE, K
TSHELL	REAL*8	OUTER CANISTER WALL AVERAGE TEMPERATURE, K
TTUBE	REAL*8	AVERAGE COOLING FLUID TUBE TEMPERATURE, K
TV	REAL*4	INNER VOID SURFACE TEMPERATURE, K
U	REAL*8	OVERALL HEAT TRANSFER COEFFICIENT, W/CM2/K
V	REAL*8	COOLING FLUID VELOCITY, CM/SEC
VOL	REAL*8	ELEMENT VOLUME ARRAY, CM3
VOLL	REAL*8	TOTAL LIQUID PCM VOLUME, CM3
VOLS	REAL*8	TOTAL SOLID PCM VOLUME, CM3
VOLT	REAL*8	TOTAL VOLUME, CM3
VOLV	REAL*8	TOTAL VOID VOLUME, CM3
VVF	REAL*8	VOID VOLUME FRACTION
WALLFR1	REAL*8	RADIAL HEAT TRANSFER WALL FRACTION AT INNER RADIUS
WALLFR2	REAL*8	RADIAL HEAT TRANSFER WALL FRACTION AT MEAN RADIUS
WALLFR3	REAL*8	RADIAL HEAT TRANSFER WALL FRACTION AT OUTER RADIUS
XF	REAL*8	ELEMENT LIQUID PCM MASS FRACTION
YF	REAL*8	ELEMENT LIQUID PCM VOLUME FRACTION
Z	REAL*8	AXIAL COORDINATE, CM
ZCHARL	REAL*8	AXIAL DEPENDENT CHARACTERISTIC LENGTH ARRAY, CM
ZKLE	REAL*8	AXIAL DEPENDENT ENHANCED CONDUCTIVITY ARRAY, W/CM/K
ZNU	REAL*8	AXIAL DEPENDENT NUSSELT NUMBER ARRAY
ZRA	REAL*8	AXIAL DEPENDENT RAYLEIGH NUMBER ARRAY, CM
ZRM	REAL*8	AXIAL DEPENDENT SOLID–LIQUID INTERFACE POSITION, CM

Appendix A3. Video Animations

A video tape which animates the transient, numerical results from two-dimensional canister analyses was created at the NASA Lewis Research Center (LeRC) advanced Graphics Visualization Laboratory (G-VIS Lab). The animation visually depicts canister temperatures, temperature gradients, and PCM phase distributions through the combined use of color fringe and isotherm contour plotting techniques. A data set containing temperature predictions for a single 91 minute TES charge-discharge cycle at 6-second intervals is read in and animated by the LeRC-developed program SVP (Scientific Visualization Program). SVP is run on the LeRC VM mainframe system through a Silicon Graphics IRIS4D/120 workstation. The graphical output from SVP is transferred to an Abekas A60 Digital Video Disk Recorder with which animation loops and segments are defined and displayed at various speeds. In conjunction with the A60, an Abekas A34 Solo unit is used for editing and video special effects before the final video sequences are transferred to 1 inch video tape, 3/4 inch (Umatic) or VHS videocassette for presentation. This procedure is repeated for each of three cases of two-dimensional canister analyses: without a void model, with a void model, and with void and free convection models.

The animated numerical results are displayed in real time at 100:1 or 300:1 time compression ratios. For example, temperature predictions from a 91 minute cycle displayed at a 300:1 time compression ratio would have a viewing time of 91/300 minutes or 18.2 seconds. This kind of visualization provides an effective method to confirm the accuracy of numerical predictions, more thoroughly interpret spatial and temporal relationships, and observe complex phenomena which can not be observed in experiments. From a practical standpoint, visualization of numerical predictions reduces the task of reviewing a 2-inch thick computer output listing containing 182,000 tabular temperature predictions (10 by 20 finite-difference elements x 91 minute cycle x 10 up-dates per minute = 182,000 predictions) to viewing an 18.2 second video tape presentation.

The 12-minute, VHS video tape animating two-dimensional canister temperature predictions is available for viewing by contacting the author or the Cleveland State University Department of Mechanical Engineering (Dr. Mounir B. Ibrahim).

National Aeronautics and
Space Administration

Report Documentation Page

1. Report No.
NASA TM-103731

2. Government Accession No.

3. Recipient's Catalog No.

4. Title and Subtitle
Multi-Dimensional Modeling of a Thermal Energy Storage Canister

5. Report Date
January 1991

6. Performing Organization Code

7. Author(s)
Thomas W. Kerslake

8. Performing Organization Report No.
E-5966

10. Work Unit No.
474-52-10

9. Performing Organization Name and Address
National Aeronautics and Space Administration
Lewis Research Center
Cleveland, Ohio 44135-3191

11. Contract or Grant No.

13. Type of Report and Period Covered
Technical Memorandum

12. Sponsoring Agency Name and Address
National Aeronautics and Space Administration
Washington, D.C. 20546-0001

14. Sponsoring Agency Code

15. Supplementary Notes
This report was submitted as a dissertation in partial fulfillment of the requirements for the degree Master of Science in Mechanical Engineering at the Cleveland State University in December 1990. Responsible person, Thomas W. Kerslake (216) 433-5373.

16. Abstract
The Solar Dynamic Power Module being developed for Space Station Freedom uses a eutectic mixture of LiF-CaF_2 phase change material (PCM) contained in toroidal canisters for thermal energy storage. Presented herein are the results from heat transfer analyses of a PCM containment canister. One- and two-dimensional finite-difference computer models are developed to analyze heat transfer in the canister walls, PCM, void, and heat engine working fluid coolant. The modes of heat transfer considered include conduction in canister walls and solid PCM, conduction and pseudo—free convection in liquid PCM, conduction and radiation across PCM vapor filled void regions and forced convection in the heat engine working fluid. Void shape, location, growth or shrinkage (due to density difference between the solid and liquid PCM phases) are prescribed based on engineering judgement. The PCM phase change process is analyzed using the enthalpy method. The discussion of results focuses on how canister thermal performance is affected by free convection in the liquid PCM and void heat transfer. Characterizing these effects is important for interpreting the relationship between ground-based canister performance (in 1-g) and expected on-orbit performance (in micro-g). Void regions accentuate canister hot spots and temperature gradients due to their large thermal resistance. Free convection reduces the extent of PCM superheating and lowers canister temperatures during a portion of the PCM thermal charge period. Surprisingly small differences in canister thermal performance result from operation on the ground and operation on-orbit. This lack of a strong gravity dependency is attributed to the large contribution of container walls in overall canister energy redistribution by conduction.

17. Key Words (Suggested by Author(s))
Phase change material; Thermal energy storage; Solar dynamic power; Space Station Freedom; Enthalpy method; Void; Gravity dependence; Free convection

18. Distribution Statement
Unclassified – Unlimited
Subject Category 20

19. Security Classif. (of this report)
Unclassified

20. Security Classif. (of this page)
Unclassified

21. No. of pages
190

22. Price*
A09

*For sale by the National Technical Information Service, Springfield, Virginia 22161

National Aeronautics and
Space Administration

Lewis Research Center
Cleveland, Ohio 44135

Official Business
Penalty for Private Use $300

FOURTH CLASS MAIL

ADDRESS CORRECTION REQUESTED

U.S. MAIL

Postage and Fees Paid
National Aeronautics and
Space Administration
NASA-451

NASA